Some Facts about Operator-Splitting and Alternating Direction Methods

Roland Glowinski, Tsorng–Whay Pan and Xue–Cheng Tai.

Abstract The main goal of this chapter is to give the reader a (relatively) brief overview of operator-splitting, augmented Lagrangian and ADMM methods and algorithms. Following a general introduction to these methods, we will give several applications in Computational Fluid Dynamics, Computational Physics, and Imaging. These applications will show the flexibility, modularity, robustness and versatility of these methods. Some of these applications will be illustrated by the results of numerical experiments; they will confirm the capabilities of operator-splitting methods concerning the solution of problems still considered complicated by today standards.

1 Introduction

In 2004, the first author of this chapter was awarded the SIAM Von Kármán Prize for his various contributions to Computational Fluid Dynamics, the direct numerical simulation of particulate flow in particular. Consequently, he was asked by some people at SIAM to contribute an article to SIAM Review, related to the Von Kármán lecture he gave at the 2004 SIAM meeting in Portland, Oregon. Since *operator-splitting* was playing a most crucial role in the result presented during his Portland lecture, he decided to write, jointly with several collaborators (including the second author), a review article on operator-splitting methods, illustrated by several

Roland Glowinski
Department of Mathematics, University of Houston, Houston, TX 77204, USA, and Department of Mathematics, Hong-Kong Baptist University, Hong Kong, e-mail: roland@math.uh.edu

Tsorng–Whay Pan
Department of Mathematics, University of Houston, Houston, TX 77204, USA, e-mail: pan@math.uh.edu

Xue–Cheng Tai
Department of Mathematics, University of Bergen, Norway, e-mail: tai@mi.uib.no

selected applications. One of the main reasons for that review article was that, to the best of our knowledge at the time, the last comprehensive publication on the subject was [121], a book-size article (266 pages) published in 1990, in the Volume I of the Handbook of Numerical Analysis. Our article was rejected, on the grounds that it was untimely. What is ironical is that the very day (of August 2005) we received the rejection e-mail message, we were having a meeting with computational scientists at Los Alamos National Laboratory (LANL) telling us that one of their *main priorities* was further investigating the various properties of operator-splitting methods, considering that these methods were (and still are) applied at LANL to solve a large variety of challenging, mostly multi-physics, problems. Another event emphasizing the importance of operator-splitting methods was the December 2005 conference, at Rice University in Houston, commemorating "50 Years of Alternating-Direction Methods" and honoring *J. Douglas, D. Peaceman* and *H. Rachford*, the inventors of those particular operator-splitting methods bearing their name. Actually, it was striking to observe during this conference that, at the time, most members of the *Partial Differential Equations* and *Optimization* communities were ignoring that most alternating-direction methods for initial value-problems are closely related to primal-dual algorithms such as *ADMM* (Alternating Direction Methods of Multipliers). In order to create a bridge between these two communities, we updated the failed SIAM Review paper and submitted it elsewhere, leading to [73] (clearly, a publication in a SIAM journal would have had more impact, worldwide). Our goal in this chapter is to present a (kind of) updated variant of [73], less CFD (resp., more ADMM) oriented. It will contain in particular applications to *Imaging*, a topic barely mentioned in reference [73]. The content of this chapter is as follows:

In Section 2, we will discuss the numerical solution of *initial value problems* by *operator-splitting* time-discretization schemes such as Peaceman-Rachford's, Douglas-Rachford's, Lie's, Strang's, Marchuk-Yanenko's, and by the fractional θ-scheme, a three-stage variation, introduced in [67] and [68], of Peaceman-Rachford's scheme. We will conclude this section by some remarks on the parallelization of operator-splitting schemes.

Section 3 will be dedicated to *augmented Lagrangian* and *ADMM algorithms*. We will show in particular that some augmented Lagrangian and ADMM algorithms are nothing but disguised operator-splitting methods (justifying thus the ADMM terminology).

Following [73], we will discuss in Section 4 the operator-splitting based *direct numerical simulation of particulate flow*, in the particular case of mixtures of incompressible viscous fluids and rigid solid particles.

In Section 5, we will discuss the application of operator-splitting methods to the solution of two problems from Physics, namely the *Gross-Pitaevskii* equation, a *nonlinear Schrödinger equation* modelling *Bose-Einstein condensates*, and the *Zakharov* system, a model for the *propagation of Langmuir waves in ionized plasma*.

Next, in Section 6, we will discuss applications of augmented Lagrangian and ADMM algorithms to the solution of problems from *Imaging*, a highly popular topic nowadays (actually, the renewed interest in ADMM type algorithms that we observe

currently can be largely explained by their application to Image Processing; see [156, 170]).

Finally, in Section 7, we will return to various issues that we left behind in the preceding sections of this chapter: these include augmentation parameter selection, an analysis of the asymptotic behavior of the Peaceman-Rachford and Douglas-Rachford schemes, and various comments concerning high order accurate operator-splitting schemes. Also, owing to the fact that one of the success stories of operator-splitting methods has been the numerical solution of the Navier-Stokes equations modeling viscous flow, we will conclude this section (and the chapter) by providing a (non-exhaustive) list of related references.

In addition to all the other chapters of this volume, material related to operator-splitting, augmented Lagrangian and ADMM algorithms can be found in [72] (see also the references therein). More references will be given in the following sections.

2 Operator-splitting schemes for the time discretization of initial value problems

2.1 Generalities

Let us consider the following autonomous initial value problem:

$$
\begin{cases}
\dfrac{d\phi}{dt} + A(\phi) = 0 \text{ on } (0,T) \text{ (with } 0 < T \le +\infty), \\
\phi(0) = \phi_0.
\end{cases}
\tag{1}
$$

Operator A maps the vector space V into itself and we suppose that $\phi_0 \in V$. We suppose also that A has a *non-trivial decomposition* such as

$$
A = \sum_{j=1}^{J} A_j,
\tag{2}
$$

with $J \ge 2$ (by *non-trivial* we mean that the operators A_j are individually simpler than A).

A question which arises naturally is clearly:

Can we take advantage of decomposition (2) for the solution of (1)?

It has been known for many years (see for example [36]) that the answer to the above question is definitely *yes*.

Many schemes have been designed to take advantage of the decomposition (2) when solving (1); several of them will be briefly discussed in the following paragraphs.

2.2 Time-discretization of (1) by Lie's scheme

Let $\triangle t(>0)$ be a time-discretization step (for simplicity, we suppose $\triangle t$ fixed,); we denote $n\triangle t$ by t^n. With ϕ^n denoting an approximation of $\phi(t^n)$, *Lie's scheme* reads as follows (for its derivation see, e.g., [70] (Chapter 6) and Chapter 1, Section 2, of this book):

$$\phi^0 = \phi_0; \tag{3}$$

then, for $n \geq 0$, $\phi^n \to \phi^{n+1}$ via

$$\begin{cases} \dfrac{d\phi_j}{dt} + A_j(\phi_j) = 0 \text{ on } (t^n, t^{n+1}), \\ \phi_j(t^n) = \phi^{n+(j-1)/J}; \phi^{n+j/J} = \phi_j(t^{n+1}), \end{cases} \tag{4}$$

for $j = 1, \dots, J$.

If (1) is taking place in a finite dimensional space and if the operators A_j are smooth enough, then $\|\phi(t^n) - \phi^n\| = O(\triangle t)$, function ϕ being the solution of (1).

Remark 1. The above scheme applies also for *multivalued* operators (such as the *subdifferentials* of proper lower semi-continuous convex functionals), but in such a case first order accuracy is not guaranteed anymore. A related application will be given in Section 2.7.

Remark 2. The above scheme is easy to generalize to *non-autonomous* problems by observing that

$$\begin{cases} \dfrac{d\phi}{dt} + A(\phi, t) = 0, \\ \phi(0) = \phi_0 \end{cases} \Leftrightarrow \begin{cases} \dfrac{d\phi}{dt} + A(\phi, \theta) = 0, \\ \dfrac{d\theta}{dt} - 1 = 0, \\ \phi(0) = \phi_0, \theta(0) = 0. \end{cases}$$

Remark 3. Scheme (3)-(4) is semi-constructive in the sense that we still have to solve the initial value sub-problems in (4) for each j. Suppose that we discretize these sub-problems using *just one step of the backward Euler scheme*. The resulting scheme reads as follows:

$$\phi^0 = \phi_0; \tag{5}$$

then, for $n \geq 0$, $\phi^n \to \phi^{n+1}$ via the solution of

$$\frac{\phi^{n+j/J} - \phi^{n+(j-1)/J}}{\triangle t} + A_j(\phi^{n+j/J}) = 0, \tag{6}$$

for $j = 1, \dots, J$.

Scheme (5)-(6) is known as the *Marchuk-Yanenko scheme* (see, e.g., refs. [121] and [70] (Chapter 6)) for more details. Several chapters of this volume are making use of the Marchuk-Yanenko scheme.

2.3 Time-discretization of (1) by Strang's symmetrized scheme

In order to improve the accuracy of Lie's scheme, G. Strang suggested a *symmetrized* variant of scheme (3)-(4) (ref. [153]). When applied to non-autonomous problems, in the case where $J = 2$, we obtain (with $t^{n+1/2} = (n+1/2)\triangle t$):

$$\phi^0 = \phi_0; \qquad (7)$$

then, for $n \geq 0$, $\phi^n \to \phi^{n+1/2} \to \widehat{\phi}^{n+1/2} \to \phi^{n+1}$ via

$$\begin{cases} \dfrac{d\phi_1}{dt} + A_1(\phi_1, t) = 0 \text{ on } (t^n, t^{n+1/2}), \\ \phi_1(t^n) = \phi^n; \phi^{n+1/2} = \phi_1(t^{n+1/2}), \end{cases} \qquad (8)$$

$$\begin{cases} \dfrac{d\phi_2}{dt} + A_2(\phi_2, t^{n+1/2}) = 0 \text{ on } (0, \triangle t), \\ \phi_2(0) = \phi^{n+1/2}; \widehat{\phi}^{n+1/2} = \phi_2(\triangle t), \end{cases} \qquad (9)$$

$$\begin{cases} \dfrac{d\phi_1}{dt} + A_1(\phi_1, t) = 0 \text{ on } (t^{n+1/2}, t^{n+1}), \\ \phi_1(t^{n+1/2}) = \widehat{\phi}^{n+1/2}; \phi^{n+1} = \phi_1(t^{n+1}). \end{cases} \qquad (10)$$

If (1) is taking place in a finite dimensional space and if operators A_1 and A_2 are smooth enough, then $\|\phi(t^n) - \phi^n\| = O(|\triangle t|^2)$, function ϕ being the solution of (1).

Remark 4. In order to preserve the second order accuracy of scheme (7)-(10) (assuming it takes place) we have to solve the initial value problems in (8), (9) and (10) by schemes which are themselves second order accurate (at least); these schemes are highly dependent of the properties of A_1 and A_2. The sub-problems (8), (9) and (10) are all particular cases of

$$\begin{cases} \dfrac{d\phi}{dt} + B(\phi, t) = 0 \text{ on } (t_0, t_f), \\ \phi(t_0) = \phi_0. \end{cases} \qquad (11)$$

Suppose now that B is a (positively) monotone operator; following [70] (Chapter 6), we advocate using for the numerical integration of (11) the *second order implicit Runge-Kutta scheme* below:

$$\begin{cases} \phi^0 = \phi_0; \\ \text{for } q = 0, \ldots, Q-1, \phi^q \to \phi^{q+\theta} \to \phi^{q+1-\theta} \to \phi^{q+1} \text{ via} \\ \begin{cases} \dfrac{\phi^{q+\theta} - \phi^q}{\theta \tau} + B(\phi^{q+\theta}, t^{q+\theta}) = 0, \\ \phi^{q+1-\theta} = \dfrac{1-\theta}{\theta} \phi^{q+\theta} + \dfrac{2\theta - 1}{\theta} \phi^q, \\ \dfrac{\phi^{q+1} - \phi^{q+1-\theta}}{\theta \tau} + B(\phi^{q+1}, t^{q+1}) = 0, \end{cases} \end{cases} \qquad (12)$$

where in (12):

- $Q(\geq 1)$ is an integer and $\tau = \dfrac{t_f - t_0}{Q}$.
- $\phi^{q+\alpha}$ is an approximation of $\phi(t^{q+\alpha})$, with $t^{q+\alpha} = t_0 + (q+\alpha)\tau$.
- $\theta = 1 - \dfrac{1}{\sqrt{2}}$.

It is shown in [70] (Chapter 2) that the implicit Runge-Kutta scheme (12) is *stiff A-stable* and "nearly" third-order accurate. It has been used, in particular, in [70] and [162] for the numerical simulation of incompressible viscous flow.

Remark 5. The main (if not the unique) drawback of Strang's symmetrized scheme (7)-(10) concerns its ability at capturing the *steady state solutions* of (1) (when $T = +\infty$), assuming that such solutions do exist. Indeed, the *splitting error* associated with scheme (7)-(10) prevents using large values of $\triangle t$ when integrating (1) from $t = 0$ to $t = +\infty$; if the sequence $\{\phi^n\}_{n\geq 0}$ converges to a limit, this limit is not, in general, a steady state solution of (1), albeit being close to one for small values of $\triangle t$ (a similar comment applies also to the sequences $\{\phi^{n+1/2}\}_{n\geq 0}$ and $\{\widehat{\phi}^{n+1/2}\}_{n\geq 0}$). A simple way to-partly-overcome this difficulty is to use variable time discretization steps: for example, in (8), (9) and (10), one can replace $\triangle t$ by τ_n (the sequence $\{\tau_n\}_{n\geq 0}$ verifying $\tau_n > 0$, $\lim\limits_{n\to\infty} \tau_n = 0$ and $\sum\limits_{n=0}^{\infty} \tau_n = +\infty$), and then define t^{n+1} and $t^{n+1/2}$ by $t^{n+1} = t^n + \tau_n \ \forall n \geq 0, t^0 = 0$, and $t^{n+1/2} = t^n + \tau^n/2$, respectively. A more sophisticated way to fix the asymptotic behavior of scheme (7)-(10) is to proceed as in the chapter by *McNamara* and *Strang* in this book (Chapter 3).

Remark 6. More comments on scheme (7)-(10) can be found in, e.g., [70] (Chapter 6), [72] (Chapter 3) and various chapters of this volume, Chapter 3 in particular. Among these comments, the generalization of the above scheme to those situations where $J \geq 3$ in (2) has been discussed. Conceptually, the case $J \geq 3$ is no more complicated than $J = 2$. Focusing on $J = 3$, we can return (in a non-unique way) to the case $J = 2$ by observing that

$$A = A_1 + A_2 + A_3 = A_1 + (A_2 + A_3) = (A_1 + A_2) + A_3 \qquad (13)$$
$$= (A_1 + \frac{1}{2}A_2) + (\frac{1}{2}A_2 + A_3).$$

The first (resp., second and third) arrangement in (13) leads to 5 (resp., 7 and 9) initial value sub-problems per time step. Scheme (7)-(10), combined with the first arrangement in (13), has been applied in [81] to the computation of the periodic solution of a nonlinear integro-differential equation from Electrical Engineering.

2.4 Time-discretization of (1) by Peaceman-Rachford's alternating direction method

Another candidate for the numerical solution of the initial value problem (1), or of its non-autonomous variant

$$\begin{cases} \dfrac{d\phi}{dt} + A(\phi, t) = 0 \text{ on } (0, T), \\ \phi(0) = \phi_0. \end{cases} \tag{14}$$

is provided, if $J = 2$ in (2), by the *Peaceman-Rachford scheme* (introduced in [139]). The idea behind the Peaceman-Rachford scheme is quite simple: the notation being like in Sections 2.1, 2.2 and 2.3, one divides the time interval $[t^n, t^{n+1}]$ into two subintervals of length $\triangle t/2$ using the mid-point $t^{n+1/2}$. Then assuming that the approximate solution ϕ^n is known at t^n one computes first $\phi^{n+1/2}$ using over $[t^n, t^{n+1/2}]$ a scheme of the *backward Euler* type with respect to A_1 and of the *forward Euler* type with respect to A_2; one proceeds similarly over $[t^{n+1/2}, t^{n+1}]$, switching the roles of A_1 and A_2. The following scheme, due to *Peaceman and Rachford* (see [139]), realizes precisely this program when applied to the solution of the initial value problem (14):

$$\begin{cases} \phi^0 = \phi_0; \\ \text{for } n \geq 0, \ \phi^n \to \phi^{n+1/2} \to \phi^{n+1} \text{ via the solution of} \\ \dfrac{\phi^{n+1/2} - \phi^n}{\triangle t/2} + A_1(\phi^{n+1/2}, t^{n+1/2}) + A_2(\phi^n, t^n) = 0, \\ \dfrac{\phi^{n+1} - \phi^{n+1/2}}{\triangle t/2} + A_1(\phi^{n+1/2}, t^{n+1/2}) + A_2(\phi^{n+1}, t^{n+1}) = 0. \end{cases} \tag{15}$$

The *convergence* of the *Peaceman-Rachford scheme* (15) has been proved in [118] and [84] under quite general *monotonicity* assumptions concerning the operators A_1 and A_2 (see also [64], [65] and [110]); indeed, A_1 and/or A_2 can be nonlinear, unbounded and even multi-valued. In general, scheme (15) is *first order accurate* at best; however, if the operators A_1 and A_2 are linear, time independent and *commute* then scheme (15) is *second order accurate* (that is $\|\phi^n - \phi(t^n)\| = O(|\triangle t|^2)$), ϕ being the solution of problem (1)). Further properties of scheme (15) can be found in, e.g., [121], [70] (Chapter 2) and [72] (Chapter 3), including its *stability*, and its *asymptotic behavior* if $T = +\infty$; concerning this last issue, a sensible advice is to use another scheme to compute steady state solutions, scheme (15) *not being stiff A-stable*.

Remark 7. Scheme (15) belongs to the *alternating direction method* family. The reason of that terminology is well-known: one of the very first applications of scheme (15) was the numerical solution of the *heat equation*

$$\frac{\partial \phi}{\partial t} - \frac{\partial^2 \phi}{\partial x^2} - \frac{\partial^2 \phi}{\partial y^2} = f,$$

completed by initial and boundary conditions. After finite difference discretization, the roles of A_1 and A_2 were played by the square matrices approximating the operators $-\dfrac{\partial^2}{\partial x^2}$ and $-\dfrac{\partial^2}{\partial y^2}$, respectively, explaining the terminology.

Remark 8. We observe that operators A_1 and A_2 play essentially *symmetrical* roles in scheme (15).

Remark 9. For those fairly common situations where operator A_2 is *uni-valued*, but operator A_1 is "nasty" (discontinuous and/or multi-valued, etc.), we should use the following equivalent formulation of the Peaceman-Rachford scheme (15):

$$\begin{cases} \phi^0 = \phi_0; \\ \text{for } n \geq 0, \ \phi^n \to \phi^{n+1/2} \to \phi^{n+1} \text{ via the solution of} \\ \dfrac{\phi^{n+1/2} - \phi^n}{\triangle t/2} + A_1(\phi^{n+1/2}, t^{n+1/2}) + A_2(\phi^n, t^n) = 0, \\ \dfrac{\phi^{n+1} - 2\phi^{n+1/2} + \phi^n}{\triangle t/2} + A_2(\phi^{n+1}, t^{n+1}) = A_2(\phi^n, t^n). \end{cases} \qquad (16)$$

2.5 Time-discretization of (1) by Douglas-Rachford's alternating direction method

We assume that $J = 2$ in (2).

The *Douglas-Rachford* scheme (introduced in [57]) is a variant of the *Peaceman-Rachford* scheme (15); when applied to the numerical solution of the initial value problem (14) (the non-autonomous generalization of (1)), it takes the following form:

$$\begin{cases} \phi^0 = \phi_0; \\ \text{for } n \geq 0, \ \phi^n \to \widehat{\phi}^{n+1} \to \phi^{n+1} \text{ via the solution of} \\ \dfrac{\widehat{\phi}^{n+1} - \phi^n}{\triangle t} + A_1(\widehat{\phi}^{n+1}, t^{n+1}) + A_2(\phi^n, t^n) = 0, \\ \dfrac{\phi^{n+1} - \phi^n}{\triangle t} + A_1(\widehat{\phi}^{n+1}, t^{n+1}) + A_2(\phi^{n+1}, t^{n+1}) = 0. \end{cases} \qquad (17)$$

The Douglas-Rachford scheme (17) has clearly a *predictor-corrector* flavor.

The convergence of the *Douglas-Rachford scheme* (17) has been proved in [118] and [84] under quite general *monotonicity* assumptions concerning the operators A_1 and A_2 (see also [64], [65] and [110]); indeed, A_1 and/or A_2 can be nonlinear, unbounded and even multi-valued. In general, scheme (17) is first order accurate at best (even if the operators A_1 and A_2 are linear, time independent and commute, assumptions implying second order accuracy for the Peaceman-Rachford scheme). Further properties of scheme (17) can be found in, e.g., [121], [70] (Chapter 2) and [72] (Chapter 3), including its *stability*, and its *asymptotic behavior* if $T = +\infty$. Concerning this last issue, a sensible advice is to use another scheme to compute

steady state solutions, scheme (17) *not being stiff A-stable*, a property it shares with the Peaceman-Rachford scheme (15).

Remark 10. Unlike the Peaceman-Rachford scheme (15), we observe that the roles played by operators A_1 and A_2 are *non-symmetrical* in scheme (17); actually, numerical experiments confirm that fact: for example, for the same $\triangle t$ the speed of convergence to a steady state solution may depend of the choice one makes for A_1 and A_2. As a rule of thumb, we advocate taking for A_2 the operator with the best continuity and monotonicity properties (see, for example, [62] (Chapter 3), [63] (Chapter 3) and [74] (Chapter 3) for more details).

Remark 11. Unlike scheme (15), scheme (17) is easy to generalize to operator decompositions involving *more than two operators*. Consider thus the numerical integration of (14) when $J \geq 3$ in (2). Following *J. Douglas* in [54] and [55] we generalize scheme (17) by

$$\phi^0 = \phi_0; \tag{18}$$

then for $n \geq 0$, ϕ^n being known, compute $\phi^{n+1/J}$, ..., $\phi^{n+j/J}$, ..., ϕ^{n+1} via the solution of

$$\begin{cases} \dfrac{\phi^{n+1/J} - \phi^n}{\triangle t} + \dfrac{1}{J-1}A_1(\phi^{n+1/J}, t^{n+1}) + \dfrac{J-2}{J-1}A_1(\phi^n, t^n) \\ \qquad + \displaystyle\sum_{i=2}^{J} A_i(\phi^n, t^n) = 0, \end{cases} \tag{19.1}$$

$$\begin{cases} \dfrac{\phi^{n+j/J} - \phi^n}{\triangle t} + \displaystyle\sum_{i=1}^{j-1}\left[\dfrac{1}{J-1}A_i(\phi^{n+i/J}, t^{n+1}) + \dfrac{J-2}{J-1}A_i(\phi^n, t^n)\right] \\ \qquad + \dfrac{1}{J-1}A_j(\phi^{n+j/J}, t^{n+1}) + \dfrac{J-2}{J-1}A_j(\phi^n, t^n) \\ \qquad + \displaystyle\sum_{i=j+1}^{J} A_i(\phi^n, t^n) = 0, \end{cases} \tag{19.j}$$

$$\begin{cases} \dfrac{\phi^{n+1} - \phi^n}{\triangle t} + \displaystyle\sum_{i=1}^{J-1}\left[\dfrac{1}{J-1}A_i(\phi^{n+i/J}, t^{n+1}) + \dfrac{J-2}{J-1}A_i(\phi^n, t^n)\right] \\ \qquad + \dfrac{1}{J-1}A_J(\phi^{n+1}, t^{n+1}) + \dfrac{J-2}{J-1}A_J(\phi^n, t^n) = 0, \end{cases} \tag{19.J}$$

Above, $\phi^{n+i/J}$ and $\phi^{n+j/J}$ denote approximate solutions at steps i and j of the computational process; *they do not denote* approximations of $\phi(t^{n+i/J})$ and $\phi(t^{n+j/J})$ (unless $i = j = J$).

Remark 12. This is the Douglas-Rachford analog of Remark 9: for those situations where A_1 is a "bad" operator (in the sense of Remark 9), we should use (assuming that A_2 is uni-valued) the following *equivalent* formulation of the Douglas-Rachford scheme (17):

$$\begin{cases} \phi^0 = \phi_0; \\ \text{for } n \geq 0, \, \phi^n \to \widehat{\phi}^{n+1} \to \phi^{n+1} \text{ via the solution of} \\ \dfrac{\widehat{\phi}^{n+1} - \phi^n}{\triangle t} + A_1(\widehat{\phi}^{n+1}, t^{n+1}) + A_2(\phi^n, t^n) = 0, \\ \dfrac{\phi^{n+1} - \widehat{\phi}^{n+1}}{\triangle t} + A_2(\phi^{n+1}, t^{n+1}) = A_2(\phi^n, t^n). \end{cases} \qquad (20)$$

Remark 13. To those wondering how to choose between the Peaceman-Rachford and Douglas-Rachford schemes, we will say that, on the basis of many numerical experiments, it seems that the second scheme is more robust and faster for those situations where one of the operators is *non-smooth* (multi-valued or singular, for example), particularly if one is interested by capturing steady state solutions. Actually, a better advice could be: consider using the *fractional θ-scheme* to be discussed in Section 2.6, below. Indeed, we have encountered situations where this θ-scheme outperforms both the Peaceman-Rachford and Douglas-Rachford schemes, for steady state computations in particular; such an example is provided by the *anisotropic Eikonal equation*, a nonlinear hyperbolic problem to be briefly discussed in Section 2.7. We will return to the Peaceman-Rachford vs Douglas-Rachford issue in Section 7.

2.6 Time-discretization of (1) by a fractional θ-scheme

This scheme (introduced in [67], [68] for the solution of the *Navier-Stokes equations*) is a variant of the *Peaceman-Rachford* scheme (15). Let θ belong to the open interval $(0, 1/2)$ (in practice, $\theta \in [1/4, 1/3]$); the fractional θ -scheme, applied to the solution of the initial value problem (14) (the non-autonomous generalization of (1)), reads as follows if $A = A_1 + A_2$:

$$\begin{cases} \phi^0 = \phi_0; \\ \text{for } n \geq 0, \, \phi^n \to \phi^{n+\theta} \to \phi^{n+1-\theta} \to \phi^{n+1} \text{ via the solution of} \\ \dfrac{\phi^{n+\theta} - \phi^n}{\theta \triangle t} + A_1(\phi^{n+\theta}, t^{n+\theta}) + A_2(\phi^n, t^n) = 0, \\ \dfrac{\phi^{n+1-\theta} - \phi^{n+\theta}}{(1-2\theta)\triangle t} + A_1(\phi^{n+\theta}, t^{n+\theta}) + A_2(\phi^{n+1-\theta}, t^{n+1-\theta}) = 0, \\ \dfrac{\phi^{n+1} - \phi^{n+1-\theta}}{\theta \triangle t} + A_1(\phi^{n+1}, t^{n+1}) + A_2(\phi^{n+1-\theta}, t^{n+1-\theta}) = 0. \end{cases} \qquad (21)$$

Remark 14. One should avoid confusion between scheme (21) and the following solution method for the initial value problem (14) (with $0 \leq \theta \leq 1$)

$$\begin{cases} \phi^0 = \phi_0; \\ \text{for } n \geq 0, \ \phi^n \to \phi^{n+1} \text{ via the solution of} \\ \dfrac{\phi^{n+1} - \phi^n}{\triangle t} + \theta A(\phi^{n+1}, t^{n+1}) + (1 - \theta)A(\phi^n, t^n) = 0, \end{cases} \tag{22}$$

which is also known as a θ-scheme. We observe that if $\theta = 1$ (resp., $\theta = 0$, $\theta = 1/2$) scheme (22) reduces to *backward Euler's* scheme (resp., *forward Euler's* scheme, a *Crank-Nicolson's* type scheme). Another "interesting" value is $\theta = 2/3$ (for reasons detailed in, e.g., [70] (Chapter 2) and [72] (Chapter 3)). By the way, it is to avoid confusion between schemes (21) and (22) that some practitioners (*S. Turek*, in particular) call the first one a fractional θ-scheme. $\quad \square$

The stability and convergence properties of scheme (21) have been discussed in [70] (Chapter 2) and [72] (Chapter 3) for very simple finite dimensional situations where A_1 and A_2 are both positive multiples of the same symmetric positive definite matrix. Numerical experiments have shown that the good properties verified by scheme (21) for those simple linear situations, in particular its *stiff A-stability* for θ well-chosen, still hold for more complicated problems, such as the numerical simulation of *unsteady incompressible viscous flow* modeled by the *Navier-Stokes equations* (as shown in, e.g., [23], [41], [69] and [70]).

Remark 15. We observe that operators A_1 and A_2 play *non-symmetrical* roles in scheme (21). Since, at each time step, one has to solve two problems (resp., one problem) associated with operator A_1 (resp., A_2) a natural choice is to take for A_1 the operator leading to the sub-problems which are the easiest to solve (that is, whose solution is the less time consuming). Less naive criteria may be used to choose A_1 and A_2, such as the *regularity* (or lack of regularity) of these operators.

Remark 16. If one takes $A_1 = A$ and $A_2 = 0$ in (21), the above scheme reduces to the Runge-Kutta scheme (12), with A replacing B.

Remark 17. The fractional θ-scheme (21) is a *symmetrized scheme*. From that point of view, it has some analogies with *Strang's symmetrized scheme* (7)-(10), discussed in Section 2.3.

Remark 18. This is the fractional θ-scheme analog of Remarks 9 and 12. For those situations where A_1 is a "bad" operator (in the sense of Remark 9), we advocate using the following *equivalent* formulation of the θ-scheme (21):

$$\begin{cases} \phi^0 = \phi_0; \\ \text{for } n \geq 0, \ \phi^n \to \phi^{n+\theta} \to \phi^{n+1-\theta} \to \phi^{n+1} \text{ via the solution of} \\ \dfrac{\phi^{n+\theta} - \phi^n}{\theta \triangle t} + A_1(\phi^{n+\theta}, t^{n+\theta}) + A_2(\phi^n, t^n) = 0, \\ \dfrac{\theta \phi^{n+1-\theta} - (1-\theta)\phi^{n+\theta} + (1-2\theta)\phi^n}{\theta(1-2\theta)\triangle t} + A_2(\phi^{n+1-\theta}, t^{n+1-\theta}) = A_2(\phi^n, t^n), \\ \dfrac{\phi^{n+1} - \phi^{n+1-\theta}}{\theta \triangle t} + A_1(\phi^{n+1}, t^{n+1}) + A_2(\phi^{n+1-\theta}, t^{n+1-\theta}) = 0. \end{cases} \tag{23}$$

2.7 Two applications: smallest eigenvalue computation and solution of an anisotropic Eikonal equation

2.7.1 Synopsis

It is not an exaggeration to say that applications of operator-splitting methods are everywhere, new ones occurring "almost" every day; indeed, some well-known methods and algorithms are *disguised* operator-splitting schemes as we will show in Section 2.7.2, concerning the computation of the *smallest eigenvalue of a real symmetric matrix*. In Section 2.7.3, we will apply the fractional θ-scheme (21) to the solution of an *Eikonal equation* modeling *wave propagation in anisotropic media*. More applications will be discussed in Sections 4 and 5.

2.7.2 Application to some eigenvalue computation

Suppose that $\mathbf{A}$ is a real $d \times d$ *symmetric* matrix. Ordering the eigenvalues of $\mathbf{A}$ as follows: $\lambda_1 \leq \lambda_2 \leq \cdots \leq \lambda_d$, our goal is to compute λ_1. We have (with obvious notation)

$$\lambda_1 = \min_{\mathbf{v} \in S} \mathbf{v}^t \mathbf{A} \mathbf{v}, \quad with \ S = \{\mathbf{v} | \mathbf{v} \in I\!\!R^d, \|\mathbf{v}\| = 1\}, \tag{24}$$

the norm in (24) being the canonical Euclidean one. The *constrained minimization* problem in (24) is equivalent to

$$\min_{\mathbf{v} \in I\!\!R^d} \left[\frac{1}{2} \mathbf{v}^t \mathbf{A} \mathbf{v} + I_S(\mathbf{v}) \right], \tag{25}$$

where, in (25), the functional $I_S : I\!\!R^d \to I\!\!R \cup \{+\infty\}$ is defined as follows

$$I_S(\mathbf{v}) = \begin{cases} 0 & if \ \mathbf{v} \in S, \\ +\infty & otherwise, \end{cases}$$

implying that I_S is the *indicator functional* of the sphere S. Suppose that $\mathbf{u}$ is a solution of (25) (that is a minimizer of the functional in (25)); we have then

$$\mathbf{A}\mathbf{u} + \partial I_S(\mathbf{u}) \ni \mathbf{0}, \tag{26}$$

$\partial I_S(\mathbf{u})$ in (26) being a (kind of) generalized gradient of functional I_S at $\mathbf{u}$ (∂I_S is a multivalued operator). Next, we associate with the (necessary) optimality system (26) the following initial value problem (*flow* in the *Dynamical System* terminology):

$$\begin{cases} \dfrac{d\mathbf{u}}{dt} + \mathbf{A}\mathbf{u} + \partial I_S(\mathbf{u}) \ni \mathbf{0} \ \text{in} \ (0, +\infty), \\ \mathbf{u}(0) = \mathbf{u}_0. \end{cases} \tag{27}$$

If one applies the Marchuk-Yanenko scheme (5)-(6) to the solution of problem (27), one obtains (with $\tau = \triangle t$):

$$\begin{cases} \mathbf{u}^0 = \mathbf{u}_0, \\ \text{for } n \geq 0, \mathbf{u}^n \to \mathbf{u}^{n+1/2} \to \mathbf{u}^{n+1} \text{ via the solution of} \\ \dfrac{\mathbf{u}^{n+1/2} - \mathbf{u}^n}{\tau} + \mathbf{A}\mathbf{u}^{n+1/2} = \mathbf{0}, \\ \dfrac{\mathbf{u}^{n+1} - \mathbf{u}^{n+1/2}}{\tau} + \partial I_S(\mathbf{u}^{n+1}) \ni \mathbf{0}. \end{cases} \tag{28}$$

The *first* finite difference equation in (28) implies

$$\mathbf{u}^{n+1/2} = (\mathbf{I} + \tau\mathbf{A})^{-1}\mathbf{u}^n. \tag{29}$$

On the other hand, the *second* finite difference equation in (28) can be interpreted as a necessary optimality condition for the following minimization problem

$$\min_{\mathbf{v} \in S} \left[\frac{1}{2}\|\mathbf{v}\|^2 - \mathbf{v}^t \mathbf{u}^{n+1/2} \right]. \tag{30}$$

Since $\|\mathbf{v}\| = 1$ over S, the solution of problem (30) is given by

$$\mathbf{u}^{n+1} = \frac{\mathbf{u}^{n+1/2}}{\|\mathbf{u}^{n+1/2}\|}. \tag{31}$$

It follows from (29) and (31) that algorithm (28) is nothing but the *inverse power method with shift*, a well-known algorithm from *Numerical Linear Algebra*. Indeed, if

$$0 < \tau < \frac{1}{\max(0_+, -\lambda_1)},$$

and if the projection of $\mathbf{u}_0$ on the vector space spanned by the eigenvectors of $\mathbf{A}$ associated with λ_1 is different from $\mathbf{0}$, we can easily prove that the sequence $\{\mathbf{u}^n\}_{n \geq 0}$ converges to an eigenvector of $\mathbf{A}$ associated with λ_1 and also that

$$\lim_{n \to +\infty} (\mathbf{u}^n)^t \mathbf{A}\mathbf{u}^n = \lambda_1.$$

Clearly, numerical analysts have not been waiting for operator-splitting to compute matrix eigenvalues and eigenvectors; on the other hand, operator-splitting has provided efficient algorithms for the solution of complicated problems from Differential Geometry, Mechanics, Physics, Physico-Chemistry, Finance, etc., including some nonlinear eigenvalue problems, as shown in, e.g., [72] (Chapter 7).

2.7.3 Application to the solution of an anisotropic Eikonal equation from acoustics

The next application of operator-splitting, that we are going to (briefly) consider in this chapter, was brought to our attention recently (December 2014) by our colleagues *S. Leung* and *J. Qian*. It concerns the numerical solution of the following *nonlinear hyperbolic* partial differential equation

$$|\nabla \tau| - \frac{|1 - \mathbf{V} \cdot \nabla \tau|}{c} = 0 \ \ in \ \Omega, \tag{32}$$

encountered in *Acoustics* and known as the *anisotropic Eikonal equation*. In (32), we have (see [40] for more details):

- $\Omega \subset \mathbb{R}^d$, with $d \geq 2$.
- $\tau(x)$ is the time of *1st arrival of the wave front* at $x \in \Omega$.
- $c > 0$ is the *wave propagation speed* in the medium filling Ω, assuming that this medium is at rest (the so-called *background medium*).
- Assuming that the ambient medium is moving, $\mathbf{V}$ is its *moving velocity*; we assume that $\mathbf{V} \in (L^\infty(\Omega))^d$.

Fast-sweeping methods have been developed for the efficient numerical solution of the classical Eikonal equation

$$|\nabla \tau| = \frac{1}{c} \ \ in \ \Omega, \tag{33}$$

(see, e.g., [104] and [182]); these methods provide automatically *viscosity solutions* in the sense of *Crandall* and *Lions* (see [38] for this notion). Unfortunately, as shown in [40], the fast sweeping methods developed for the solution of (33) cannot handle (32), unless one modifies them significantly, as done in [40]. Actually, there exists an alternative, simpler to implement, to the method developed in [40]: it relies on the operator-splitting methods discussed in Sections 2.3, 2.4, 2.5 and 2.6, and takes advantage of the fact that the fast-sweeping methods developed for the solution of (33) can be easily modified in order to handle equations such as

$$\alpha \tau - \beta \nabla^2 \tau + |\nabla \tau| = f \tag{34}$$

and

$$\alpha \tau - \beta \nabla^2 \tau - \frac{|1 - \mathbf{V} \cdot \nabla \tau|}{c} = f, \tag{35}$$

with $\alpha > 0$ and $\beta \geq 0$. Therefore, in order to solve problem (32), we associate with it the following initial value problem:

$$\begin{cases} (I - \varepsilon \nabla^2)\dfrac{\partial \tau}{\partial t} + |\nabla \tau| - \dfrac{|1 - \mathbf{V} \cdot \nabla \tau|}{c} = 0 \ \ in \ \Omega \times (0, +\infty), \\ \tau(0) = \tau_0, \end{cases} \tag{36}$$

whose steady state solutions are also solutions of (32). In (36), ε is a non-negative parameter (a regularizing one if $\varepsilon > 0$) and $\tau(t)$ denotes the function $t \rightarrow \tau(x,t)$. Actually, additional conditions are required to have solution uniqueness, typical ones being τ specified on a subset of $\overline{\Omega}(= \Omega \cup \partial\Omega)$, possibly reduced to just one point (a point source for the wave). A typical choice for τ_0 is the corresponding solution of problem (33).

The results reported in [75] show that, with $\theta = 1/3$, the fractional θ-scheme discussed in Section 2.6 outperforms the Strang's, Peaceman-Rachford's and Douglas-Rachford's schemes when applied to the computation of the steady state solutions of (36). The resulting algorithm reads as follows:

$$
\begin{cases}
\tau^0 = \tau_0; \\
\text{for } n \geq 0, \ \tau^n \rightarrow \tau^{n+\theta} \rightarrow \tau^{n+1-\theta} \rightarrow \tau^{n+1} \text{ via the solution of} \\
(I - \varepsilon\nabla^2)\dfrac{\tau^{n+\theta} - \tau^n}{\theta\triangle t} + |\nabla\tau^{n+\theta}| - \dfrac{|1 - \mathbf{V}\cdot\nabla\tau^n|}{c} = 0, \\
(I - \varepsilon\nabla^2)\dfrac{\tau^{n+1-\theta} - \tau^{n+\theta}}{(1-2\theta)\triangle t} + |\nabla\tau^{n+\theta}| - \dfrac{|1 - \mathbf{V}\cdot\nabla\tau^{n+1-\theta}|}{c} = 0, \\
(I - \varepsilon\nabla^2)\dfrac{\tau^{n+1} - \tau^{n+1-\theta}}{\theta\triangle t} + |\nabla\tau^{n+1}| - \dfrac{|1 - \mathbf{V}\cdot\nabla\tau^{n+1-\theta}|}{c} = 0.
\end{cases} \tag{37}
$$

The three problems in (37) being particular cases of (34) and (35), their finite difference analogues can be solved by fast-sweeping algorithms. Physical considerations suggest that $\triangle t$ has to be of the order of the space discretization step h. Actually, the numerical results reported in [75] show that, unlike the other schemes discussed in Sections 2.2 to 2.5, scheme (37), with $\theta = 1/3$, has very good convergence properties, even for large values of the ratio $\dfrac{\triangle t}{h}$ (100, typically). If $\varepsilon = 0$ (resp., h^2), these numerical experiments suggest that the number of iterations (time steps), necessary to achieve convergence to a steady state solution, varies (roughly) like $h^{-1/2}$ (resp., $h^{-1/3}$), for two and three-dimensional test problems (see [75] for further results and more details). Clearly, preconditioning does pay here (a well-known fact, in general).

Remark 19. Some readers may wonder why the authors of [75] gave the role of A_1 (resp., A_2) to the operator $\tau \rightarrow |\nabla\tau|$ (resp., $\tau \rightarrow -\dfrac{1}{c}|1 - \mathbf{V}\cdot\nabla\tau|$), and not the other way around. Let us say to these readers that the main reason behind that choice was preliminary numerical experiments showing that, for the same values of α and β, problem (34) is cheaper to solve that problem (35).

2.8 Time-discretization of (1) by a parallel splitting scheme

The splitting schemes presented so far have a sequential nature, i.e. the sub-problems associated with the decomposed operators are solved in a sequential man-

ner. Actually, it is also possible to solve the sub-problems in parallel, as shown just below, using the following variant of Marchuk-Yanenko's scheme:

$$
\begin{cases}
\phi^0 = \phi_0; \\
\text{for } n \geq 0, \text{ we obtain } \phi^{n+1} \text{ from } \phi^n \text{ by solving first} \\
\dfrac{\phi^{n+j/2J} - \phi^n}{J\triangle t} + A_j(\phi^{n+j/2J}, t^{n+1}) = 0, \text{ for } j = 1,\ldots,J, \\
\phi^{n+1} \text{ being then obtained by averaging as follows} \\
\phi^{n+1} = \dfrac{1}{J} \sum_{j=1}^{J} \phi^{n+j/2J}.
\end{cases}
\tag{38}
$$

Scheme (38) is nothing but Algorithm 5.1 in [119]. Under suitable conditions, it has been proved in the above reference that scheme (38) is first order accurate, that is $\|\phi^n - \phi(t^n)\| = O(\triangle t)$. A parallelizable algorithm with second order accuracy is presented also in [119]. The main advantage of the above schemes is that the sub-problems can be solved in parallel. Clearly, this parallel splitting idea can be used for computing the steady state solutions of (1). As observed in [155], the sub-problems (or at least some of them) can also be solved in parallel if the corresponding operator A_j has the right decomposition properties.

3 Augmented Lagrangian algorithms and Alternating Direction Methods of Multipliers

3.1 Introduction

It is our opinion that a review chapter like this one has to include some material about *augmented Lagrangian* algorithms, including of course their relationships with *alternating direction methods*. On the other hand, since augmented Lagrangian algorithms and alternating direction methods of multipliers, and their last known developments, are discussed, with many details, in other chapters of this book, we will not say much about these methods in this section. However, we will give enough information so that the reader may follow Section 6 (dedicated to *Image Processing*) without spending too much time consulting the other chapters (or other references).

In Section 3.2 we will introduce several *augmented Lagrangian algorithms*, and show in Section 3.3 how these algorithms relate to the *alternating direction methods* discussed in Sections 2.4 (*Peaceman-Rachford's*) and 2.5 (*Douglas-Rachford's*).

This section is largely inspired by Chapter 4 of [72].

3.2 Decomposition-coordination methods by augmented Lagrangians

3.2.1 Abstract problem formulation. Some examples

A large number of problems in *Mathematics, Physics, Engineering, Economics, Data Processing, Imaging, etc.* can be formulated as

$$u = \arg\min_{v \in V}[F(Bv) + G(v)], \tag{39}$$

where: (i) V and H are Banach spaces. (ii) $B \in \mathscr{L}(V,H)$. (iii) $F : H \to \mathbb{R} \cup \{+\infty\}$ and $G : V \to \mathbb{R} \cup \{+\infty\}$ are *proper, lower semi-continuous* and *convex* functionals verifying $\mathrm{dom}(F \circ B) \cap \mathrm{dom}(G) \neq \emptyset$, implying that problem (39) may have solutions.

Example 1. This first example concerns the following variational problem:

$$u = \arg\min_{v \in H_0^1(\Omega)} \left[\frac{\mu}{2} \int_\Omega |\nabla v|^2 \, dx + \tau_y \int_\Omega |\nabla v| \, dx - \varpi \int_\Omega v \, dx\right], \tag{40}$$

where: (i) Ω is a bounded domain (that is an bounded open connected subset) of $\mathbb{R}^2$; we denote by Γ the boundary of Ω. (ii) $dx = dx_1 dx_2$. (iii) μ and τ_y are two positive constants. (iv) $|\nabla v|^2 = \left|\frac{\partial v}{\partial x_1}\right|^2 + \left|\frac{\partial v}{\partial x_2}\right|^2$ (v) The space $H_0^1(\Omega)$ (a Sobolev space) is defined by

$$H_0^1(\Omega) = \{v \,|\, v \in L^2(\Omega), \partial v / \partial x_i \in L^2(\Omega), \forall i = 1, 2, v|_\Gamma = 0\}, \tag{41}$$

the two derivatives in (41) being in the *sense of distributions* (see, e.g., [148], [157] for this notion). Since Ω is bounded, $H_0^1(\Omega)$ is a Hilbert space for the inner product $\{v, w\} \to \int_\Omega \nabla v \cdot \nabla w \, dx$, and the associated norm. Problem (40) is a well-known problem from *non-Newtonian fluid mechanics*; it models the *flow of an incompressible visco-plastic fluid* (of the *Bingham* type) in an infinitely long cylinder of cross-section Ω, ϖ being the *pressure drop per unit length* and u the flow *axial velocity*. In (40), μ denotes the fluid *viscosity* and τ_y its *plasticity yield* (see, e.g., [59] and [83] for further information on visco-plastic fluid flows; see also the references therein). It follows from, e.g., [66] and [72], that the variational problem (40) has a unique solution.

Problem (40) is a particular case of (39) with $V = H_0^1(\Omega)$, $H = (L^2(\Omega))^2$, $B = \nabla$, $F(\mathbf{q}) = \int_\Omega |\mathbf{q}| \, dx$, and $G(v) = \frac{\mu}{2} \int_\Omega |\nabla v|^2 \, dx - \varpi \int_\Omega v \, dx$; other decompositions are possible.

Close variants of problem (40) are encountered in *imaging*, as shown in Section 6 (and other chapters of this volume).

Example 2. It concerns the following variant of problem (40):

$$u = \arg\min_{v \in K} \left[\frac{\mu}{2} \int_{\Omega} |\nabla v|^2 \, dx - C \int_{\Omega} v \, dx \right], \tag{42}$$

where Ω is a bounded domain of $I\!R^2$, μ is a *positive constant* and

$$K = \{v | v \in H_0^1(\Omega), |\nabla v| \le 1 \text{ a.e. in } \Omega\}.$$

It is a classical result (see, e.g., [59]) that (42) models, in an appropriate system of mechanical units, the *torsion* of an infinitely long cylinder of cross-section Ω, made of an *elastic-plastic* material, C being the *torsion angle per unit length* and u a *stress potential*. It follows from, e.g., [66] and [72], that the variational problem (42) has a unique solution.

Problem (42) is a particular case of problem (39) with $V = H_0^1(\Omega)$, $H = (L^2(\Omega))^2$, $B = \nabla$, $G(v) = \frac{\mu}{2} \int_{\Omega} |\nabla v|^2 \, dx - C \int_{\Omega} v \, dx$, and $F(\mathbf{q}) = I_{\mathcal{K}}(\mathbf{q})$, $I_{\mathcal{K}}(\cdot)$ being the *indicator functional* of the *closed convex non-empty* subset $\mathcal{K}$ of H defined by

$$\mathcal{K} = \{\mathbf{q} | \mathbf{q} \in H, |\mathbf{q}| \le 1 \text{ a.e. in } \Omega\}.$$

Other decompositions are possible.

Remark 20. We recall that, we have, (from the definition of *indicator functionals*)

$$I_{\mathcal{K}}(\mathbf{q}) = \begin{cases} 0 \text{ if } \mathbf{q} \in \mathcal{K}, \\ +\infty \text{ otherwise,} \end{cases}$$

implying, from the properties of $\mathcal{K}$, that $I_{\mathcal{K}} : H \to I\!R \cup \{+\infty\}$ is *convex, proper* and *lower semi-continuous*. □

Numerical methods for the solution of problem (42) can be found in, e.g., [66] and [76].

3.2.2 Primal-dual methods for the solution of problem (39): ADMM algorithms

In order to solve problem (39), we are going to use a strategy introduced in [77] and [78] (to the best of our knowledge). The starting point is the obvious *equivalence* between (39) and the following *linearly constrained* optimization problem:

$$\{u, Bu\} = \arg\min_{\{v,q\} \in W} j(v,q), \tag{43}$$

where

$$j(v,q) = F(q) + G(v),$$

and

$$W = \{\{v,q\} | v \in V, q \in H, Bv - q = 0\}.$$

From now on, we will assume that V and H are (real) *Hilbert spaces*, the *H-norm* being denoted by $|\cdot|$ and the associated inner-product by $(\cdot,\cdot)$. The next step is quite natural: we associate with the minimization problem (43) a *Lagrangian* functional $\mathscr{L}$ defined by

$$\mathscr{L}(v,q;\mu) = j(v,q) + (\mu, Bv - q),$$

and an *augmented Lagrangian* functional $\mathscr{L}_r$ defined (with $r > 0$) by

$$\mathscr{L}_r(v,q;\mu) = \mathscr{L}(v,q;\mu) + \frac{r}{2}|Bv - q|^2. \tag{44}$$

One can easily prove that the functionals $\mathscr{L}$ and $\mathscr{L}_r$ share the same saddle-points over $(V \times H) \times H$, and also that, if $\{\{u,p\},\lambda\}$ is such a saddle-point, then u is a solution of problem (39) and $p = Bu$. A classical algorithm to compute saddle-points is the so-called *Uzawa algorithm*, popularized by [3] (a book dedicated to the study of *Economics equilibria*), and further discussed in, e.g., [76]. Applying a close variant of the Uzawa algorithm to the computation of the saddle-points of $\mathscr{L}_r$ over $(V \times H) \times H$, we obtain

$$\begin{cases} \lambda^0 \text{ is given in } H; \\ \text{for } n \geq 0, \ \lambda^n \to \{u^n, p^n\} \to \lambda^{n+1} \text{ via} \\ \{u^n, p^n\} = \arg \min_{\{v,q\} \in V \times H} \mathscr{L}_r(v,q;\lambda^n), \\ \lambda^{n+1} = \lambda^n + \rho(Bu^n - p^n), \end{cases} \tag{45}$$

an algorithm called *ALG*1 by some practitioners, following a terminology introduced in [78] (an alternative name could have been *augmented Lagrangian Uzawa algorithm* which summarizes quite well what algorithm (45) is all about).

Concerning the *convergence* of *ALG*1 it has been proved in, e.g., [62], [63], [66] and [74] (see also [78]), that if:

(i) $\mathscr{L}$ has a saddle-point $\{\{u,p\},\lambda\}$ over $(V \times H) \times H$.

(ii) B is an injection and $R(B)$ is closed in H.

(iii) $\lim_{|q| \to +\infty} \dfrac{F(q)}{|q|} = +\infty.$

(iv) $F = F_0 + F_1$ with F_0 and F_1 proper, lower semi-continuous and convex, with F_0 Gateaux-differentiable, and uniformly convex on the bounded sets of H

(the above properties imply that problem (39) has a unique solution), then we have, $\forall \, r > 0$ and if

$$0 < \rho < 2r,$$

the following convergence result

$$\lim_{n \to +\infty} \{u^n, p^n\} = \{u, Bu\} \text{ in } V \times H, \tag{46}$$

where u is the solution of problem (39); moreover, the convergence result (46) holds $\forall \, \lambda^0 \in H$. The convergence of the multiplier sequence $\{\lambda^n\}_{n \geq 0}$ is no better than

weak in general, implying that the criterion used to stop *ALG*1 has to been chosen carefully. Of course, in *finite dimension*, the properties of B, F and G implying convergence are *less demanding* than in *infinite dimension*; for example, the *existence* of a solution to problem (39) is *sufficient* to imply the *existence* of a *saddle-point*.

The main difficulty with the Uzawa algorithm (45) is clearly the solution of the minimization problem it contains. An obvious choice to solve this problem is to use a *relaxation* method (as advocated in [77], [78]). Suppose that, as advocated in the two above references (which show that, indeed, for the nonlinear elliptic problem discussed there the number of relaxation iterations reduces quickly to two), we limit the number of relaxation iterations to one when solving the minimization problem in (45): we obtain then the following primal-dual algorithm (called *ALG*2 by some practitioners):

$$\{u^{-1}, \lambda^0\} \text{ is given in } V \times H; \tag{47}$$

for $n \geq 0$, $\{u^{n-1}, \lambda^n\} \rightarrow p^n \rightarrow u^n \rightarrow \lambda^{n+1}$ via

$$p^n = \arg\min_{q \in H} \mathscr{L}_r(u^{n-1}, q; \lambda^n), \tag{48}$$

$$u^n = \arg\min_{v \in V} \mathscr{L}_r(v, p^n; \lambda^n), \tag{49}$$

$$\lambda^{n+1} = \lambda^n + \rho(Bu^n - p^n). \tag{50}$$

Assuming that

$$0 < \rho < \frac{1 + \sqrt{5}}{2} r,$$

with the other assumptions implying the convergence of *ALG*1 still holding, we have

$$\lim_{n \to +\infty} \{u^n, p^n\} = \{u, Bu\} \text{ in } V \times H,$$

where u is the solution of problem (39). Convergence proofs can be found in [62], [63], [66] and [74].

A simple variant (called *ALG*3) of algorithm (47)-(50) is obtained by updating the multiplier a first time immediately after (48); we obtain then

$$\{u^{-1}, \lambda^0\} \text{ is given in } V \times H, \tag{51}$$

for $n \geq 0$, $\{u^{n-1}, \lambda^n\} \rightarrow p^n \rightarrow \lambda^{n+1/2} \rightarrow u^n \rightarrow \lambda^{n+1}$ via

$$p^n = \arg\min_{q \in H} \mathscr{L}_r(u^{n-1}, q; \lambda^n), \tag{52}$$

$$\lambda^{n+1/2} = \lambda^n + \rho(Bu^{n-1} - p^n). \tag{53}$$

$$u^n = \arg\min_{v \in V} \mathscr{L}_r(v, p^n; \lambda^{n+1/2}), \tag{54}$$

$$\lambda^{n+1} = \lambda^{n+1/2} + \rho(Bu^n - p^n). \tag{55}$$

Most practitioners prefer *ALG*2 to *ALG*3, the main reason being that *ALG*2 is more robust than *ALG*3, in general.

Remark 21. If one takes $\rho = r$ in (47)-(50) and (51)-(55), the algorithms we obtain belong to the *Alternating Direction Methods of Multipliers* (*ADMM*) family (a terminology we will justify in Section 3.3). The convergence of *ADMM* related algorithms is rather well established in the *convex* case (see, for example, [18], [61], [95]; see also the references therein and other chapters of this book, the one by *M. Burger, A. Sawatzky & G. Steidl* in particular). On the other hand, one is still lacking a general theory for the convergence of algorithms such as *ALG*1, *ALG*2 and *ALG*3 when applied to the solution of *non-convex variational problems*. Nevertheless, the above algorithms have been successfully applied to the solution of non-convex problems as shown, for example, in [42], [72] (Chapter 4), [74], and other chapters of this book, Chapters 6 and 7, in particular.

Remark 22. An important issue with the above primal-dual algorithms is how to vary r and ρ *dynamically* in order to improve the speed of convergence of these algorithms. This issue has been addressed in, e.g., [18], [34], [45], [46] (see also the references therein).

Remark 23. An overlooked ([34] being a notable exception) property of primal-dual algorithms such as *ALG*1, *ALG*2 and *ALG*3 is that they may be constructive still, in those not so uncommon situations where in (39) one has $\mathrm{dom}(F \circ B) \cap \mathrm{dom}(G) = \emptyset$, implying that problem (39) has no solutions, strictly speaking. On the basis of the numerical results reported in [42] (see also [72] (Chapter 4) and Chapter 7 of this volume), we conjecture that if the parameters ρ and r are properly chosen, the sequence $\{\{u^n, p^n\}\}_{n \geq 0}$ converges to a pair $\{u, p\}$ minimizing the functional

$$\{v, q\} \rightarrow G(v) + F(q)$$

over the set

$$\{\{v, q\}\} | \{v, q\} \in \mathrm{dom}(G) \times \mathrm{dom}(F), |Bv - q| = \min_{\{w, \varpi\} \in \mathrm{dom}(G) \times \mathrm{dom}(F)} |Bw - \varpi|\},$$

while the sequence $\{\lambda^n\}_{n \geq 0}$ diverges *arithmetically* (that is, $|\lambda^n| \rightarrow +\infty$ like n multiplied by a positive constant, that is slowly). If the above convergence/divergence result holds true (which seems to be the case for the non-convex problem discussed in [42]), it implies that the above primal-dual algorithms solve problem (39) in a *least-squares sense*, a most remarkable property indeed, testifying of the robustness of these algorithms. The above results look natural, but the optimization experts we consulted had trouble to give us a precise reference (or a proof).

Remark 24. We encountered situations (in *incompressible finite elasticity* in particular; see, e.g., [74] for details) where a safe way to proceed with the above primal-dual algorithms is as follows: Employ *ALG*1 with a well-balanced (that is neither to small nor too large) stopping criterion for the relaxation algorithm used to solve the minimization problem in (45); it has been observed quite often that the number

of relaxation iterations necessary to compute $\{u^n, p^n\}$ from λ^n goes down quickly to one or two (an observation at the origin of *ALG*2), implying that starting with *ALG*1, the algorithm switches automatically to *ALG*2. It is not uncommon that this implementation of *ALG*1 produces an algorithm faster (CPU-wise) than *ALG*2 and *ALG*3, when solving "hard" problems. □

Further information on the convergence of *Lagrange multiplier based iterative methods* can be found in other chapters of this volume, and in, e.g., [45], [60], [62], [63], [66], [74] and [100] (see also the many references therein).

3.3 On the relationship between Alternating Direction Methods and ALG2, ALG3

As reported in [71] and [72] (Chapter 4) some previously unknown relationships between *alternating direction methods* and *augmented Lagrangian algorithms* were identified in 1975 by T.F. Chan and the first author of this chapter, while investigating the numerical solution of some simple nonlinear elliptic problems by various iterative methods (see [30] for details). Indeed, let us consider the particular case of problem (39) where $V = H$, $B = I$ and F and G are both differentiable over V; then, assuming that $\rho = r$, *ALG*2 (that is algorithm (47)-(50)) takes the following form:

$$\{u^{-1}, \lambda^0\} \text{ is given in } V \times H; \tag{56}$$

for $n \geq 0$, $\{u^{n-1}, \lambda^n\} \to p^n \to u^n \to \lambda^{n+1}$ via

$$r(p^n - u^{n-1}) + DF(p^n) - \lambda^n = 0, \tag{57}$$

$$r(u^n - p^n) + DG(u^n) + \lambda^n = 0, \tag{58}$$

$$\lambda^{n+1} = \lambda^n + r(u^n - p^n), \tag{59}$$

where DF (resp., DG) denotes the differential of F (resp., G). By elimination of λ^n and λ^{n+1} in (57)-(59), we obtain

$$r(p^n - u^{n-1}) + DF(p^n) + DG(u^{n-1}) = 0,$$

$$r(u^n - u^{n-1}) + DF(p^n) + DG(u^n) = 0,$$

which imply in turn (after changing $n - 1$ in n):

$$r(p^{n+1} - u^n) + DF(p^{n+1}) + DG(u^n) = 0, \tag{60}$$

$$r(u^{n+1} - u^n) + DF(p^{n+1}) + DG(u^{n+1}) = 0. \tag{61}$$

Comparing to (17) shows that in this particular case, *ALG*2 is a disguised form of the *Douglas-Rachford* scheme discussed in Section 2.5, with $r = 1/\triangle t$ and DF (resp., DG) playing the role of A_1 (resp., A_2). A similar interpretation holds for *ALG*3: in-

deed, if we assume again that $V = H$, $B = I$ and F and G are differentiable, then, if $\rho = r$, algorithm (51)-(55) reduces to the *Peaceman-Rachford* scheme (15) discussed in Section 2.4. The above equivalence result can be generalized to situations where F and/or G are not differentiable.

The reasons for which *ALG*2 and *ALG*3 are called *Alternating Direction Methods of Multipliers* (*ADMM*) by many practitioners should be clear now. For further information and details on these primal-dual equivalences, see the discussion by M. Yan and W. Yin in Chapter 4 of this book.

4 Operator-splitting methods for the direct numerical simulation of particulate flow

4.1 Generalities. Problem formulation

It is the (necessarily biased) opinion of the authors of this chapter that the *direct numerical simulation of particulate flow* has been one of the success stories of operator-splitting methods, justifying thus a dedicated section in this chapter, despite the fact that this story has been told in several publications (see, e.g., [70] (Chapters 8 & 9), [73] and [79], and the references therein). For simplicity, we will discuss only the one-particle case (however, the results of numerical experiments involving more than one particle will be presented).

Let Ω be a bounded, connected and open region of $\mathbb{R}^d$ ($d = 2$ or 3 in applications); the boundary of Ω is denoted by Γ. We suppose that Ω contains:

(i) A Newtonian incompressible viscous fluid of density ρ_f and viscosity μ_f ; ρ_f and μ_f are both positive constants.
(ii) A rigid body B of boundary ∂B, mass M, center of mass G, and inertia $\mathbf{I}$ at the center of mass (see Figure 1, for additional details).

The fluid occupies the region $\Omega \setminus \overline{B}$ and we suppose that *distance* $(\partial B(0), \Gamma) > 0$. From now on, $\mathbf{x} = \{x_i\}_{i=1}^d$ will denote the generic point of $\mathbb{R}^d$, $d\mathbf{x} = dx_1 \ldots dx_d$, while $\phi(t)$ will denote the function $\mathbf{x} \to \phi(\mathbf{x}, t)$. Assuming that the only external force is *gravity*, the *fluid flow-rigid body motion* coupling is modeled by

$$\rho_f \left(\frac{\partial \mathbf{u}}{\partial t} + (\mathbf{u} \cdot \nabla)\mathbf{u} \right) - \mu_f \nabla^2 \mathbf{u} + \nabla p = \rho_f \mathbf{g} \ \ in \ \Omega \setminus \overline{B(t)}, \text{ a.e. } t \in (0,T), \ (62)$$

$$\nabla \cdot \mathbf{u}(t) = 0 \ in \ \Omega \setminus \overline{B(t)}, \text{ a.e. } t \in (0,T), \tag{63}$$

$$\mathbf{u}(t) = \mathbf{u}_\Gamma(t) \ on \ \Gamma, \text{ a.e. } t \in (0,T), \ with \ \int_\Gamma \mathbf{u}_\Gamma(t) \cdot \mathbf{n} \, d\Gamma = 0, \tag{64}$$

$$\mathbf{u}(0) = \mathbf{u}_0 \ in \ \Omega \setminus \overline{B(0)} \ with \ \nabla \cdot \mathbf{u}_0 = 0, \tag{65}$$
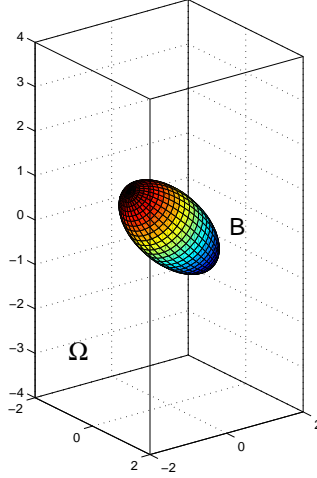
and

Fig. 1 Visualization of the rigid body and of a part of the flow region

$$\frac{dG}{dt} = \mathbf{V}, \tag{66}$$

$$M \frac{d\mathbf{V}}{dt} = M\mathbf{g} + \mathbf{R}_H, \tag{67}$$

$$\frac{d(\mathbf{I}\boldsymbol{\omega})}{dt} = \mathbf{T}_H, \tag{68}$$

$$G(0) = G_0, \mathbf{V}(0) = \mathbf{V}_0, \boldsymbol{\omega}(0) = \boldsymbol{\omega}_0, B(0) = B_0. \tag{69}$$

In relations (62)-(69):

- Vector $\mathbf{u} = \{u_i\}_{i=1}^{d}$ is the *fluid flow velocity* and p is the *pressure*.
- $\mathbf{u}_0$ and $\mathbf{u}_\Gamma$ are given vector-valued functions.
- $\mathbf{V}$ is the *velocity of the center of mass* of body B, while $\boldsymbol{\omega}$ is the angular velocity.
- $\mathbf{R}_H$ and $\mathbf{T}_H$ denote, respectively, the *resultant* and the *torque* of the *hydrodynamical forces*, namely the forces that the fluid exerts on B; we have, actually,

$$\mathbf{R}_H = \int_{\partial B} \boldsymbol{\sigma}\mathbf{n}\,d\gamma \ \ and \ \ \mathbf{T}_H = \int_{\partial B} \overrightarrow{G\mathbf{x}} \times \boldsymbol{\sigma}\mathbf{n}\,d\gamma. \tag{70}$$

In (70) the *stress-tensor* $\boldsymbol{\sigma}$ is defined by $\boldsymbol{\sigma} = 2\mu_f D(\mathbf{u}) - p\mathbf{I}_d$, with $D(\mathbf{v}) = \frac{1}{2}(\boldsymbol{\nabla}\mathbf{v} + (\boldsymbol{\nabla}\mathbf{v})^t)$, while $\mathbf{n}$ is a unit normal vector at ∂B and $\mathbf{I}_d$ is the *identity tensor*.

Concerning the compatibility conditions on ∂B we have: (i) the forces exerted by the fluid on the solid body *balance* those exerted by the solid body on the fluid, and we shall assume that: (ii) the *no-slip boundary condition* holds, namely

$$\mathbf{u}(\mathbf{x},t) = \mathbf{V}(t) + \boldsymbol{\omega}(t) \times \overrightarrow{G(t)\mathbf{x}}, \ \forall \mathbf{x} \in \partial B(t). \tag{71}$$

Remark 25. System (62)-(65) (resp., (66)-(69)) is of the *incompressible Navier-Stokes* (resp., *Euler-Newton*) type. Also, the above model can be generalized to multiple-particles situations and/or non-Newtonian incompressible viscous fluids. □

The (local in time) *existence of weak solutions* for problems such as (62)-(69) has been proved in [52], assuming that, at $t = 0$, the particles do not touch Γ and each other (see also [87] and [145]). Concerning the numerical solution of (62)-(69), (71) several approaches are encountered in the literature, among them: (i) The *Arbitrary Lagrange-Euler* (*ALE*) methods; these methods, which rely on *moving meshes*, are discussed in, e.g., [98], [103] and [127]. (ii) The *fictitious boundary* method discussed in, e.g., [165], and (iii) the non-boundary fitted *fictitious domain* methods discussed in, e.g., [70], [79] and [140], [141] (and in Section 4.2, hereafter). Among other things, the methods in (ii) and (iii) have in common that the meshes used for the flow computations do not have to match the boundary of the particles.

Remark 26. Even if theory suggests that collisions may never take place in finite time (if we assume that the particles have smooth shapes and that the flow is still modeled by the Navier-Stokes equations as long as the particles do not touch each other, or Γ), near collisions take place, and after discretization particles may collide. These phenomena can be handled by introducing (as done in, e.g., [70] (Chapter 8) and [79]) well-chosen short range repulsion potentials reminiscent of those encountered in *Molecular Dynamics*, or by using *Kuhn-Tucker multipliers* to authorize particle motions with *contact* but *no overlapping* (as done in, e.g., [128] and [129]). More information on the numerical treatment of particles in flow, can be found in, e.g., [152] (and the references therein), and of course in Google.

4.2 A fictitious domain formulation

Considering the fluid-rigid body mixture as a unique (heterogeneous) medium we are going to derive a *fictitious domain* based variational formulation to model its motion. The principle of this derivation is pretty simple: it relies on the following steps (see, e.g., [70] and [79] for more details), where in *Step a* we denote by $\mathbf{S} : \mathbf{T}$ the *Fröbenius* inner product of the tensors $\mathbf{S}$ and $\mathbf{T}$, that is (with obvious notation) $\mathbf{S} : \mathbf{T} = \sum_{1 \leq i,j \leq d} s_{ij} t_{ij}$:

Step a. Start from the following *global weak* formulation (of the *virtual power* type):

$$
\left\{
\begin{aligned}
&\rho_f \int_{\Omega \setminus \overline{B(t)}} \left[\frac{\partial \mathbf{u}}{\partial t} + (\mathbf{u} \cdot \nabla)\mathbf{u} \right] \cdot \mathbf{v} \, d\mathbf{x} + 2\mu_f \int_{\Omega \setminus \overline{B(t)}} \mathbf{D}(\mathbf{u}) : \mathbf{D}(\mathbf{v}) \, d\mathbf{x} \\
&- \int_{\Omega \setminus \overline{B(t)}} p \nabla \cdot \mathbf{v} \, d\mathbf{x} + M \frac{d\mathbf{V}}{dt} \cdot \mathbf{Y} + \frac{d(\mathbf{I}\boldsymbol{\omega})}{dt} \cdot \boldsymbol{\theta} \\
&= \rho_f \int_{\Omega \setminus \overline{B(t)}} \mathbf{g} \cdot \mathbf{v} \, d\mathbf{x} + M\mathbf{g} \cdot \mathbf{Y}, \\
&\forall \{\mathbf{v}, \mathbf{Y}, \boldsymbol{\theta}\} \in (H^1(\Omega \setminus \overline{B(t)}))^d \times I\!\!R^d \times \boldsymbol{\Theta} \ \text{and} \ \text{verifying} \\
&\mathbf{v} = 0 \ \text{on} \ \Gamma, \ \mathbf{v}(\mathbf{x}) = \mathbf{Y} + \boldsymbol{\theta} \times \overrightarrow{G(t)\mathbf{x}}, \forall \mathbf{x} \in \partial B(t), \ t \in (0,T), \\
&\text{with} \ \boldsymbol{\Theta} = I\!\!R^3 \ \text{if} \ d = 3, \ \boldsymbol{\Theta} = \{(0,0,\theta) \mid \theta \in I\!\!R\} \ \text{if} \ d = 2,
\end{aligned}
\right. \tag{72}
$$

$$
\int_{\Omega \setminus \overline{B(t)}} q \nabla \cdot \mathbf{u}(t) \, d\mathbf{x} = 0, \forall q \in L^2(\Omega \setminus \overline{B(t)}), \ t \in (0,T), \tag{73}
$$

$$
\mathbf{u}(t) = \mathbf{u}_\Gamma(t) \ \text{on} \ \Gamma, \ t \in (0,T), \tag{74}
$$

$$
\mathbf{u}(\mathbf{x},t) = \mathbf{V}(t) + \boldsymbol{\omega}(t) \times \overrightarrow{G(t)\mathbf{x}}, \forall \mathbf{x} \in \partial B(t), \ t \in (0,T), \tag{75}
$$

$$
\frac{dG}{dt} = \mathbf{V}, \tag{76}
$$

$$
\mathbf{u}(\mathbf{x},0) = \mathbf{u}_0(x), \forall \mathbf{x} \in \Omega \setminus \overline{B(0)}, \tag{77}
$$

$$
G(0) = G_0, \ \mathbf{V}(0) = \mathbf{V}_0, \ \boldsymbol{\omega}(0) = \boldsymbol{\omega}_0, \ B(0) = B_0. \tag{78}
$$

Step b. Fill B with the surrounding fluid and impose a rigid body motion to the fluid inside B.

Step c. Modify the global weak formulation (72)-(78) accordingly, taking advantage of the fact that if $\mathbf{v}$ is a rigid body motion velocity field, then $\nabla \cdot \mathbf{v} = 0$ and $\mathbf{D}(\mathbf{v}) = \mathbf{0}$.

Step d. Use a *Lagrange multiplier* defined over B to force the rigid body motion inside B.

Assuming that B is made of a homogeneous material of density ρ_s, the above program leads to:

$$
\left\{
\begin{aligned}
&\rho_f \int_\Omega \left[\frac{\partial \mathbf{u}}{\partial t} + (\mathbf{u} \cdot \nabla)\mathbf{u} \right] \cdot \mathbf{v} \, d\mathbf{x} + 2\mu_f \int_\Omega \mathbf{D}(\mathbf{u}) : \mathbf{D}(\mathbf{v}) \, d\mathbf{x} - \int_\Omega p \nabla \cdot \mathbf{v} \, d\mathbf{x} \\
&+ (1 - \rho_f/\rho_s) \left[M \frac{d\mathbf{V}}{dt} \cdot \mathbf{Y} + \frac{d(\mathbf{I}\boldsymbol{\omega})}{dt} \cdot \boldsymbol{\theta} \right] + < \boldsymbol{\lambda}, \mathbf{v} - \mathbf{Y} - \boldsymbol{\theta} \times \overrightarrow{G(t)\mathbf{x}} >_{B(t)} \\
&= \rho_f \int_\Omega \mathbf{g} \cdot \mathbf{v} \, d\mathbf{x} + (1 - \rho_f/\rho_s) M\mathbf{g} \cdot \mathbf{Y}, \ \forall \{\mathbf{v}, \mathbf{Y}, \boldsymbol{\theta}\} \in (H^1(\Omega))^d \times I\!\!R^d \times \boldsymbol{\Theta}, \\
&t \in (0,T), \ \text{with} \ \boldsymbol{\Theta} = I\!\!R^3 \ \text{if} \ d = 3, \ \boldsymbol{\Theta} = \{(0,0,\theta) \mid \theta \in I\!\!R\} \ \text{if} \ d = 2,
\end{aligned}
\right. \tag{79}
$$

$$\int_{\Omega} q\boldsymbol{\nabla}\cdot\mathbf{u}(t)\,d\mathbf{x}=0, \forall q\in L^2(\Omega),\ t\in(0,T), \tag{80}$$

$$\mathbf{u}(t)=\mathbf{u}_\Gamma(t)\ on\ \Gamma,\ t\in(0,T), \tag{81}$$

$$\begin{cases} <\boldsymbol{\mu},\mathbf{u}(\mathbf{x},t)-\mathbf{V}(t)-\boldsymbol{\omega}(t)\times\overrightarrow{G(t)\mathbf{x}}>_{B(t)}=0, \\ \forall\boldsymbol{\mu}\in\boldsymbol{\Lambda}(t)\ (=(H^1(B(t)))^d),\ t\in(0,T), \end{cases} \tag{82}$$

$$\frac{dG}{dt}=\mathbf{V}, \tag{83}$$

$$\begin{cases} G(0)=G_0,\ \mathbf{V}(0)=\mathbf{V}_0,\ \boldsymbol{\omega}(0)=\boldsymbol{\omega}_0,\ B(0)=B_0, \\ \mathbf{u}(\mathbf{x},0)=\mathbf{u}_0(\mathbf{x}),\forall\mathbf{x}\in\Omega\setminus\bar{B}_0,\ \ \mathbf{u}(x,0)=\mathbf{V}_0+\boldsymbol{\omega}_0\times\overrightarrow{G_0\mathbf{x}},\ \forall\mathbf{x}\in\bar{B}_0. \end{cases} \tag{84}$$

From a theoretical point of view, a natural choice for $<\cdot,\cdot>_{B(t)}$ is provided by, e.g.,

$$<\boldsymbol{\mu},\mathbf{v}>_{B(t)}=\int_{B(t)}[\boldsymbol{\mu}\cdot\mathbf{v}+l^2\mathbf{D}(\boldsymbol{\mu}):\mathbf{D}(\mathbf{v})]\,d\mathbf{x}; \tag{85}$$

in (85), l is a characteristic length, the diameter of B, for example. In practice, following [70] (Chapter 8) and [79], one makes things much simpler by approximating $\boldsymbol{\Lambda}(t)$ by

$$\boldsymbol{\Lambda}_h(t)=\{\boldsymbol{\mu}\mid\boldsymbol{\mu}=\sum_{j=1}^{N(t)}\boldsymbol{\mu}_j\delta(\mathbf{x}-\mathbf{x}_j),\ with\ \boldsymbol{\mu}_j\in\mathbb{R}^d,\ \forall j=1,\dots,N\}, \tag{86}$$

and the pairing in (85) by

$$<\mu,\mathbf{v}>_{(B(t),h)}=\sum_{j=1}^{N(t)}\boldsymbol{\mu}_j\cdot\mathbf{v}(\mathbf{x}_j). \tag{87}$$

In (86), (87), $\mathbf{x}\to\delta(\mathbf{x}-\mathbf{x}_j)$ is the Dirac measure at $\mathbf{x}_j$, and the set $\{\mathbf{x}_j\}_{j=1}^N$ is the union of two subsets, namely: (i) The set of the points of the velocity grid contained in $B(t)$ and whose distance at $\partial B(t)$ is $\geq ch$, h being a space discretization step and c a constant ≈ 1.(ii) A set of control points located on $\partial B(t)$ and forming a mesh whose step size is of the order of h. It is clear that, using the approach above, one forces the rigid body motion inside the particle by *collocation*.

A variant of the above fictitious domain approach is discussed in [140] and [141]; after an appropriate elimination, it does not make use of Lagrange multipliers to force the rigid body motion of the particles, but uses instead projections on velocity subspaces where the rigid body motion velocity property is verified over the particles (see [140] and [141] for details).

4.3 Solving problem (79)-(84) by operator-splitting

We do not consider *collisions*; after (formal) elimination of p and $\boldsymbol{\lambda}$, problem (79)-(84) reduces to an initial value problem of the following form

$$\frac{d\mathbf{X}}{dt} + \sum_{j=1}^{J} A_j(\mathbf{X},t) = \mathbf{0} \ on \ (0,T), \ \ \mathbf{X}(0) = \mathbf{X}_0, \tag{88}$$

where $\mathbf{X} = \{\mathbf{u},\mathbf{V},\boldsymbol{\omega},G\}$ (or $\{\mathbf{u},\mathbf{V},\mathbf{I}\boldsymbol{\omega},G\}$). A typical situation will be the one where, with $J = 4$, operator A_1 will be associated with *incompressibility*, A_2 with *advection*, A_3 with *diffusion*, A_4 with the *fictitious domain* treatment of the *rigid body motion*; other decompositions are possible as shown in, e.g., [70] (Chapter 8) and [79] (both references include a *collision operator*). The *Lie's scheme* (3), (4) applies "beautifully" to the solution of problem (79)-(84). The resulting method is quite modular implying that different space and time approximations can be used to treat the various sub-problems encountered at each time step; the only constraint is that two successive steps have to communicate (by projection in general to provide the initial condition required by each initial value sub-problem).

4.4 Numerical experiments

4.4.1 Generalities

The methodology we described (briefly) in the above paragraphs has been validated by numerous experiments (see, in particular, [70] (Chapters 8 & 9), [73], [79], [97] [137] and the related publications reported in http://www.math.uh.edu/∼pan/). In this chapter, we will consider two test problems (borrowed from [73] (Section 3.4)): The first test problem involves three particles, while the second one concerns a channel flow with 300 particles. The fictitious domain/operator-splitting approach has made the solution of these problems (almost) routine nowadays. All the flow computations have been done using the *Bercovier-Pironneau finite element approximation*; namely (see [70] (Chapters 5, 8 and 9) for details), we used a globally continuous piecewise affine approximation of the velocity (resp., the pressure) associated with a triangulation (in 2-D) or tetrahedral partition (in 3-D) $\mathscr{T}_h$ (resp., $\mathscr{T}_{2h}$) of Ω, h being a space discretization step. The pressure mesh is thus twice *coarser* than the velocity one. The calculations have been done using uniform partitions $\mathscr{T}_h$ and $\mathscr{T}_{2h}$.

4.4.2 First test problem: Settling of three balls in a vertical narrow tube

Our goal in this sub-section is to discuss the interaction of three identical balls settling in a narrow tube of rectangular cross-section, containing an incompressible Newtonian viscous fluid. Theoretically, the tube should be infinitely long, but for

Fig. 2 Projections on the x_1x_3-plane of the trajectories of the mass centers of the three particles

practicality we first consider the settling of the balls in a cylinder of length 6 whose cross-section is the rectangle $\Omega = (0,1.5) \times (0,0.25)$; this cylinder is moving with the balls in such a way that the center of the lower ball is in the horizontal symmetry plane (a possible, but less satisfying, alternative would be to specify periodicity in the vertical direction). At time $t = 0$, we suppose that the truncated cylinder coincides with the "box" $(0,1.5) \times (0,0.25) \times (0,6)$, and the centers of the balls are on the vertical axis of the cylinder at the points $x_1 = 0.75$, $x_2 = 0.125$, $x_3 = 1$, 1.3 and 1.6. The parameters for this test case are $\rho_s = 1.1$, $\rho_f = 1$, $\mu_f = 1$, the diameter of the balls being $d = 0.2$. The mesh size used to compute the velocity field (resp., the pressure) is $h_v = h = 1/96$ (resp., $h_p = 2h = 1/48$), while we took 1/1000 for the time-discretization step; the initial velocity of the flow is **0**, while the three balls are released from rest. The velocity on the cylinder wall is **0**. On the time interval $[0,15]$ the drafting, kissing and tumbling phenomenon (a terminology introduced by *D.D. Joseph*) has been observed several time before a stable quasi-horizontal configuration takes place, as shown in Figures 2, 3 and 4. The averaged vertical velocity of the balls is 2.4653 on the time interval $[13,15]$, while the *averaged particle Reynolds number* is 49.304 on the same time interval, a clear evidence that inertia has to be taken into account.
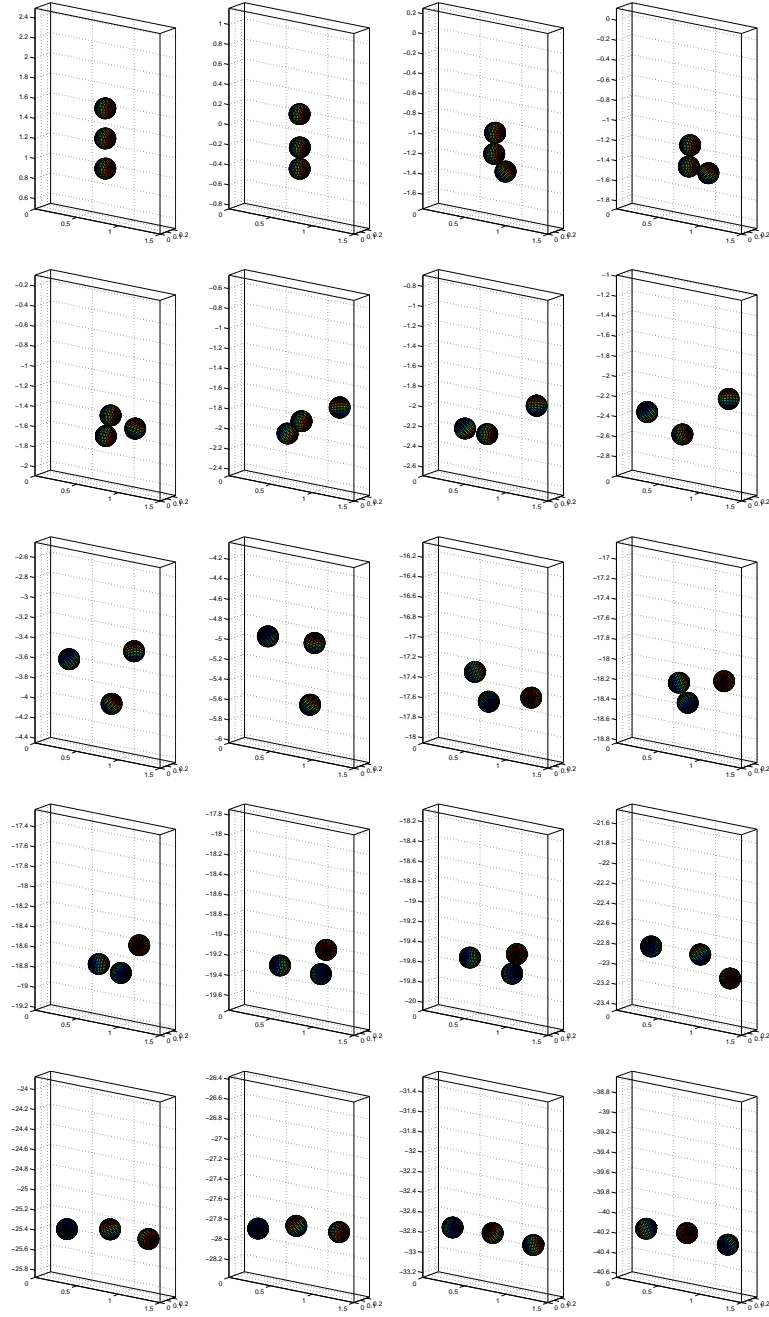
Fig. 3 Relative positions of the three balls at $t = 0$, 0.4, 0.6, 0.65, 0.7, 0.8, 0.9, 1, 1.5, 2, 6, 6.25, 6.4, 6.6, 6.7, 8, 9, 10, 12 and 15 (from left to right and from top to bottom)
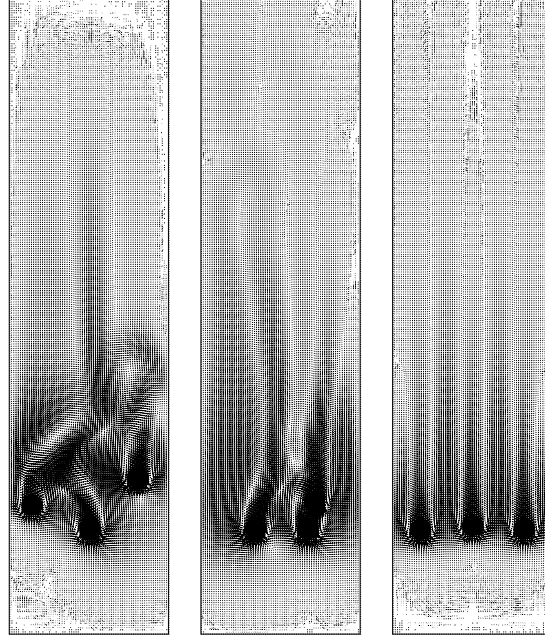
Fig. 4 Visualization of the flow and of the particles at $t = 1.1$, 6.6 and 15.

4.4.3 Motion of 300 neutrally buoyant disks in a two-dimensional horizontal channel

This second test problem involving 300 particles and a *solid volume/fluid volume* of the order of 0.38, collisions (or near-collisions) have to be accounted for in the simulations; to do so, we have used the methods discussed in [70] (Chapter 8) and [79]. Another peculiarity of this test problem is that $\rho_s = \rho_f$ for all the particles (a neutrally buoyant situation). Indeed, neutrally buoyant models are more delicate to handle than those in the general case since $1 - \rho_f/\rho_s = 0$ in (79); however this difficulty can be overcome as shown in [136]. For this test problem, we have: (a) $\Omega = (0, 42) \times (0, 12)$. (b) Ω contains the mixture of a Newtonian incompressible viscous fluid of density $\rho_f = 1$ and viscosity $\mu_f = 1$, with 300 identical rigid solid disks of density $\rho_f = 1$ and diameter 0.9. (c) At $t = 0$, fluid and particles are at rest, the particle centers being located at the points of a regular lattice. (d) The mixture is put into motion by a uniform pressure drop of 10/9 per unit length (without the particles the corresponding steady flow would have been of the Poiseuille type with 20 as maximal flow speed). (e) The boundary conditions are given by $\mathbf{u}(x_1, x_2, t) = \mathbf{0}$ if $0 \leq x_1 \leq 42$, $x_2 = 0$ and 12, and $0 \leq t \leq 400$ (no-slip boundary condition on the horizontal parts of the boundary), and then $\mathbf{u}(0, x_2, t) = \mathbf{u}(42, x_2, t)$, $0 < x_2 < 12$, $0 \leq t \leq 400$ (space-periodic in the Ox_1 direction). (f) $h_{\mathbf{v}} = h = 1/10$, $h_p = 2h = 1/5$, the time-discretization step being 1/1000.
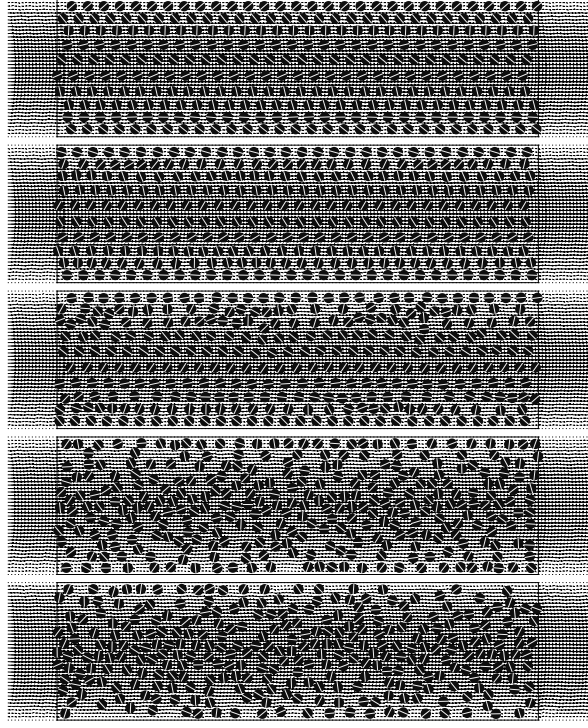
Fig. 5 Positions of the 300 particles at $t = 100$, 107.8, 114, 200 and 400 (from top to bottom).

The particle distribution at $t = 100$, 107.8, 114, 200 and 400 has been visualized on Figures 5. These figures show that, initially, we have the sliding motion of horizontal particle layers, then after some critical time a chaotic flow-motion takes place in very few time units, the highest particle concentration being along the channel axis (actually, a careful inspection of the results shows that the transition to chaos takes place just after $t =$107.8). The maximal speed at $t =$400 is 7.9, implying that the corresponding particle Reynolds number is very close to 7.1. On Figure 6 we show the averaged solid fraction as a function of x_2, the averaging space-time set being $\{\{x_1,t\}|0 \le x_1 \le 42, 380 \le t \le 400\}$; the particle aggregation along the channel horizontal symmetry axis appears very clearly from this figure since the solid fraction is close to 0.58 at $x_2 = 6$ while the global solid fraction is 0.38 (vertical line in the figure). Finally, we have visualized on Figure 7 the x_1-averaged horizontal component of the mixture velocity at $t = 400$, as a function of x_2. The dashed line corresponds to a horizontal velocity distribution of the steady flow of the same fluid, with no particle in the channel, for the same pressure drop; the corresponding velocity profile is (of course) of the Poiseuille type and shows that the mixture behaves like a viscous fluid whose viscosity is (approximately) 2.5 larger than μ_f . Actually, a closer inspection (see [136] for details) shows that the mixture behaves like a non-
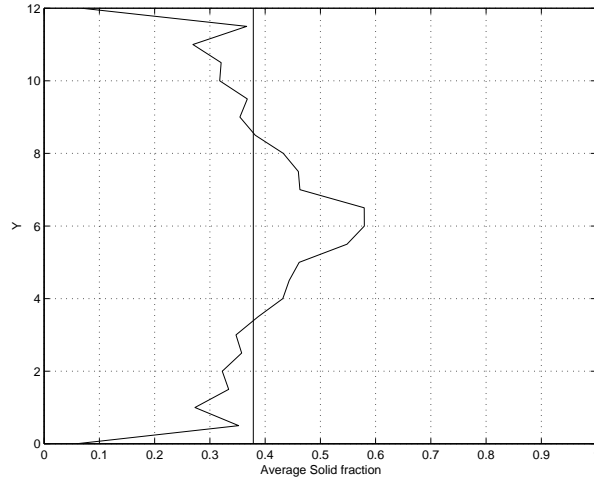
Fig. 6 Averaged solid fraction distribution.
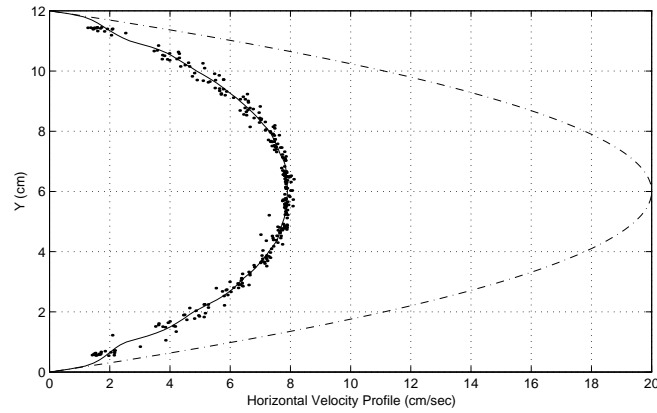
Fig. 7 Horizontal velocity distribution at $t = 400$.

Newtonian incompressible viscous fluid of the power law type, for an exponent $s = 1.7093$ ($s = 2$ corresponding to a Newtonian fluid and $s = 1$ to a perfectly plastic material). Figures 5, 6 and 7 show also that, as well-known, some *order may be found in chaos*.

For more details and further results and comments on pressure driven neutrally buoyant particulate flows in two-dimensional channels (including simulations with much larger numbers of particles, the largest one being 1,200) see [70] (Chapter 9) and [97].

5 Operator-splitting methods for the numerical solution of nonlinear problems from condensate and plasma physics

5.1 Introduction

Operator-splitting methods have been quite successful at solving problems in *Computational Physics*, beside those from *Computational Mechanics* (*CFD* in particular). Among these successful applications let us mention those involving *nonlinear Schrödinger equations*, as shown, for example, by [9], [10], [44] and [102]. On the basis of some very inspiring articles (see, e.g., [9], [10] and [102]) he wrote on the above topic, the editors asked their colleague *Peter Markowich* to contribute a related chapter for this book; unfortunately, Professor Markowich being busy elsewhere had to say no. Considering the importance of nonlinear Schrödinger related problems, it was decided to (briefly) discuss in this chapter the solution of some of them by operator-splitting methods (see also Chapter 15 on the propagation of laser pulses along optical fibers). In Section 5.2, we will discuss the operator-splitting solution of the celebrated *Gross-Pitaevskii* equation for *Bose-Einstein condensates*, then, in Section 5.3, we will discuss the solution of the *Zakharov system* modeling the *propagation of Langmuir waves in ionized plasma*.

5.2 On the solution of the Gross-Pitaevskii equation

A *Bose-Einstein condensate* (BEC) is a state of matter of a dilute gas of bosons cooled to temperatures very close to absolute zero. Under such conditions, a large fraction of the bosons occupies the lowest quantum state, at which point macroscopic quantum phenomena become apparent. The existence of Bose-Einstein condensates was predicted in the mid-1920s by *S. N. Bose* and *A. Einstein*. If dilute enough, the time evolution of a BEC is described by the following *Gross-Pitaevskii equation* (definitely of the *nonlinear Schrödinger* type and given here in a-dimensional form (following [9])):

$$i\varepsilon \frac{\partial \boldsymbol{\psi}}{\partial t} = -\frac{\varepsilon^2}{2}\nabla^2\boldsymbol{\psi} + V_d(x)\boldsymbol{\psi} + K_d|\boldsymbol{\psi}|^2\boldsymbol{\psi} \text{ in } \Omega \times (0,T), \tag{89}$$

where, in (89), $\boldsymbol{\psi}$ is a complex-valued function of x and t, $i = \sqrt{-1}$, Ω is an open connected subset of $I\!R^d$ (with $d = 1$, 2 or 3), the real-valued function V_d denotes an external potential, and the real-valued parameter K_d is representative of the particles interactions. Equation (89) has to be completed by boundary and initial conditions. Equation (89) has motivated a very large literature from both physical and mathematical points of view. Let us mention among many others [1], [9], [125] and [126] (see also the many references therein). To solve equation (89) numerically we need to complete it by *boundary* and *initial conditions*: from now on, we will assume that

$$\boldsymbol{\psi}(x,0) = \boldsymbol{\psi}_0(x), \ x \in \Omega, \tag{90}$$

and (denoting by Γ the boundary of Ω)

$$\boldsymbol{\psi} = 0 \text{ on } \Gamma \times (0,T). \tag{91}$$

The boundary conditions in (91) have been chosen for their simplicity, and also to provide an alternative to the *periodic boundary conditions* considered in [9]. An important (and very easy to prove) property of the solution of the initial boundary value problem (89)-(91) reads as:

$$\frac{d}{dt} \int_\Omega |\boldsymbol{\psi}(x,t)|^2 \, dx = 0 \text{ on } (0,T],$$

implying that

$$\int_\Omega |\boldsymbol{\psi}(x,t)|^2 \, dx = \int_\Omega |\boldsymbol{\psi}_0(x)|^2 \, dx \text{ on } [0,T]. \tag{92}$$

As done before, we denote by $\boldsymbol{\psi}(t)$ the function $x \to \boldsymbol{\psi}(x,t)$. Let $\triangle t(> 0)$ be a time discretization step and denote $(n+\alpha)\triangle t$ by $t^{n+\alpha}$; applying to problem (89)-(91) the Strang's symmetrized scheme (7)-(10) of Section 2.3, we obtain:

$$\boldsymbol{\psi}^0 = \boldsymbol{\psi}_0; \tag{93}$$

for $n \geq 0, \boldsymbol{\psi}^n \to \boldsymbol{\psi}^{n+1/2} \to \widehat{\boldsymbol{\psi}}^{n+1/2} \to \boldsymbol{\psi}^{n+1}$ as follows

$$\begin{cases} i\dfrac{\partial \boldsymbol{\psi}}{\partial t} + \dfrac{\varepsilon}{2}\nabla^2 \boldsymbol{\psi} = 0 \ \text{ in } \Omega \times (t^n, t^{n+1/2}), \\ \boldsymbol{\psi} = 0 \ \text{ on } \Gamma \times (t^n, t^{n+1/2}), \\ \boldsymbol{\psi}(t^n) = \boldsymbol{\psi}^n; \ \boldsymbol{\psi}^{n+1/2} = \boldsymbol{\psi}(t^{n+1/2}), \end{cases} \tag{94}$$

$$\begin{cases} i\varepsilon\dfrac{\partial \boldsymbol{\psi}}{\partial t} = V_d(x)\boldsymbol{\psi} + K_d|\boldsymbol{\psi}|^2 \boldsymbol{\psi} \ \text{ in } \Omega \times (0,\triangle t), \\ \boldsymbol{\psi} = 0 \ \text{ on } \Gamma \times (0,\triangle t), \\ \boldsymbol{\psi}(0) = \boldsymbol{\psi}^{n+1/2}; \ \widehat{\boldsymbol{\psi}}^{n+1/2} = \boldsymbol{\psi}(\triangle t), \end{cases} \tag{95}$$

$$\begin{cases} i\dfrac{\partial \boldsymbol{\psi}}{\partial t} + \dfrac{\varepsilon}{2}\nabla^2 \boldsymbol{\psi} = 0 \ \text{ in } \Omega \times (t^{n+1/2}, t^{n+1}), \\ \boldsymbol{\psi} = 0 \ \text{ on } \Gamma \times (t^{n+1/2}, t^{n+1}), \\ \boldsymbol{\psi}(t^{n+1/2}) = \widehat{\boldsymbol{\psi}}^{n+1/2}; \ \boldsymbol{\psi}^{n+1} = \boldsymbol{\psi}(t^{n+1}). \end{cases} \tag{96}$$

On the solution of (95): Let us denote by ψ_1 (resp., ψ_2) the real (resp., imaginary) part of $\boldsymbol{\psi}$; from (95), we have

$$\begin{cases} \varepsilon\dfrac{\partial \psi_1}{\partial t} = V_d(x)\psi_2 + K_d|\boldsymbol{\psi}|^2 \psi_2 \ \text{ in } \Omega \times (0,\triangle t), \\ \varepsilon\dfrac{\partial \psi_2}{\partial t} = -V_d(x)\psi_1 - K_d|\boldsymbol{\psi}|^2 \psi_1 \ \text{ in } \Omega \times (0,\triangle t), \end{cases} \tag{97}$$

Multiplying by ψ_1 (resp., ψ_2) the 1st (resp., the 2nd) equation in (97), we obtain by addition

$$\frac{\partial}{\partial t}|\boldsymbol{\psi}(x,t)|^2 = 0 \text{ on}(0,\triangle t), \text{ a.e. } x \in \Omega,$$

which implies in turn that

$$|\boldsymbol{\psi}(x,t)| = |\boldsymbol{\psi}(x,0)| = |\boldsymbol{\psi}^{n+1/2}| \text{ on}(0,\triangle t), \text{ a.e. } x \in \Omega. \tag{98}$$

It follows then from (95) and (98) that

$$\begin{cases} i\varepsilon\dfrac{\partial \boldsymbol{\psi}}{\partial t} = V_d(x)\boldsymbol{\psi} + K_d|\boldsymbol{\psi}^{n+1/2}|^2 \boldsymbol{\psi} \text{ in } \Omega \times (0,\triangle t), \\ \boldsymbol{\psi} = 0 \text{ on } \Gamma \times (0,\triangle t), \\ \boldsymbol{\psi}(0) = \boldsymbol{\psi}^{n+1/2}; \; \widehat{\boldsymbol{\psi}}^{n+1/2} = \boldsymbol{\psi}(\triangle t), \end{cases}$$

which implies for $\widehat{\boldsymbol{\psi}}^{n+1/2}$ the following closed-form solution

$$\widehat{\boldsymbol{\psi}}^{n+1/2} = e^{-i\frac{\triangle t}{\varepsilon}\left(V_d + K_d|\boldsymbol{\psi}^{n+1/2}|^2\right)} \boldsymbol{\psi}^{n+1/2}. \tag{99}$$

On the solution of (94) and (96): The initial boundary value problems in (94) and (96) are particular cases of

$$\begin{cases} i\dfrac{\partial \boldsymbol{\phi}}{\partial t} + \dfrac{\varepsilon}{2}\nabla^2\boldsymbol{\phi} = 0 \text{ in } \Omega \times (t_0,t_f), \\ \boldsymbol{\phi} = 0 \text{ on } \Gamma \times (t_0,t_f), \\ \boldsymbol{\phi}(t_0) = \boldsymbol{\phi}_0. \end{cases} \tag{100}$$

The above *linear Schrödinger problem* is a very classical one. Its solution is obviously given by

$$\boldsymbol{\phi}(t) = e^{i\frac{\varepsilon}{2}(t-t_0)\nabla^2}\boldsymbol{\phi}_0, \; \forall t \in [t_0,t_f]. \tag{101}$$

Suppose that $\Omega = (0,a) \times (0,b) \times (0,c)$ with $0 < a < +\infty$, $0 < b < +\infty$ and $0 < c < +\infty$; since the eigenvalues, and related eigenfunctions, of the negative Laplace operator $-\nabla^2$, associated with the homogeneous Dirichlet boundary conditions are known explicitly, and given, for p, q and r positive integers, by

$$\begin{cases} \lambda_{pqr} = \pi^2\left(\dfrac{p^2}{a^2} + \dfrac{q^2}{b^2} + \dfrac{r^2}{c^2}\right), \\ w_{pqr}(x_1,x_2,x_3) = 2\sqrt{\dfrac{2}{abc}}\sin\left(p\pi\dfrac{x_1}{a}\right)\sin\left(q\pi\dfrac{x_2}{b}\right)\sin\left(r\pi\dfrac{x_3}{c}\right) \end{cases} \tag{102}$$

(we have then $\int_\Omega |w_{pqr}(x)|^2\,dx = 1$) it follows from (101) that

$$\boldsymbol{\phi}(x,t) = \sum_{1 \le p,q,r < +\infty} \phi_{pqr}^0 e^{-i\frac{\varepsilon}{2}\lambda_{pqr}(t-t_0)} w_{pqr}(x), \text{ with } \phi_{pqr}^0 = \int_\Omega w_{pqr}(y)\boldsymbol{\phi}_0(y)\,dy. \tag{103}$$

In practice, one takes $1 \le p \le P$, $1 \le q \le Q$, $1 \le r \le R$, and uses the *Fast Fourier Transform* (FFT) to compute the coefficients $\boldsymbol{\phi}^0_{pqr}$ and then $\boldsymbol{\phi}(x,t)$.

For those more general situations where the solutions of the following *linear eigenvalue problem*

$$\begin{cases} \{w,\lambda\} \in H^1_0(\Omega) \times \mathbb{R}, \ \int_\Omega |w(x)|^2 \, dx = 1, \ \lambda > 0, \\ \int_\Omega \nabla w \cdot \nabla v \, dx = \lambda \int_\Omega wv \, dx, \ \forall v \in H^1_0(\Omega), \end{cases} \tag{104}$$

are not known explicitly, one still has several options to solve (100), an obvious one being:

Approximate (104) by

$$\begin{cases} \{w,\lambda\} \in V_h \times \mathbb{R}, \ \int_\Omega |w(x)|^2 \, dx = 1, \ \lambda > 0, \\ \int_\Omega \nabla w \cdot \nabla v \, dx = \lambda \int_\Omega wv \, dx, \ \forall v \in V_h, \end{cases} \tag{105}$$

where V_h is a finite dimensional sub-space of $H^1_0(\Omega)$. Then, as in, e.g., [17], [82] use an eigensolver (like the one discussed in [113]) to compute the first $Q(\le N = \dim V_h)$ eigen-pairs solutions of (105), such that (with obvious notation) $\int_\Omega w_p w_q \, dx = 0$ $\forall p,q$, $1 \le p,q \le Q$, $p \ne q$, and denote by V_Q the finite dimensional space span by the basis $\{w_q\}^Q_{q=1}$. Next, proceeding as in the continuous case we approximate the solution of problem (100) by $\boldsymbol{\phi}_Q$ defined by

$$\boldsymbol{\phi}_Q(x,t) = \sum_{q=1}^Q \boldsymbol{\phi}^0_q e^{-i\frac{\varepsilon}{2}\lambda_q(t-t_0)} w_q(x), \ \text{with} \ \boldsymbol{\phi}^0_q = \int_\Omega w_q(y) \boldsymbol{\phi}_0(y) \, dy. \tag{106}$$

For the space V_h in (105), we can use these *finite element* approximations of $H^1_0(\Omega)$ discussed for example in [37], [66] (Appendix 1) and [72] (Chapter 1) (see also the references therein).

Another approach, less obvious but still natural, is to observe that if $\boldsymbol{\phi}$, the unique solution of (100) is smooth enough, it is also the unique solution of

$$\begin{cases} \dfrac{\partial^2 \boldsymbol{\phi}}{\partial t^2} + \dfrac{\varepsilon^2}{4} \nabla^4 \boldsymbol{\phi} = 0 \ \text{in} \ \Omega \times (t_0,t_f), \\ \boldsymbol{\phi} = 0 \ \text{and} \ \nabla^2 \boldsymbol{\phi} = 0 \ \text{on} \ \Gamma \times (t_0,t_f), \\ \boldsymbol{\phi}(t_0) = \boldsymbol{\phi}_0, \ \dfrac{\partial \boldsymbol{\phi}}{\partial t}(t_0) = i\dfrac{\varepsilon}{2}\nabla^2 \boldsymbol{\phi}_0 (= \boldsymbol{\phi}_1), \end{cases} \tag{107}$$

a well-known model in *elasto-dynamics* (vibrations of simply supported plates). From Q, a positive integer, we define a time discretization step τ by $\tau = \dfrac{t_f - t_0}{Q}$. The initial-boundary value problem (107) is clearly equivalent to

$$
\begin{cases}
\dfrac{\partial \boldsymbol{\phi}}{\partial t} = \mathbf{v} \ \text{ in } \Omega \times (t_0, t_f), \\[2mm]
\dfrac{\partial \mathbf{v}}{\partial t} + \dfrac{\varepsilon^2}{4} \nabla^4 \boldsymbol{\phi} = 0 \ \text{ in } \Omega \times (t_0, t_f), \\[2mm]
\boldsymbol{\phi} = 0 \text{ and } \nabla^2 \boldsymbol{\phi} = 0 \ \text{ on } \Gamma \times (t_0, t_f), \\[2mm]
\boldsymbol{\phi}(t_0) = \boldsymbol{\phi}_0, \ \mathbf{v}(t_0) = i\dfrac{\varepsilon}{2}\nabla^2 \boldsymbol{\phi}_0 (= \mathbf{v}_0).
\end{cases}
\tag{108}
$$

A time-discretization scheme for (107) (via (108)), combining good accuracy, stability and energy conservation properties (see, e.g., [14]) reads as follows (with $\{\boldsymbol{\phi}^q, \mathbf{v}^q\}$ an approximation of $\{\boldsymbol{\phi}, \mathbf{v}\}$ at $t^q = t_0 + q\tau$):

$$
\begin{cases}
\boldsymbol{\phi}^0 = \boldsymbol{\phi}_0, \ \mathbf{v}^0 = \mathbf{v}_0; \\[1mm]
\text{for } q = 0, \cdots, Q-1, \text{ compute } \{\boldsymbol{\phi}^{q+1}, \mathbf{v}^{q+1}\} \text{ from } \{\boldsymbol{\phi}^q, \mathbf{v}^q\} \text{ via the solution of} \\[1mm]
\begin{cases}
\dfrac{\boldsymbol{\phi}^{q+1} - \boldsymbol{\phi}^q}{\tau} = \dfrac{1}{2}(\mathbf{v}^{q+1} + \mathbf{v}^q), \\[2mm]
\dfrac{\mathbf{v}^{q+1} - \mathbf{v}^q}{\tau} + \dfrac{\varepsilon^2}{8}\nabla^4(\boldsymbol{\phi}^{q+1} + \boldsymbol{\phi}^q) = 0 \ \text{ in } \Omega, \\[2mm]
\boldsymbol{\phi}^{q+1} = 0 \text{ and } \nabla^2 \boldsymbol{\phi}^{q+1} = 0 \ \text{ on } \Gamma.
\end{cases}
\end{cases}
\tag{109}
$$

By elimination of $\mathbf{v}^{q+1}$ it follows from (109) that $\boldsymbol{\phi}^{q+1}$ is solution of

$$
\begin{cases}
\boldsymbol{\phi}^{q+1} + \dfrac{(\tau\varepsilon)^2}{8}\nabla^4 \boldsymbol{\phi}^{q+1} = \boldsymbol{\phi}^q + \tau\mathbf{v}^q - \dfrac{(\tau\varepsilon)^2}{8}\nabla^4 \boldsymbol{\phi}^q \ \text{ in } \Omega, \\[2mm]
\boldsymbol{\phi}^{q+1} = 0 \text{ and } \nabla^2 \boldsymbol{\phi}^{q+1} = 0 \ \text{ on } \Gamma,
\end{cases}
\tag{110}
$$

a bi-harmonic problem which is well-posed in $H_0^1(\Omega) \cap H^2(\Omega)$. Next, one obtains easily $\mathbf{v}^{q+1}$ from

$$
\mathbf{v}^{q+1} = \frac{\tau}{2}(\boldsymbol{\phi}^{q+1} - \boldsymbol{\phi}^q) - \mathbf{v}^q.
$$

For the solution of the bi-harmonic problem (110) we advocate those mixed finite element approximations and conjugate gradient algorithms used in various chapters of [72] (see also the references therein).

5.3 On the solution of Zakharov systems

In 1972, *V.E. Zakharov* introduced a mathematical model describing the *propagation of Langmuir waves* in *ionized plasma* (ref. [180]). This model reads as follows (after rescaling):

$$
\begin{cases}
i\dfrac{\partial u}{\partial t} + \nabla^2 u = un, \\[2mm]
\dfrac{\partial^2 n}{\partial t^2} - \nabla^2 n + \nabla^2(|u|^2) = 0,
\end{cases}
\tag{111}
$$

where the complex-valued function u is associated with a highly oscillating *electric field*, while the real-valued function n denotes the *fluctuation of the plasma-ion density* from its equilibrium state. In this section, following [102], we will apply the *symmetrized Strang operator-splitting scheme* (previously discussed in Section 2.3 of this chapter) to the following generalization of the above equations:

$$
\begin{cases}
i\dfrac{\partial u}{\partial t} + \nabla^2 u + 2\lambda |u|^2 u + 2un = 0, \\
\dfrac{1}{c^2}\dfrac{\partial^2 n}{\partial t^2} - \nabla^2 n + \mu \nabla^2(|u|^2) = 0,
\end{cases}
\tag{112}
$$

where λ and μ are real numbers and $c(>0)$ is the wave propagation speed. Following again [102], we will assume, for simplicity, that the physical phenomenon modelled by (112) takes place on the bounded interval $(0,L)$, with u, n, $\partial u/\partial x$ and $\partial n/\partial x$ *space-periodic*, during the time interval $[0,T]$. Thus, (112), completed by initial conditions, reduces to:

$$
\begin{cases}
i\dfrac{\partial u}{\partial t} + \dfrac{\partial^2 u}{\partial x^2} + 2\lambda |u|^2 u + 2un = 0 \ \text{ in } (0,L)\times(0,T), \\
\dfrac{1}{c^2}\dfrac{\partial^2 n}{\partial t^2} - \dfrac{\partial^2 n}{\partial x^2} + \mu\dfrac{\partial^2}{\partial x^2}(|u|^2) = 0 \ \text{ in } (0,L)\times(0,T), \\
u(0,t) = u(L,t), \ \dfrac{\partial u}{\partial x}(0,t) = \dfrac{\partial u}{\partial x}(L,t) \ \text{ on } (0,T), \\
n(0,t) = n(L,t), \ \dfrac{\partial n}{\partial x}(0,t) = \dfrac{\partial n}{\partial x}(L,t) \ \text{ on } (0,T), \\
u(0) = u_0, \ n(0) = n_0, \ \dfrac{\partial n}{\partial t}(0) = n_1.
\end{cases}
\tag{113}
$$

As done previously in this chapter, we denote by $\phi(t)$ the function $x \to \phi(x,t)$.

Remark 27. Albeit considered by some as too simple from a physical point of view, *space-periodic boundary conditions* are common in plasma physics. They have been used for example in [131], a most celebrated article dedicated to the mathematical analysis of the behavior of plasma entropy (see also [163] which relates a discussion that *C. Villani* had with *E. Lieb* concerning precisely the use of space-periodic boundary conditions in plasma physics). □

From the rich structure of the Zakharov's system (113) it is not surprising that a variety of *operator-splitting schemes* can be applied to its numerical solution, several of these schemes being described in [102] (see also the references therein concerning splitting schemes not described in [102]). A first step to the application of operator-splitting scheme to the time-discretization of problem (113) is to introduce the function $p = \dfrac{\partial n}{\partial t}$ and to rewrite (113) as:

$$
\begin{cases}
i\dfrac{\partial u}{\partial t} + \dfrac{\partial^2 u}{\partial x^2} + 2\lambda |u|^2 u + 2un = 0 \ \ \text{in} \ (0,L) \times (0,T), \\[2mm]
\dfrac{\partial n}{\partial t} - p = 0 \ \ \text{in} \ (0,L) \times (0,T), \\[2mm]
\dfrac{1}{c^2} \dfrac{\partial p}{\partial t} - \dfrac{\partial^2 n}{\partial x^2} + \mu \dfrac{\partial^2}{\partial x^2}(|u|^2) = 0 \ \ \text{in} \ (0,L) \times (0,T), \\[2mm]
u(0,t) = u(L,t), \ \dfrac{\partial u}{\partial x}(0,t) = \dfrac{\partial u}{\partial x}(L,t) \ \ \text{on} \ (0,T), \\[2mm]
n(0,t) = n(L,t), \ \dfrac{\partial n}{\partial x}(0,t) = \dfrac{\partial n}{\partial x}(L,t) \ p(0,t) = p(L,t) \ \ \text{on} \ (0,T), \\[2mm]
u(0) = u_0, \ n(0) = n_0, \ p(0) = n_1.
\end{cases}
\tag{114}
$$

Applying the Strang's symmetrized scheme to the time-discretization of problem (114), one obtains (among other possible schemes, and with $t^{q+\alpha} = (q+\alpha)\triangle t$):

$$
\{u^0, n^0, p^0\} = \{u_0, n_0, n_1\}.
\tag{115}
$$

For $q \geq 0$, $\{u^q, n^q, p^q\} \to \{u^{q+1/2}, n^{q+1/2}, p^{q+1/2}\} \to \{\hat{u}^{q+1/2}, \hat{n}^{q+1/2}, \hat{p}^{q+1/2}\} \to \{u^{q+1}, n^{q+1}, p^{q+1}\}$ via

$$
\begin{cases}
i\dfrac{\partial u}{\partial t} + \dfrac{\partial^2 u}{\partial x^2} = 0 \ \ \text{in} \ (0,L) \times (t^q, t^{q+1/2}), \\[2mm]
\dfrac{\partial n}{\partial t} - \dfrac{p}{2} = 0 \ \ \text{in} \ (0,L) \times (t^q, t^{q+1/2}), \\[2mm]
\dfrac{1}{c^2}\dfrac{\partial p}{\partial t} - \dfrac{\partial^2 n}{\partial x^2} = 0 \ \ \text{in} \ (0,L) \times (t^q, t^{q+1/2}), \\[2mm]
u(0,t) = u(L,t), \ \dfrac{\partial u}{\partial x}(0,t) = \dfrac{\partial u}{\partial x}(L,t) \ \ \text{on} \ (t^q, t^{q+1/2}), \\[2mm]
n(0,t) = n(L,t), \ \dfrac{\partial n}{\partial x}(0,t) = \dfrac{\partial n}{\partial x}(L,t), \ p(0,t) = p(L,t) \ \ \text{on} \ (t^q, t^{q+1/2}), \\[2mm]
u(t^q) = u^q, \ n(t^q) = n_q, \ p(t^q) = p^q; \\[2mm]
u^{q+1/2} = u(t^{q+1/2}), n^{q+1/2} = n(t^{q+1/2}), p^{q+1/2} = p(t^{q+1/2}),
\end{cases}
\tag{116}
$$

$$
\begin{cases}
i\dfrac{\partial u}{\partial t} + 2\lambda |u|^2 u + 2un = 0 \ \ \text{in} \ (0,L) \times (0,\triangle t), \\[2mm]
\dfrac{\partial n}{\partial t} - \dfrac{p}{2} = 0 \ \ \text{in} \ (0,L) \times (0,\triangle t), \\[2mm]
\dfrac{1}{c^2}\dfrac{\partial p}{\partial t} + \mu \dfrac{\partial^2}{\partial x^2}(|u|^2) = 0 \ \ \text{in} \ (0,L) \times (0,\triangle t), \\[2mm]
u(0,t) = u(L,t), \ \dfrac{\partial u}{\partial x}(0,t) = \dfrac{\partial u}{\partial x}(L,t) \ \ \text{on} \ (0,\triangle t), \\[2mm]
n(0,t) = n(L,t), \ \dfrac{\partial n}{\partial x}(0,t) = \dfrac{\partial n}{\partial x}(L,t), \ p(0,t) = p(L,t) \ \ \text{on} \ (0,\triangle t), \\[2mm]
u(0) = u^{q+1/2}, \ n(0) = n^{q+1/2}, \ p(0) = p^{q+1/2}; \\[2mm]
\hat{u}^{q+1/2} = u(\triangle t), \hat{n}^{q+1/2} = n(\triangle t), \hat{p}^{q+1/2} = p(\triangle t),
\end{cases}
\tag{117}
$$

$$\begin{cases} i\dfrac{\partial u}{\partial t} + \dfrac{\partial^2 u}{\partial x^2} = 0 \text{ in } (0,L) \times (t^{q+1/2}, t^{q+1}), \\[2mm] \dfrac{\partial n}{\partial t} - \dfrac{p}{2} = 0 \text{ in } (0,L) \times (t^{q+1/2}, t^{q+1}), \\[2mm] \dfrac{1}{c^2}\dfrac{\partial p}{\partial t} - \dfrac{\partial^2 n}{\partial x^2} = 0 \text{ in } (0,L) \times (t^{q+1/2}, t^{q+1}), \\[2mm] u(0,t) = u(L,t), \ \dfrac{\partial u}{\partial x}(0,t) = \dfrac{\partial u}{\partial x}(L,t) \text{ on } (t^{q+1/2}, t^{q+1}), \\[2mm] n(0,t) = n(L,t), \ \dfrac{\partial n}{\partial x}(0,t) = \dfrac{\partial n}{\partial x}(L,t), \ p(0,t) = p(L,t) \text{ on } (t^{q+1/2}, t^{q+1}), \\[2mm] u(t^{q+1/2}) = \hat{u}^{q+1/2}, \ n(t^{q+1/2}) = \hat{n}^{q+1/2}, \ p(t^{q+1/2}) = \hat{p}^{q+1/2}; \\[2mm] u^{q+1} = u(t^{q+1}), n^{q+1} = n(t^{q+1}), p^{q+1} = p(t^{q+1}). \end{cases}$$

(118)

Scheme (115)-(118) is clearly equivalent to

$$\{u^0, n^0, p^0\} = \{u_0, n_0, n_1\}.$$

(119)

For $q \geq 0$, $\{u^q, n^q, p^q\} \rightarrow \{u^{q+1/2}, n^{q+1/2}, p^{q+1/2}\} \rightarrow \{\hat{u}^{q+1/2}, \hat{n}^{q+1/2}, \hat{p}^{q+1/2}\} \rightarrow \{u^{q+1}, n^{q+1}, p^{q+1}\}$ via

$$\begin{cases} i\dfrac{\partial u}{\partial t} + \dfrac{\partial^2 u}{\partial x^2} = 0 \text{ in } (0,L) \times (t^q, t^{q+1/2}), \\[2mm] \dfrac{2}{c^2}\dfrac{\partial^2 n}{\partial t^2} - \dfrac{\partial^2 n}{\partial x^2} = 0 \text{ in } (0,L) \times (t^q, t^{q+1/2}), \\[2mm] u(0,t) = u(L,t), \ \dfrac{\partial u}{\partial x}(0,t) = \dfrac{\partial u}{\partial x}(L,t) \text{ on } (t^q, t^{q+1/2}), \\[2mm] n(0,t) = n(L,t), \ \dfrac{\partial n}{\partial x}(0,t) = \dfrac{\partial n}{\partial x}(L,t) \text{ on } (t^q, t^{q+1/2}), \\[2mm] u(t^q) = u^q, \ n(t^q) = n_q, \ \dfrac{\partial n}{\partial t}(t^q) = p^q/2; \\[2mm] u^{q+1/2} = u(t^{q+1/2}), n^{q+1/2} = n(t^{q+1/2}), p^{q+1/2} = 2\dfrac{\partial n}{\partial t}(t^{q+1/2}), \end{cases}$$

(120)

$$\begin{cases} i\dfrac{\partial u}{\partial t} + 2\lambda |u|^2 u + 2un = 0 \text{ in } (0,L) \times (0, \triangle t), \\[2mm] \dfrac{2}{c^2}\dfrac{\partial^2 n}{\partial t^2} + \mu\dfrac{\partial^2}{\partial x^2}(|u|^2) = 0 \text{ in } (0,L) \times (0, \triangle t), \\[2mm] u(0,t) = u(L,t), \ \dfrac{\partial u}{\partial x}(0,t) = \dfrac{\partial u}{\partial x}(L,t) \text{ on } (0, \triangle t), \\[2mm] n(0,t) = n(L,t), \ \dfrac{\partial n}{\partial x}(0,t) = \dfrac{\partial n}{\partial x}(L,t) \text{ on } (0, \triangle t), \\[2mm] u(0) = u^{q+1/2}, \ n(0) = n^{q+1/2}, \ \dfrac{\partial n}{\partial t}(0) = p^{q+1/2}/2; \\[2mm] \hat{u}^{q+1/2} = u(\triangle t), \hat{n}^{q+1/2} = n(\triangle t), \hat{p}^{q+1/2} = 2\dfrac{\partial n}{\partial t}(\triangle t), \end{cases}$$

(121)

$$\begin{cases} i\dfrac{\partial u}{\partial t} + \dfrac{\partial^2 u}{\partial x^2} = 0 \ \ \text{in } (0,L) \times (t^{q+1/2}, t^{q+1}), \\[2mm] \dfrac{2}{c^2}\dfrac{\partial^2 n}{\partial t^2} - \dfrac{\partial^2 n}{\partial x^2} = 0 \ \ \text{in } (0,L) \times (t^{q+1/2}, t^{q+1}), \\[2mm] u(0,t) = u(L,t), \ \dfrac{\partial u}{\partial x}(0,t) = \dfrac{\partial u}{\partial x}(L,t) \ \ \text{on } (t^{q+1/2}, t^{q+1}), \\[2mm] n(0,t) = n(L,t), \ \dfrac{\partial n}{\partial x}(0,t) = \dfrac{\partial n}{\partial x}(L,t) \ \ \text{on } (t^{q+1/2}, t^{q+1}), \\[2mm] u(t^{q+1/2}) = \hat{u}^{q+1/2}, \ n(t^{q+1/2}) = \hat{n}^{q+1/2}, \ \dfrac{\partial n}{\partial t}(t^{q+1/2}) = \hat{p}^{q+1/2}/2; \\[2mm] u^{q+1} = u(t^{q+1}), n^{q+1} = n(t^{q+1}), p^{q+1} = 2\dfrac{\partial n}{\partial t}(t^{q+1}). \end{cases} \tag{122}$$

The *linear Schrödinger* and *wave equations* in (120) and (122) are uncoupled, implying that they can be solved by a variety of classical *spectral* or *finite difference* methods taking advantage of the space-periodic boundary conditions. On the other hand, the nonlinear system (121) can be solved *pointwise*: Indeed, since u and n are *real-valued* functions, it follows from the first and fifth equations in (121) that

$$|u(x,t)| = |u^{q+1/2}(x)|, \ \forall t \in [0, \triangle t], \ x \in [0, L]. \tag{123}$$

It follows then from (121) and (123) that the solution n in (121) is also a solution of the following *linear* problem

$$\begin{cases} \dfrac{\partial^2 n}{\partial t^2} = -\dfrac{\mu}{2}c^2\dfrac{\partial^2}{\partial x^2}(|u^{q+1/2}|^2) \ \ \text{in } (0,L) \times (0, \triangle t), \\[2mm] n(0,t) = n(L,t) \ \ \text{on } (0, \triangle t), \\[2mm] n(0) = n^{q+1/2}, \ \dfrac{\partial n}{\partial t}(0) = p^{q+1/2}/2. \end{cases} \tag{124}$$

The closed form solution of (124) is given by

$$n(x,t) = n^{q+1/2}(x) + \dfrac{1}{2}p^{q+1/2}(x)t - \dfrac{\mu}{4}c^2\dfrac{\partial^2}{\partial x^2}(|u^{q+1/2}|^2)t^2 \ \ \text{on } (0,L) \times (0, \triangle t), \tag{125}$$

implying, in particular, that

$$\hat{n}^{q+1/2} = n^{q+1/2} + \dfrac{\triangle t}{2}p^{q+1/2} - \dfrac{\mu}{4}(c\triangle t)^2\dfrac{\partial^2}{\partial x^2}(|u^{q+1/2}|^2).$$

Finally, to obtain the u solution of system (121), we observe that (n being known from (125)) it is the *unique* solution of the following *non-autonomous linear* initial value problem

$$\begin{cases} i\dfrac{\partial u}{\partial t} + 2(\lambda|u^{q+1/2}|^2 + n)u = 0 \ \ \text{in } (0,L) \times (0, \triangle t), \\[2mm] u(0,t) = u(L,t) \ \ \text{on } (0, \triangle t), \\[2mm] u(0) = u^{q+1/2}, \end{cases} \tag{126}$$

a particular case of

$$\begin{cases} i\dfrac{\partial \phi}{\partial t} + 2(\lambda |\boldsymbol{\psi}|^2 + v)\phi = 0 \ \text{ in } (0,L) \times (t_0, t_f), \\ \phi(0,t) = \phi(L,t) \ \text{ on } (t_0, t_f), \\ \phi(t_0) = \phi_0, \end{cases} \tag{127}$$

$\boldsymbol{\psi}$ (resp., v) being a given complex (resp., real)-valued function of x (resp., of $\{x,t\}$). With $M \geq 1$ an integer, let us define τ, a time-discretization step, by $\tau = \dfrac{t_f - t_0}{M}$, and $t^m = t_0 + m\tau$. To solve (127) we advocate the following time-discretization scheme of the *Crank-Nicolson* type:

$$\phi^0 = \phi_0. \tag{128}$$

For $m = 0, \cdots, M-1$, $\phi^m \to \phi^{m+1}$ via the solution of

$$\begin{cases} i\dfrac{\phi^{m+1} - \phi^m}{\tau} + \left[\lambda |\boldsymbol{\psi}|^2 + \dfrac{v(t^{m+1}) + v(t^m)}{2}\right](\phi^{m+1} + \phi^m) = 0 \ \text{ in } (0,L), \\ \phi^{m+1}(0) = \phi^{m+1}(L). \end{cases} \tag{129}$$

Problem (129), can be solved point-wise (in practice at the grid-points of a finite difference one- dimensional "grid"). Scheme (128)-(129) is *second-order accurate* and *modulus preserving* (that is, verifies $|\phi^{m+1}| = |\phi^m|$, $\forall m = 0, \ldots, M-1$). On $[0,L]$, $\phi^{m+1}(x)$ is obtained via the solution of a 2×2 linear system (for those who prefer to use real arithmetic).

Remark 28. In [102], one advocates using instead of n the function $n - \mu|u|^2$. The numerical results reported in the above publication clearly show that operator-splitting provides efficient methods for the numerical solution of the Zakharov's system (112).

6 Applications of augmented Lagrangian and ADMM algorithms to the solution of problems from Imaging

6.1 Variational models for image processing

6.1.1 Generalities

Usually, *image processing* refers to the processing and analysis of digital images. Variational models have become an essential part of image processing, such models relying on the minimization of a well-chosen energy functional, the minimization problem reading typically as

$$u = \arg \min_{v \in V} \left[E_{fitting}(v) + E_{regularizing}(v) \right]. \tag{130}$$

As shown above, the energy functional has two parts, namely a *fitting* part and a *regularizing* one. In the following we will present various variational image processing models and show that the operator-splitting and ADMM methodology provides efficient methods for the numerical solution of the related minimization problems. We will start our discussion with the well-known *Rudin-Osher-Fatemi* (ROF) model, and then follow with the presentation of some higher order models. Before going into more details, some remarks are in order, namely:

Remark 29. Most of the models we are going to consider below are not fully understood yet from a mathematical point of view, two of the main issues being, in (130), the choice of the space *V* and the weak-continuity properties of the energy functional. This will not prevent us to use these continuous models, for the simplicity of their formalism which facilitates the derivation of algorithms whose discrete analogues have provable convergence properties.

Remark 30. For image processing problems, the computational domain is always a rectangle, the image pixels providing a natural mesh for space discretization. This particularity makes easy, in general, the finite difference discretization of problem (130) and the implementation of iterative solution algorithms. The methodology we are going to discuss is not restricted to rectangular domains, however for domains with curved boundaries using finite-difference discretization may become complicated near the boundary; an elegant way to overcome this difficulty is to employ finite element approximations, as done in, e.g., [133].

Remark 31. A very detailed analysis of ADMM algorithms for the solution of image processing problems can be found in the chapter of this book by *M. Burger, A. Sawatzky & G. Steidl* (Chapter 8).

6.1.2 Total variation and the ROF model

One of the most popular variational models for image processing was proposed by *Rudin*, *Osher*, and *Fatemi* in their seminal work (ROF model) [144]. In [144], a denoised image is obtained by minimizing the following energy functional

$$E(v) = \frac{1}{2} \int_{\Omega} |f - v|^2 \, dx + \eta \int_{\Omega} |\nabla v| \, dx, \tag{131}$$

where: $dx = dx_1 dx_2$, $f : \Omega \to \mathbb{R}$ is a given noisy image defined on Ω, $\int_{\Omega} |\nabla v| \, dx$ stands for the total variation of the trial function v (see [157] and [169] for a definition of the notion of total variation), and $\eta > 0$ is a positive tuning parameter controlling how much noise will be removed. The remarkable feature of the ROF model lies in its effectiveness in preserving object edges while removing noise. In fact, the total variation regularizer has been widely employed to accomplish other image processing tasks such as deblurring, segmentation, and registration.

In order to incorporate more geometrical information into the regularizer, a number of higher order regularization models have been proposed and used for im-

age processing and computer vision problems. The ROF model has several unfavorable features. The main caveat is the stair-case effect, that is, the resulting cleaned image would present blocks even though the desired image may be smooth. Other undesirable properties include corner smearing and loss of image contrast. To remedy these drawbacks, a very rich list of results exists in the literature, see [2, 31, 120, 183, 186]. Despite the effectiveness of these models in removing the staircase effect, it is often a challenging issue to minimize the corresponding functionals. Note that if the functional E contains second-order derivatives of v, the related Euler-Lagrange equation is a fourth-order linear or nonlinear partial differential equation.

6.1.3 Regularization using $TV2$

In [120], *Lysaker et al.* directly incorporated second order derivative information into the image denoising process, by proposing to minimize the following energy functional

$$E(v) = \frac{1}{2} \int_{\Omega} |f - v|^2 \, dx + \eta \int_{\Omega} \sqrt{(v_{x_1 x_1})^2 + 2(v_{x_1 x_2})^2 + (v_{x_2 x_2})^2} \, dx \qquad (132)$$

This higher order energy functional is much simpler than the Elastica regularizer that we shall introduce later. Numerically, this regularizer shows rather good performance with noise suppression and edge preservation. In the literature, there exists quite a number of related models, see [20, 24, 25, 26, 28, 39, 53, 58, 89, 99, 101, 134, 138, 147, 171, 146, 181]. The well-posedness of the variational problem associated with the energy functional in (132), and its gradient flow equation, have been studied in [88, 130]. High order models, such as the one associated with the energy in (132), have been discussed in, e.g., [15, 24, 32, 149, 177].

6.1.4 Regularization using the Euler's Elastica energy

In order to 'clean' a given function $f : \Omega \to \mathbb{R}$, the *Euler's Elastica* model relies on the minimization of the following energy functional

$$E(v) = \frac{1}{2} \int_{\Omega} |f - v|^2 \, dx + \int_{\Omega} \left[a + b \left| \nabla \cdot \frac{\nabla v}{|\nabla v|} \right|^2 \right] |\nabla v| \, dx. \qquad (133)$$

In (133), a and b are non-negative with $a + b > 0$. These two constants have to be chosen properly, depending of the application under consideration. The image processing model associated with the above energy functional comes from the Euler's Elastica energy for curves (see [31, 124] for the derivation of this energy): indeed, for a given curve $\Gamma \subset \mathbb{R}^2$ with curvature κ, the Euler's Elastica energy is defined (with obvious notation) by $\int_{\Gamma} (a + b\kappa^2) \, ds$. For a function v , the curvature of the

level curve $\Gamma_c := \{x | v(x) = c\}$ is $\kappa = \nabla \cdot \dfrac{\nabla v}{|\nabla v|}$ (if $\nabla v \neq \mathbf{0}$). Thus, the Euler's Elastica energy for the level curve Γ_c is given by

$$l(c) = \int_{\Gamma_c} \left[a + b \left| \nabla \cdot \frac{\nabla v}{|\nabla v|} \right|^2 \right] ds.$$

Summing up (integrating) the Euler's Elastica energy over all the level curves Γ_c, it follows from the co-area formula (see [168]) that the total Euler's Elastica energy is given by

$$\int_{-\infty}^{\infty} l(c)\, dc = \int_{-\infty}^{\infty} \int_{\Gamma_c} \left[a + b \left| \nabla \cdot \frac{\nabla v}{|\nabla v|} \right|^2 \right] ds\, dc = \int_{\Omega} \left[a + b \left| \nabla \cdot \frac{\nabla v}{|\nabla v|} \right|^2 \right] |\nabla v|\, dx.$$

6.1.5 Regularization using the image graph mean curvature

In [183], the authors proposed a variational image processing model making use of the mean curvature of the graph of function f, that is of the surface $\{x, y, z = f(x,y)\}$, to remove the noise. More specifically, the model considered in [183] employs the L^1 norm of the mean curvature of the above graph as a regularizer, the associated energy functional being defined by

$$E(v) = \frac{1}{2} \int_{\Omega} |f - v|^2\, dx + \eta \int_{\Omega} \left| \nabla \cdot \frac{\nabla v}{\sqrt{1 + |\nabla v|^2}} \right| dx. \qquad (134)$$

Above, $\eta\,(> 0)$ is a tuning parameter and the term $\dfrac{\nabla v}{\sqrt{1 + |\nabla v|^2}}$ is the mean curvature of the surface $\phi(x,y,z) = 0$ with $\phi(x,y,z) = u(x,y) - z$. Clearly, the model tries to fit the given noisy image surface $\{x, y, z = f(x,y)\}$ with a surface $\{x, y, z = u(x,y)\}$, u being a minimizer of the L^1-mean curvature energy functional (134). This idea goes back to much earlier publications, [108] for example. The model can sweep noise while keeping object edges, and it also avoids the staircase effect. More importantly, as discussed in [186], the model is also capable of preserving image contrasts as well as object corners.

6.1.6 Interface problems: Chan-Vese segmentation model, labeling techniques, min-cut and continuous max-flow

In image processing, computer vision, etc., one encounters operations more complicated than denoising, *segmentation* being one of them. These applications require mathematical models more complicated (in some sense) than those considered in Sections 6.1.2 to 6.1.5, one of them being the *Chan-Vese* model introduced in [33]. Actually (as obvious from [33]), the *snake and active contour* model (ref. [106]) and

the *Mumford-Shah* model (ref. [132]) can be viewed as ancestors of the Chan-Vese model. Using the notation of [33], the Chan-Vese segmentation model relies on the minimization of the following energy functional:

$$E_{CV}(\phi, d_1, d_2) = \lambda_1 \int_{\Omega} |f - d_1|^2 H(\phi) \, dx + \lambda_2 \int_{\Omega} |f - d_2|^2 [1 - H(\phi)] \, dx \qquad (135)$$
$$+ \mu \int_{\Omega} |\nabla H(\phi)| \, dx + \nu \int_{\Omega} H(\phi) \, dx,$$

where in (135): (i) ϕ is a level set function whose zero level curves set represents the segmentation boundary. (ii) $H(\cdot)$ is the Heaviside function. (iii) d_1 and d_2 are two real numbers. (iv) λ_1, λ_2 and μ (resp., ν) are positive (resp., non-negative) tuning parameters (in many applications, one takes $\lambda_1 = \lambda_2 = 1$). The Euler-Lagrange equation associated with the minimization of the functional in (135) has been derived in [33]. In the above reference the associated gradient flow has been time-discretized by an explicit scheme to compute the solution of the above minimization problem (after an appropriate finite difference space discretization). Operator- splitting and ADMM can be used to develop algorithms with much faster convergence properties than the above explicit schemes; we will return on this issue in Section 6.2. Let us denote $H(\phi)$ by v; there is clearly equivalence between minimizing the functional defined by (135) and

$$\begin{cases} \displaystyle \inf_{\{v, d_1, d_2\} \in V \times \mathbb{R} \times \mathbb{R}} [\lambda_1 \int_{\Omega} |f - d_1|^2 v \, dx + \lambda_2 \int_{\Omega} |f - d_2|^2 [1 - v] \, dx \\ \qquad\qquad + \mu \int_{\Omega} |\nabla v| \, dx + \nu \int_{\Omega} v \, dx], \end{cases} \qquad (136)$$

where $V = \{v | v \in L^{\infty}(\Omega), v(x) \in \{0, 1\}, \text{a.e. in } \Omega, \nabla v \in L^1(\Omega)\}$. The model associated with (136) was proposed in [117] and referred as a *binary level set* based model. More generally, we can consider the minimization, over the above set V, of energy functionals such as E_{potts} defined by

$$E_{potts}(v) = \int_{\Omega} f_1 v \, dx + \int_{\Omega} f_2 [1 - v] \, dx + \int_{\Omega} g |\nabla v| \, dx, \qquad (137)$$

where f_1 and f_2 are given functions indicating the possibility that a point belongs to phase 0 or to phase 1, and where g is a non-negative function, possibly constant; if d_1 and d_2 are fixed in (136), the Chan-Vase model becomes a particular case of the model associated with the functional E_{potts} defined by (137). It was recently observed (see [173, 176]) that minimizing E_{potts} over the above V is a (kind of) continuous *min-cut problem*, itself equivalent (by duality) to a *max-flow problem*. Indeed, let us consider the following continuous max-flow problem

$$\begin{cases} \displaystyle \sup_{q_s, q_f, \mathbf{v}} \int_{\Omega} q_s \, dx \text{ subject to} \\ q_s \leq f_1, q_t \leq f_2, |\mathbf{v}| \leq g, \\ \nabla \cdot \mathbf{v} = q_s - q_t \text{ in } \Omega, \mathbf{v} \cdot \mathbf{n} = 0 \text{ on } \Gamma (= \partial \Omega), \end{cases} \qquad (138)$$

where in (138)): (i) $\mathbf{v} = \{v_1, v_2\}$ and $|\mathbf{v}| = \sqrt{v_1^2 + v_2^2}$, $\mathbf{v}$ being the flow inside Ω. (ii) $\mathbf{n}$ is the unit outward vector normal at Γ. (iii) q_s (resp., q_t) represents a flow *from a source* (resp., *to a sink*). (iv) f_1 and f_2 are as in (137). We can also define $|\mathbf{v}|$ by $|\mathbf{v}| := |v_1| + |v_2|$; if we do so, the discretized max-flow problem can be solved by traditional graph cut methods. It follows from [176] that a dual of the max flow problem (138) reads as:

$$\inf_{\mu \in \Lambda} \left[\int_\Omega f_1(1-\mu)\,dx + \int_\Omega f_2\mu\,dx + \int_\Omega g|\nabla\mu|\,dx \right], \qquad (139)$$

where $\Lambda = \{\mu | \mu \in L^\infty(\Omega), 0 \le \mu(x) \le 1, \text{a.e. in } \Omega\} \cap W^{1,1}(\Omega)$. We have recovered thus the functional E_{potts} from (137) and shown a link between the Chan-Vese model and the max-flow problem. The dual problem (139) is known as a (continuous) *min-cut problem*. Actually, *Chan, Esedoglu* and *Nikolova* have shown in [29] that there is equivalence between (139) and minimizing over $V = \{v | v \in L^\infty(\Omega), v(x) \in \{0,1\}, \text{ a.e. in } \Omega, \nabla v \in L^1(\Omega)\}$ the functional E_{potts} defined by (137), a most remarkable result indeed since problem (139) is a convex variational problem whose discrete variants can be solved by ADMM type algorithms (see [5, 6, 7, 8, 114, 173, 174, 175, 176, 179] for more details and generalizations).

Remark 32. In (136), (138) and (139), it is on purpose that we used inf (resp., sup) instead of min (resp., max) since we have no guarantee that the minimizing sequences of the functionals under consideration will converge weakly in the space or set where the minimization takes place.

Remark 33. Suppose that in (138) we replace the constraint $|\mathbf{v}| \le g$ by $|v_1| \le g_1$ and $|v_2| \le g_2$, everything else being the same; then, the dual problem of the associated variant of (138) reads (with Λ as in (139)) as

$$\inf_{\mu \in \Lambda} \left[\int_\Omega f_1(1-\mu)\,dx + \int_\Omega f_2\mu\,dx + \int_\Omega \left(g_1 \left| \frac{\partial\mu}{\partial x_1} \right| + g_2 \left| \frac{\partial\mu}{\partial x_2} \right| \right) dx \right],$$

clearly a close variant of (139). Similarly, if we replace in (138) the constraint $|\mathbf{v}| \le g$ by $|v_1| + |v_2| \le g$, we obtain (as expected) the following dual problem

$$\inf_{\mu \in \Lambda} \left[\int_\Omega f_1(1-\mu)\,dx + \int_\Omega f_2\mu\,dx + \int_\Omega g \, \sup\left(\left| \frac{\partial\mu}{\partial x_1} \right|, \left| \frac{\partial\mu}{\partial x_2} \right| \right) dx \right],$$

the set Λ being as above.

6.1.7 Segmentation models with higher order regularization

As could have been expected, first order segmentation models have limitations (discussed in [132]). To give an example let us consider the situation depicted in Figure 8(a) where some parts of the four letters have been erased: albeit one can easily recognize the four letters, first order segmentation models such as Chan-Vese's, might
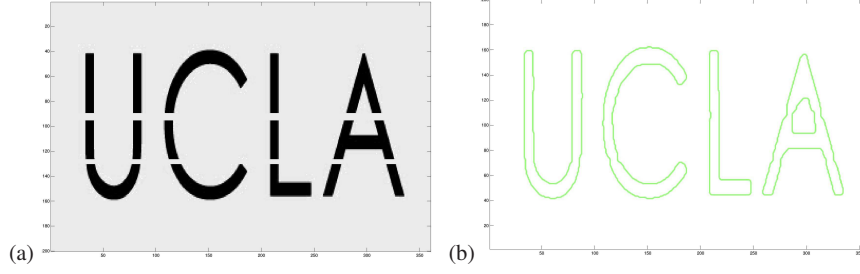
(a)

(b)

Fig. 8 Broken letters "UCLA" and its connected segmentation.

often capture the existing boundary instead of restoring the missing ones, as illustrated in Figure 8(b). In *inpainting* problems (see [31, 124]), missing image information is also recovered, but within given regions assigned in advance. In contrast, one would like to have a segmentation model that can interpolate the missing boundaries automatically without specifying the region of interest. To this end, one may employ the Euler's Elastica functional as a novel regularization term in the Chan-Vese's model (135), in order to replace the weighted *TV* term. Doing so we obtain the following energy functional (we assume $v = 0$, here):

$$E_{CVE}(\phi, d_1, d_2) = \lambda_1 \int_\Omega |f - d_1|^2 H(\phi) \, dx + \lambda_2 \int_\Omega |f - d_2|^2 [1 - H(\phi)] \, dx \quad (140)$$

$$+ \left[a + b \left(\nabla \cdot \frac{\nabla \phi}{|\nabla \phi|} \right)^2 \right] |\nabla H(\phi)| \, dx$$

where λ_1, λ_2, a and b are positive parameters. If ϕ is the signed distance level set function, it can be proved that the last term in (140) is equal to the Euler's elastica energy of the segmentation curve. This regularization was originally proposed and used in the celebrated paper on *segmentation with depth* by Nitzberg, Mumford and Shiota (ref. [135]). Actually, it has also been used in [31] (resp., [184, 185]) for the solution of the in-painting (resp., illusory contour) problem. In [146], linear programming was used to minimize (after space discretization) curvature dependent functionals, the functional defined by (140) being one of those considered in this article.

Remark 34. Observe that since (formally at least, but this can be justified using a well-chosen regularization of the Heaviside function, such as $\xi \to \frac{1}{2} \left[1 + \frac{\xi}{\sqrt{\varepsilon^2 + \xi^2}} \right]$) $\frac{\nabla \phi}{|\nabla \phi|} = \frac{\nabla H(\phi)}{|\nabla H(\phi)|}$, only the sign $H(\phi)$ of the function ϕ is needed when solving the segmentation problem via the functional in (140). This property suggests, as done in [117], to use a binary level set representation via the introduction of the function $v = H(\phi)$. Such a change of function was also used in [29] for finding the global minimizer associated with the Chan-Vese's model. More general binary level set

representations with global minimization techniques have been developed (see, e.g., [7, 173, 174, 176, 178]) using the relationships existing between graph cuts, binary labeling and continuous max flow problems. Since $\nabla \cdot \dfrac{\nabla \phi}{|\nabla \phi|} = \nabla \cdot \dfrac{\nabla H(\phi)}{|\nabla H(\phi)|}$, one can rewrite the functional in (140) as

$$E_{(v,d_1,d_2)} = \lambda_1 \int_{\Omega} |f - d_1|^2 v\,dx + \lambda_2 \int_{\Omega} |f - d_2|^2 [1 - v]\,dx \qquad (141)$$

$$+ \left[a + b \left(\nabla \cdot \frac{\nabla v}{|\nabla v|} \right)^2 \right] |\nabla v|\,dx$$

with the values taken by v being either 0 or 1. Strictly speaking the mean curvature of the graph makes sense for "smooth" functions only; to fix this issue, one relaxes the above binary restriction by replacing it by $0 \le v \le 1$, a less constraining condition indeed.

6.2 Fast numerical algorithms for variational image processing models based on operator- splitting and augmented Lagrangian methods (ALM)

In this section, we will present operator-splitting and ALM based fast numerical algorithms, for the numerical treatment of variational image processing models.

6.2.1 Parallel splitting schemes for the ROF model

The first model that we are going to consider is the ROF model discussed in Section 6.1.2. The formal *Euler-Lagrange equation* associated with the minimization of the (strictly convex) functional in (131) reads as

$$-\eta \nabla \cdot \frac{\nabla u}{|\nabla u|} + u = f \text{ in } \Omega, \quad \frac{\nabla u}{|\nabla u|} \cdot \mathbf{n} = 0 \text{ on } \partial \Omega. \qquad (142)$$

with $\mathbf{n}$ the outward unit vector normal at $\partial \Omega$. In order to solve the nonlinear non-smooth elliptic equation (142) we associate with it an initial value problem and look for steady-state solutions. We consider thus

$$\begin{cases} \dfrac{\partial u}{\partial t} - \eta \nabla \cdot \dfrac{\nabla u}{|\nabla u|} + u = f \text{ in } \Omega \times (0, +\infty), \\ \dfrac{\nabla u}{|\nabla u|} \cdot \mathbf{n} = 0 \text{ on } \partial \Omega \times (0, +\infty), \\ u(0) = u_0, \end{cases} \qquad (143)$$

an obvious choice for u_0 in (143) being $u_0 = f$. Actually to overcome the difficulty associated with the non-smoothness of the elliptic operator in (142) and (143), we consider the following regularized variant of (143):

$$\begin{cases} \dfrac{\partial u}{\partial t} - \eta \nabla \cdot \dfrac{\nabla u}{\sqrt{|\nabla u|^2 + \varepsilon^2}} + u = f \text{ in } \Omega \times (0, +\infty), \\ \dfrac{\partial u}{\partial n} = 0 \text{ on } \partial \Omega \times (0, +\infty), \\ u(0) = u_0, \end{cases} \tag{144}$$

with ε a small positive number. The simplest time-stepping scheme we can think about to capture the steady state solution of (144) is clearly the *forward-Euler scheme*. Let $\triangle t(> 0)$ be a time-discretization step; applied to the solution of (144) the forward Euler scheme produces the following algorithm:

$$u^0 = u_0. \tag{145}$$

For $n \geq 0$, $u^n \to u^{n+1}$ via

$$\begin{cases} \dfrac{u^{n+1} - u^n}{\triangle t} - \eta \nabla \cdot \dfrac{\nabla u^n}{\sqrt{|\nabla u^n|^2 + \varepsilon^2}} + u^n = f \text{ in } \Omega, \\ \dfrac{\partial u^{n+1}}{\partial n} = 0 \text{ on } \partial \Omega. \end{cases} \tag{146}$$

In practice, scheme (145)-(146) is applied to a discrete variant of (144) obtained by finite difference or finite element space discretization. Scheme (145)-(146) being explicit and the condition number of the operator in (146) rather large, its conditional stability requires small time steps leading to a slow convergence to a steady state solution. Suppose that Ω is the rectangle $(0,a) \times (0,b)$; in order to improve the speed of convergence to a steady state solution, we are going to apply to the solution of (144) the parallelizable operator-splitting scheme discussed in Section 2.8, taking advantage of the following decomposition of the operator in (144)

$$-\eta \nabla \cdot \dfrac{\nabla u}{\sqrt{|\nabla u|^2 + \varepsilon^2}} + u - f = A_1(u) + A_2(u), \tag{147}$$

with

$$\begin{cases} A_1(u) = -\eta \dfrac{\partial}{\partial x_1} \left(\dfrac{\dfrac{\partial u}{\partial x_1}}{\sqrt{|\nabla u|^2 + \varepsilon^2}} \right) + \dfrac{1}{2}(u - f), \\ A_2(u) = -\eta \dfrac{\partial}{\partial x_2} \left(\dfrac{\dfrac{\partial u}{\partial x_2}}{\sqrt{|\nabla u|^2 + \varepsilon^2}} \right) + \dfrac{1}{2}(u - f). \end{cases} \tag{148}$$

Combining the scheme we mentioned just above with a semi-explicit time discretization of the nonlinear terms we obtain

$$u^0 = u_0. \tag{149}$$

For $n \geq 0$, $u^n \to \{u^{n+1/4}, u^{n+2/4}\} \to u^{n+1}$ via

$$\begin{cases} \dfrac{u^{n+1/4} - u^n}{2\triangle t} - \eta \dfrac{\partial}{\partial x_1} \left(\dfrac{\dfrac{\partial u^{n+1/4}}{\partial x_1}}{\sqrt{|\nabla u^n|^2 + \varepsilon^2}} \right) + \dfrac{u^{n+1/4}}{2} = \dfrac{f}{2} \text{ in } \Omega, \\[4mm] \dfrac{\partial u^{n+1/4}}{\partial x_1}(0, x_2) = \dfrac{\partial u^{n+1/4}}{\partial x_1}(a, x_2) = 0 \ \forall x_2 \in (0, b), \end{cases} \tag{150.1}$$

$$\begin{cases} \dfrac{u^{n+2/4} - u^n}{2\triangle t} - \eta \dfrac{\partial}{\partial x_2} \left(\dfrac{\dfrac{\partial u^{n+2/4}}{\partial x_2}}{\sqrt{|\nabla u^n|^2 + \varepsilon^2}} \right) + \dfrac{u^{n+2/4}}{2} = \dfrac{f}{2} \text{ in } \Omega, \\[4mm] \dfrac{\partial u^{n+2/4}}{\partial x_2}(x_1, 0) = \dfrac{\partial u^{n+2/4}}{\partial x_2}(x_1, b) = 0 \ \forall x_1 \in (0, a), \end{cases} \tag{150.2}$$

$$u^{n+1} = \frac{1}{2}(u^{n+1/4} + u^{n+2/4}). \tag{151}$$

Scheme (149)-(151) can accommodate large time steps implying a fast convergence to steady state solutions. It preserve also the symmetry of the images. Moreover since in most applications Ω is a rectangle with the image pixels uniformly distributed on it, it makes sense to use a finite difference discretization on a uniform Cartesian grid to approximate (150.1) and (150.2). For Dirichlet or Neunann boundary conditions, the finite difference discretization of (150.1) and (150.2) will produce two families of uncoupled tri-diagonal linear systems easily solvable (the good parallelization properties of the above scheme are quite obvious). The above operator-splitting scheme can be generalized to the numerical treatment of other variational models (such as Chan-Vese's, and to models involving derivatives of order higher than one, as shown in, e.g., [89]). A closely related scheme is discussed in [167].

6.2.2 A split-Bregman method and related ADMM algorithm for the ROF model

In ref. [86], *T. Goldstein* and *S. Osher* proposed and tested a fast converging iterative method for the ROF model: this algorithm, of the *split-Bregman* type, is certainly one of the fastest numerical methods for the ROF model. It was quickly realized (see [156, 170, 172]) that the Bregman algorithm discussed in [86] is equivalent to an *ADMM* one. Here, we will explain the ideas in an informal way using the continuous model whose formalism is much simpler. As stated in Remark 29, to make

our discussion more rigorous mathematically, the functional spaces for which the continuous model makes sense have to be specified (here, they are of the *bounded variation* type). This difficulty is one of the reasons explaining why some authors (as in [170]) consider discrete models, directly.

Let us denote ∇u by $\mathbf{p}$; then, it is easy to see that (from (131)) the ROF model is equivalent to the following linearly constrained minimization problem:

$$\{u, \mathbf{p}\} = \arg\min_{\substack{\{v, \mathbf{q}\} \\ \nabla v - \mathbf{q} = 0}} \left[\eta \int_\Omega |\mathbf{q}| \, dx + \frac{1}{2} \int_\Omega |v - f|^2 \, dx \right]. \qquad (152)$$

Clearly, problem (152) belongs to the family of variational problems discussed in Section 3.2, the associated augmented Lagrangian being defined (with $r > 0$) by (see, e.g., [72] (Chapter 4)):

$$\mathscr{L}_{rof}(v, \mathbf{q}; \boldsymbol{\mu}) = \eta \int_\Omega |\mathbf{q}| \, dx + \frac{1}{2} \int_\Omega |v - f|^2 \, dx \qquad (153)$$
$$+ \frac{r}{2} \int_\Omega |\nabla v - \mathbf{q}|^2 \, dx + \int_\Omega \boldsymbol{\mu} \cdot (\nabla v - \mathbf{q}) \, dx.$$

Above, $u : \Omega \to \mathbb{R}$ denotes the restored image we are looking for, $\mathbf{p} = \nabla u$, $\boldsymbol{\mu}$ is a multiplier. Due to the strict convexity of the second term, the discrete analogues of the minimization problem (152) have a unique solution. Applying algorithm *ALG*2 of Section 3.2.2 to the solution of (152) we obtain the following

Algorithm 6.1: *An augmented Lagrangian method for the ROF model*

0. Initialization: $\boldsymbol{\lambda}^0 = \mathbf{0}$, $u^0 = f$.

For $k = 0, 1, \cdots$, until convergence:

1. Compute $\mathbf{p}^{k+1}$ from

$$\mathbf{p}^{k+1} = \arg\min_{\mathbf{q} \in (L^2(\Omega))^2} \mathscr{L}_{rof}(u^k, \mathbf{q}; \boldsymbol{\lambda}^k). \qquad (154)$$

2. Compute u^{k+1} from

$$u^{k+1} = \arg\min_{v \in H^1(\Omega)} \mathscr{L}_{rof}(v, \mathbf{p}^{k+1}; \boldsymbol{\lambda}^k). \qquad (155)$$

3. Update $\boldsymbol{\lambda}^k$ by

$$\boldsymbol{\lambda}^{k+1} = \boldsymbol{\lambda}^k + r(\nabla u^{k+1} - \mathbf{p}^{k+1}). \qquad (156)$$

It was observed in [156, 170] that this augmented Lagrangian algorithm is equivalent to the split-Bregman algorithm discussed in [86]. This equivalence is also explained in [172] for compressive sensing models. The minimization sub-problems (154) have closed form solutions which can be computed point-wise; solving them is thus quite easy. The minimization sub-problems (155) (in fact their discrete analogues) reduce to discrete well-posed linear Neumann problems; the associated ma-

trix being symmetric, positive definite and sparse, these discrete elliptic problems can be solved by a large variety of direct and iterative methods (among them: sparse Cholesky, multi-level, Gauss-Seidel, conjugate gradient, FFT, etc.; see [170, 172] for more details). The convergence of algorithm (154)-(156) is discussed in [170].

Remark 35. As described above, Algorithm 6.1 is largely formal since it operates in the space $\mathbf{W} = [H^1(\Omega) \times (L^2(\Omega))^2] \times (L^2(\Omega))^2$, although the solution u of problem (131) may not have enough regularity to belong to $H^1(\Omega)$. However, Algorithm 6.1 makes sense for the discrete analogues of problem (131) and space $\mathbf{W}$ obtained by finite difference or finite element approximation; for finite element approximations in particular, the formalisms of Algorithm 6.1 and of its discrete counterparts are nearly identical. The above observation applies to most of the ADMM algorithms described below (see Remark 36, for example).

Remark 36. As shown in, e.g., [109] (for image denoising applications), Algorithm 6.1 is easy to modify in order to handle those situations where the functional $\int_\Omega |\nabla \mathbf{v}| \, dx$ is replaced by $\frac{1}{s} \int_\Omega |\nabla \mathbf{v}|^s \, dx$ with $0 < s < 1$, or by other non-convex functionals of $|\nabla \mathbf{v}|$; once discretized, these modifications of Algorithm 6.1 perform very well as shown in [109].

Remark 37. It is easy to extend algorithm (154)-(156) to the solution of the min-cut problem (139), since the additional constraint encountered in this last problem, namely $0 \leq \mu(x) \leq 1$, a.e. in Ω, is (relatively) easy to treat; actually, this extension has been done in [22] (see also [4, 27], and Section 6.2.3, below, for a number of related new approaches). As shown in [170] (page 320), and [142, 143], it is also easy to extend algorithm (154)-(156) to those situations where one uses vector-*TV* regularization in order to process vector- valued data.

6.2.3 An augmented Lagrangian method for the continuous min-cut and max-flow problems

The continuous max-flow problems (138) and (139) are dual to each other in the sense that if the function λ is solution of (139), it is a *Lagrange multiplier* for the flow conservation equation in (138). We can solve both problems simultaneously using a primal-dual method à la *ALG2* relying on the following *augmented Lagrangian* functional

$$\mathscr{L}_c(q_s, q_t, \mathbf{v}; \mu) = -\int_\Omega q_s \, dx - \int_\Omega \mu(\nabla \cdot \mathbf{v} - q_s + q_t) \, dx + \frac{r}{2} \int_\Omega (\nabla \cdot \mathbf{v} - q_s + q_t)^2 \, dx,$$
(157)

where in (157): $r > 0$, and q_s, q_t and $\mathbf{v}$ verify, a.e. in Ω, $q_s \leq f_1, q_t \leq f_2, |\mathbf{v}| \leq g$; here $|\mathbf{v}| = \sqrt{v_1^2 + v_2^2}, \forall \mathbf{v} = \{v_1, v_2\}$. Applying *ALG2* to the computation of the saddle-points of $\mathscr{L}_c$ over the set $(Q_1 \times Q_2 \times K) \times L^2(\Omega)$, where $Q_1 = \{q | q \in L^2(\Omega), q \leq f_1\}$, $Q_2 = \{q | q \in L^2(\Omega), q \leq f_2\}$, and $K = \{\mathbf{v} | \mathbf{v} \in (L^2(\Omega))^2, \nabla \cdot \mathbf{v} \in L^2(\Omega), \mathbf{v} \cdot \mathbf{n} = 0$ on $\Gamma, |\mathbf{v}| \leq g\}$, we obtain

Algorithm 6.2: *An augmented Lagrangian method for the continuous max-flow problem*

0. Initialization: $\lambda^0 = 0$, $p_s^0 = f_1$, $p_t^0 = f_2$.

For $k = 0, 1, \cdots$, until convergence:

1. Compute $\mathbf{u}^{k+1}$ from

$$\mathbf{u}^{k+1} = \arg\min_{\mathbf{v} \in K} \mathscr{L}_c(p_s^k, p_t^k, \mathbf{v}; \lambda^k). \tag{158}$$

2. Compute $\{p_s^{k+1}, p_t^{k+1}\}$ from

$$\{p_s^{k+1}, p_t^{k+1}\} = \arg\min_{\{q_s, q_t\} \in Q_1 \times Q_2} \mathscr{L}_c(q_s, q_t, \mathbf{u}^{k+1}; \lambda^k). \tag{159}$$

3. Update λ^k by

$$\lambda^{k+1} = \lambda^k - r(\nabla \cdot \mathbf{u}^{k+1} - p_s^{k+1} + p_t^{k+1}). \tag{160}$$

We observe that (159) has a closed form solution (and that p_s^{k+1} and p_t^{k+1} can be computed point-wise independently of each other). The sub-problem (158) is a simple variant of the dual of the ROF problem (that is, the unconstrained minimization of the functional in (131)). We just need to solve this problem approximately; indeed, in our implementations we just used few steps of a descent algorithm, followed by a projection on the convex set $\{\mathbf{v} | \mathbf{v} \in (L^2(\Omega))^2, |\mathbf{v}| \leq g\}$ (see [173], [176] for more details on the solution of these sub-problems). The discrete variant of algorithm (158)-(160) that we implemented (via a finite difference discretization) proved being very robust with respect to initialization and to the value of the augmentation parameter r; it is also very efficient computationally.

Remark 38. As written, algorithm (158)-(160) is applicable only to the solution of two-phase flow problems. There are several ways to generalize this algorithm to models involving more than two phases, as shown in, e.g., [5, 6, 7, 8, 173, 178]. Also, we would like to emphasize the fact that the discrete analogue of algorithm (158)-(160) we implemented has good convergence properties no matter which of the following two norms we used for the flow constraint in (138) (see Remark 33 for the dual formulation associated with (162)):

$$|\mathbf{v}|_2 = \sqrt{v_1^2 + v_2^2} \tag{161}$$

or

$$|\mathbf{v}|_1 = |v_1| + |v_2|. \tag{162}$$

If one uses the meshes classically used in digital imaging, traditional graph cut methods (like those discussed in [19]) can be used to solve the discrete min-cut and max-flow problems if one uses the norm defined by (162) to bound $\mathbf{v}$. On the other hand, the above mentioned graph cut methods cannot handle the norm defined by (161). It

is also known that the solutions of the discrete min-cut and max-flow problems suffer from the matrication error if the norm in (162) is used. Compared to graph cut methods, ADMM algorithms such as (158)-(160) can handle both norms without particular difficulty. Moreover, these augmented Lagrangian algorithms are easy to parallelize and to implement on GPUs; also, they use much less memory than traditional graph cut methods; this enables using these algorithms for high dimensional and large size images or data.

6.2.4 A split-Bregman method and related ADMM algorithm for a second order total variation model

Here, we will discuss the application of *ALG*2 (that is ADMM) to the solution of those image processing problems associated with the functional defined by (132) (also known as the *TV*2 model). The presentation follows [42, 73, 170], where the main idea is: (i) Transfer the burden of nonlinearity from the Hessian

$$\mathbf{D}^2 u \left(= \begin{pmatrix} \partial^2 u / \partial x_1^2 & \partial^2 u / \partial x_1 \partial x_2 \\ \partial^2 u / \partial x_1 \partial x_2 & \partial^2 u / \partial x_2^2 \end{pmatrix} \right)$$

to an additional unknown **p**, via the relation

$$\mathbf{p} = \mathbf{D}^2 u, \tag{163}$$

and (ii) Use a well-chosen augmented Lagrangian functional, associated with the linear relation (163). A similar idea has been (successfully) used in [42] for the augmented Lagrangian solution of the Dirichlet problem for the Monge-Ampère equation $\det \mathbf{D}^2 u = f$ (see also Chapter 7 of this book).

Back to the *TV*2 model (132), let us recall that the related minimization problem reads as

$$u = \arg\min_{v \in V} \left[\frac{1}{2} \int_\Omega |v - f|^2 \, dx + \eta \int_\Omega |\mathbf{D}^2 v| \, dx \right], \tag{164}$$

with $V = \{v | v \in L^2(\Omega), \mathbf{D}^2 v \in (L^1(\Omega))^{2 \times 2}\}$ and $|\mathbf{M}| = \sqrt{\sum_{1 \leq i,j \leq 2} m_{ij}^2}$ denoting the Fröbenius norm of matrix **M**. Proceeding as in Section 3.2.2, we observe the equivalence between (164) and

$$\{u, \mathbf{D}^2 u\} = \arg\min_{\{v, \mathbf{q}\} \in W} \left[\frac{1}{2} \int_\Omega |v - f|^2 \, dx + \eta \int_\Omega |\mathbf{q}| \, dx \right], \tag{165}$$

where

$$W = \{\{v, \mathbf{q}\} | v \in V, \mathbf{q} \in (L^1(\Omega))^{d \times d}, \mathbf{D}^2 v - \mathbf{q} = \mathbf{0}\},$$

an observation leading us to introduce the following augmented Lagrangian functional

$$\mathscr{L}_{TV2}(v, \mathbf{q}; \boldsymbol{\mu}) = \frac{1}{2} \int_{\Omega} |v - f|^2 \, dx + \eta \int_{\Omega} |\mathbf{q}| \, dx \tag{166}$$
$$+ \frac{r}{2} \int_{\Omega} |\mathbf{D}^2 v - \mathbf{q}|^2 \, dx + \int_{\Omega} \boldsymbol{\mu} : (\mathbf{D}^2 v - \mathbf{q}) \, dx,$$

where, in (166), $r > 0$, and (with obvious notation) $\mathbf{S} : \mathbf{T} = \sum_{1 \le i, j \le 2} s_{ij} t_{ij}$. Applying the methods discussed in Section 3.2.2 to the solution of the minimization problem (164) we obtain the following

Algorithm 6.3: *An augmented Lagrangian method for the TV2 model*

0. Initialization: $\boldsymbol{\lambda}^0 = \mathbf{0}$, $u^0 = f$.

For $k = 0, 1, \cdots$, until convergence:

1. Compute $\mathbf{p}^{k+1}$ from

$$\mathbf{p}^{k+1} = \arg \min_{\mathbf{q} \in (L^2(\Omega))^{2 \times 2}} \mathscr{L}_{TV2}(u^k, \mathbf{q}; \boldsymbol{\lambda}^k). \tag{167}$$

2. Compute u^{k+1} from

$$u^{k+1} = \arg \min_{v \in H^2(\Omega)} \mathscr{L}_{TV2}(v, \mathbf{p}^{k+1}; \boldsymbol{\lambda}^k). \tag{168}$$

3. Update $\boldsymbol{\lambda}^k$ by

$$\boldsymbol{\lambda}^{k+1} = \boldsymbol{\lambda}^k + r(\mathbf{D}^2 u^{k+1} - \mathbf{p}^{k+1}). \tag{169}$$

As with Algorithm 6.1 (that is (154)-(156)), the sub-problems (167) have closed-form solutions which can be computed point-wise. On the other hand, the sub-problems (168) reduce to linear bi-harmonic problems for the elliptic operator $I + r\nabla^4$; if properly discretized on a uniform grid (typically by finite differences), the discrete analogues of these bi-harmonic problems can be solved by FFT or by iterative methods (see [170] (page 324) for details).

Remark 39. Obviously, Remark 35 applies also to Algorithm 6.3, with $H^2(\Omega)$ playing here the role of $H^1(\Omega)$ there.

6.2.5 An augmented Lagrangian method for the Euler's Elastica model

The energy functional defined by (133), namely

$$E(v) = \frac{1}{2} \int_{\Omega} |f - v|^2 \, dx + \int_{\Omega} \left[a + b \left| \nabla \cdot \frac{\nabla v}{|\nabla v|} \right|^2 \right] |\nabla v| \, dx,$$

makes no sense on the subset of Ω where ∇v vanishes. Following an approach very common in *visco-plasticity* (see, e.g., [66, 83]]) one make things more rigorous by defining (following [154]) the energy functional by

$$E(v,\mathbf{m}) = \frac{1}{2}\int_\Omega |f-v|^2\,dx + \int_\Omega \left[a + b|\nabla\cdot\mathbf{m}|^2\right]|\nabla v|\,dx \qquad (170)$$

the functions v and $\mathbf{m}$ in (170) verifying

$$|\nabla v| = \mathbf{m}\cdot\nabla v,\ |\mathbf{m}| \leq 1. \qquad (171)$$

The related minimization problem reads as

$$\begin{cases} \{u,\mathbf{n}\} = \arg\min_{\{v,\mathbf{m}\}} E(v,\mathbf{m}), \\ \text{with } \{v,\mathbf{m}\} \text{ verifying (171).} \end{cases} \qquad (172)$$

Introducing the vector-valued function $\mathbf{p}$ verifying $\mathbf{p} = \nabla u$, we clearly have equivalence between (172) and

$$\begin{cases} \{u,\mathbf{p},\mathbf{n}\} = \arg\min_{\{v,\mathbf{q},\mathbf{m}\}} \left[\frac{1}{2}\int_\Omega |f-v|^2\,dx + \int_\Omega \left[a + b|\nabla\cdot\mathbf{m}|^2\right]|\mathbf{q}|\,dx\right], \\ \text{with } \{v,\mathbf{q},\mathbf{m}\} \text{ verifying } \mathbf{q} = \nabla v,\ |\mathbf{q}| = \mathbf{m}\cdot\mathbf{q},\ |\mathbf{m}| \leq 1. \end{cases} \qquad (173)$$

Following [154], we associate with the minimization problem (173) the following augmented Lagrangian functional

$$\begin{aligned} \mathcal{L}_{elas}\{v,\mathbf{q},\mathbf{m};\boldsymbol{\mu}_1,\mu_2\} = {} & \frac{1}{2}\int_\Omega |v-f|^2\,dx + \int_\Omega\left[a + b|\nabla\cdot\mathbf{m}|^2\right]|\mathbf{q}|\,dx \\ & + \frac{r_1}{2}\int_\Omega |\nabla v - \mathbf{q}|^2\,dx + r_2\int_\Omega (|\mathbf{q}| - \mathbf{q}\cdot\mathbf{m})\,dx \qquad (174) \\ & + \int_\Omega \boldsymbol{\mu}_1\cdot(\nabla v - \mathbf{q})\,dx + \int_\Omega \mu_2(|\mathbf{q}| - \mathbf{q}\cdot\mathbf{m})\,dx, \end{aligned}$$

with r_1 and r_2 both positive. Suppose that in (174) the vector-valued function $\mathbf{m}$ belongs to $\mathbf{M}$, the closed convex set of $(L^2(\Omega))^2$ defined by

$$\mathbf{M} = \{\mathbf{m}|\mathbf{m}\in(L^2(\Omega))^2, |\mathbf{m}(x)| \leq 1, \text{a.e. in } \Omega\};$$

we have then $|\mathbf{q}| - \mathbf{q}\cdot\mathbf{m} \geq 0$, implying (since $|\mathbf{q}| - \mathbf{q}\cdot\mathbf{m} = ||\mathbf{q}| - \mathbf{q}\cdot\mathbf{m}|$) that the variant of $ALG2$ described just below will force the condition $|\mathbf{q}| - \mathbf{q}\cdot\mathbf{m} = 0$ in the sense of $L^1(\Omega)$. This variant of $ALG2$ reads as follows when applied to the solution of problem (172) (below, $H(\Omega;\mathrm{div}) = \{\mathbf{v}|\mathbf{v}\in(L^2(\Omega))^2, \nabla\cdot\mathbf{v}\in L^2(\Omega)\}$):

Algorithm 6.4: *An augmented Lagrangian method for the Euler's Elastica model*

0. Initialization: $\boldsymbol{\lambda}_1^0 = \mathbf{0}$, $\lambda_2^0 = 0$, $u^0 = f$, $\mathbf{n}^0 = \mathbf{0}$.

For $k = 0, 1, \cdots$, until convergence:

1. Compute $\mathbf{p}^{k+1}$ from

$$\mathbf{p}^{k+1} = \arg\min_{\mathbf{q}\in(L^2(\Omega))^2} \mathcal{L}_{elas}(u^k,\mathbf{q},\mathbf{n}^k;\boldsymbol{\lambda}_1^k,\lambda_2^k). \qquad (175)$$

2. Compute $\mathbf{n}^{k+1}$ from

$$\mathbf{n}^{k+1} = \arg \min_{\mathbf{m} \in H(\Omega;\mathrm{div}) \cap \mathbf{M}} \mathscr{L}_{elas}(u^k, \mathbf{p}^{k+1}, \mathbf{m}; \boldsymbol{\lambda}_1^k, \lambda_2^k). \qquad (176)$$

3. Compute u^{k+1} from

$$u^{k+1} = \arg \min_{v \in H^1(\Omega)} \mathscr{L}_{elas}(v, \mathbf{p}^{k+1}, \mathbf{n}^{k+1}; \boldsymbol{\lambda}_1^k, \lambda_2^k). \qquad (177)$$

4. Update $\{\boldsymbol{\lambda}_1^k, \lambda_2^k\}$ by

$$\begin{cases} \boldsymbol{\lambda}_1^{k+1} = \boldsymbol{\lambda}_1^k + r_1(\nabla u^{k+1} - \mathbf{p}^{k+1}), \\ \lambda_2^{k+1} = \lambda_2^k + r_2(|\mathbf{p}^{k+1}| - \mathbf{p}^{k+1} \cdot \mathbf{n}^{k+1}). \end{cases} \qquad (178)$$

Below, we will give some details and comments about the solution of the sub-problems encountered when applying algorithm (175)-(176); implementation issues will be also addressed. Further information is provided in [154].

- The minimization sub-problem (175) has a unique closed-form solution which can be computed point-wise.
- The minimization sub-problem (176) is equivalent to the following *elliptic variational inequality*

$$\begin{cases} \mathbf{n}^{k+1} \in H(\Omega;\mathrm{div}) \cap \mathbf{M}, \\ b \int_{\Omega} |\mathbf{p}^{k+1}| \, \nabla \cdot \mathbf{n}^{k+1} \, \nabla \cdot (\mathbf{m} - \mathbf{n}^{k+1}) \, dx \geq \int_{\Omega} (r_2 + \lambda_2^k) \mathbf{p}^{k+1} \cdot (\mathbf{m} - \mathbf{n}^{k+1}) \, dx, \\ \forall \mathbf{m} \in H(\Omega;\mathrm{div}) \cap \mathbf{M}. \end{cases} \qquad (179)$$

We observe that the bilinear functional in the left-hand side of (179) is symmetric and positive semi-definite (indeed, $\int_{\Omega} |\mathbf{p}^{k+1}|(\nabla \cdot \mathbf{m})^2 \, dx = 0$ if $\mathbf{m} = \nabla \times \mathbf{z}$. However, the boundedness of $\mathbf{M}$ implies that the variational problem (176), (179) has solutions. For the solution of the discrete analogues of the above problem we advocate using few iterations of those *relaxation methods with projection* discussed in, e.g., [66, 76] (other methods are possible as shown in [154]).
- The minimization sub-problem (177) has a unique solution characterized by

$$\begin{cases} u^{k+1} \in H^1(\Omega), \\ \int_{\Omega} u^{k+1} v \, dx + r_1 \int_{\Omega} \nabla u^{k+1} \cdot \nabla v \, dx = \int_{\Omega} f v \, dx + \int_{\Omega} (r_1 \mathbf{p}^{k+1} - \boldsymbol{\lambda}_1^k) \cdot \nabla v \, dx \\ \forall v \in H^1(\Omega). \end{cases} \qquad (180)$$

Actually, (180) is nothing but a variational formulation of the following Neumann problem

$$\begin{cases} u^{k+1} - r_1 \nabla^2 u^{k+1} = f - \nabla \cdot (r_1 \mathbf{p}^{k+1} - \boldsymbol{\lambda}_1^k) & \text{in } \Omega, \\ r_1 \dfrac{\partial u^{k+1}}{\partial \nu} = (r_1 \mathbf{p}^{k+1} - \boldsymbol{\lambda}_1^k) \cdot \boldsymbol{\nu} & \text{on } \partial\Omega, \end{cases} \tag{181}$$

where, in (181), $\boldsymbol{\nu}$ denotes the outward unit vector normal at the boundary $\partial\Omega$ of Ω. The numerical solution of linear elliptic problems such as (181) is routine nowadays; after an appropriate space discretization it can be achieved by a large variety of direct and iterative methods (sparse Cholesky, FFT, relaxation, multilevel, etc.).

- Since the energy functional associated with the Euler's Elastica is *non-convex* (see (170)) the augmentation parameters r_1 and r_2 have to be chosen large enough to guarantee the convergence of algorithm (175)-(179). Actually, the tuning of r_1 and r_2 is a delicate issue in itself and we can expect (as shown for example in [133], for a problem involving three augmentation parameters) the optimal values of these parameters to be of different orders of magnitude with respect to the space discretization h.
- Another solution method for the Euler's Elastica is discussed in [21]. It relies on tractable convex relaxation in higher dimension.

Remark 40. In [154], an alternative method for the solution of the Euler's Elastica problem (172) is also considered. It relies on the equivalence between (172) and

$$\begin{cases} \{u, \mathbf{p}, \mathbf{n}^1, \mathbf{n}^2\} = \underset{\{v, \mathbf{q}, \mathbf{m}_1, \mathbf{m}_2\}}{\arg\min} \left[\dfrac{1}{2} \int_\Omega |f - v|^2 \, dx + \int_\Omega \left[a + b |\nabla \cdot \mathbf{m}_1|^2 \right] |\mathbf{q}| \, dx \right], \\ \text{with } \{v, \mathbf{q}, \mathbf{m}_1, \mathbf{m}_2\} \text{ verifying } \mathbf{q} = \nabla v, \ \mathbf{m}_1 = \mathbf{m}_2, \ |\mathbf{q}| = \mathbf{m}_2 \cdot \mathbf{q}, \ |\mathbf{m}_2| \le 1. \end{cases} \tag{182}$$

An augmented Lagrangian associated with (182) is clearly the one defined by

$$\mathscr{L}_{elas}\{v, \mathbf{q}, \mathbf{m}_1, \mathbf{m}_2; \boldsymbol{\mu}_1, \mu_2, \boldsymbol{\mu}_3) = \dfrac{1}{2} \int_\Omega |v - f|^2 \, dx + \int_\Omega \left[a + b |\nabla \cdot \mathbf{m}_1|^2 \right] |\mathbf{q}| \, dx$$

$$+ \dfrac{r_1}{2} \int_\Omega |\nabla v - \mathbf{q}|^2 \, dx + r_2 \int_\Omega (|\mathbf{q}| - \mathbf{q} \cdot \mathbf{m}_2) \, dx + r_3 \int_\Omega |\mathbf{m}_1 - \mathbf{m}_2|^2 \, dx \tag{183}$$

$$+ \int_\Omega \boldsymbol{\mu}_1 \cdot (\nabla v - \mathbf{q}) \, dx + \int_\Omega \mu_2 (|\mathbf{q}| - \mathbf{q} \cdot \mathbf{m}_2) \, dx + \int_\Omega \boldsymbol{\mu}_3 \cdot (\mathbf{m}_1 - \mathbf{m}_2) \, dx,$$

with r_1, r_2 and r_3 all positive. From (183), one can easily derive a variant of algorithm (175)-(178) for the solution of the minimization problem (172); such an algorithm is discussed in [154]. Actually the above reference discusses also the solution by a similar methodology of the variant of problem (172) obtained by replacing the fidelity term $\dfrac{1}{2} \int_\Omega |f - v|^2 \, dx$ by $\dfrac{1}{s} \int_\Omega |f - v|^s \, dx$ with $s \in [1, +\infty)$. Typically, one takes $s = 1$ (resp., $s = 2$) for salt-and-pepper noise (resp., Gaussian noise). Further details and generalizations are given in [154].

Remark 41. As shown in [187], the methodology we employed to solve the minimization problem (172) can be easily modified in order to handle the *Chan-Vese Elastica* model.

6.2.6 An augmented Lagrangian method for the L^1-mean curvature model

In this section, we follow closely the presentation used in [186]. The rational of the L^1-mean curvature model has been given in Section 6.1.5, leading one to consider the following minimization problem

$$u = \arg\min_{v \in V} \left[\frac{1}{2} \int_\Omega |v - f|^2 \, dx + \eta \int_\Omega \left| \nabla \cdot \frac{\nabla v}{\sqrt{1 + |\nabla v|^2}} \right| dx \right], \qquad (184)$$

where $\nabla = \{\partial/\partial x_i\}_{i=1}^2$. In (184), the choice of V is a delicate theoretical issue; indeed the safest way to proceed would be to take $V = H^2(\Omega)$ in (184), and to replace min by inf (a (kind) of justification for this approach can be found in [133]). Let observe (as in [186], where a slightly different notation is used) that

$$\nabla \cdot \frac{\nabla v}{\sqrt{1 + |\nabla v|^2}} = \nabla_3 \cdot \frac{\{\nabla v, -1\}}{|\{\nabla v, -1\}|}, \qquad (185)$$

where, in (185), $\nabla_3 = \{\partial/\partial x_1, \partial/\partial x_2, 0\}$, and where $\{\nabla v, -1\}$ denotes the 3-dimensional vector-valued function $\{\partial v/\partial x_1, \partial v/\partial x_2, -1\}$. In order to simplify (in some sense) the nonlinear structure of the minimization problem (184), we associate new unknown functions with its solution u, namely $\mathbf{p}$, $\mathbf{n}$ and ψ verifying

$$\begin{cases} \mathbf{p} = \{\nabla u, -1\}, \\ \mathbf{n} = \dfrac{\mathbf{p}}{|\mathbf{p}|}, & \text{or equivalently here } \ |\mathbf{p}| - \mathbf{p} \cdot \mathbf{n} = 0, \ |\mathbf{n}| \le 1, \\ \psi = \nabla_3 \cdot \mathbf{n}. \end{cases} \qquad (186)$$

From (185) and (186), there is clearly equivalence between (184) and

$$\begin{cases} \{u, \psi, \mathbf{p}, \mathbf{n}\} = \arg\min_{\{v, \varphi, \mathbf{q}, \mathbf{m}\}} \left[\dfrac{1}{2} \int_\Omega |v - f|^2 \, dx + \eta \int_\Omega |\varphi| \, dx \right], \\ \text{with } \{v, \varphi, \mathbf{q}, \mathbf{m}\} \text{ verifying } \mathbf{q} = \{\nabla v, -1\}, |\mathbf{q}| - \mathbf{q} \cdot \mathbf{m} = 0, |\mathbf{m}| \le 1, \nabla_3 \cdot \mathbf{m} = \varphi. \end{cases} \qquad (187)$$

In order to solve the minimization problem (184), taking advantage of its equivalence with (187), we introduce the following augmented Lagrangian functional

$$\mathcal{L}_{MC}(v,\varphi,\mathbf{q},\mathbf{z},\mathbf{m};\mu_1,\boldsymbol{\mu}_2,\mu_3,\boldsymbol{\mu}_4) = \frac{1}{2}\int_\Omega |v-f|^2\,dx + \eta\int_\Omega |\varphi|\,dx$$

$$+\frac{r_1}{2}\int_\Omega (|\mathbf{q}|-\mathbf{q}\cdot\mathbf{z})\,dx + \int_\Omega \mu_1(|\mathbf{q}|-\mathbf{q}\cdot\mathbf{z})\,dx$$

$$+\frac{r_2}{2}\int_\Omega |\{\nabla v,-1\}-\mathbf{q}|^2\,dx + \int_\Omega \boldsymbol{\mu}_2\cdot(\{\nabla v,-1\}-\mathbf{q})\,dx \qquad (188)$$

$$+\frac{r_3}{2}\int_\Omega \left|\varphi-\left(\frac{\partial m_1}{\partial x_1}+\frac{\partial m_2}{\partial x_2}\right)\right|^2\,dx + \int_\Omega \mu_3\left(\varphi-\left(\frac{\partial m_1}{\partial x_1}+\frac{\partial m_2}{\partial x_2}\right)\right)\,dx,$$

$$+\frac{r_4}{2}\int_\Omega |\mathbf{z}-\mathbf{m}|^2\,dx + \int_\Omega \boldsymbol{\mu}_4\cdot(\mathbf{z}-\mathbf{m})\,dx.$$

The additional vector-valued function $\mathbf{z}$ has been introduced in order to decouple $\nabla_3\cdot\mathbf{m}$ from the nonlinear relations verified by $\mathbf{m}$ in (187). Following [186], and taking (187) and (188) into account, we advocate the following algorithm for the solution of problem (184):

Algorithm 6.5: *An augmented Lagrangian method for the L^1-mean curvature model*

0. Initialization: $\lambda_1^0=0$, $\boldsymbol{\lambda}_2^0=\mathbf{0}$, $\lambda_3^0=0$, $\boldsymbol{\lambda}_4^0=\mathbf{0}$, $u^0=f$, $\mathbf{p}^0=\{\nabla u^0,-1\}$, $\mathbf{n}^0=$
$\mathbf{y}^0=\dfrac{\mathbf{p}^0}{|\mathbf{p}^0|}$, $\psi^0=\nabla_3\cdot\mathbf{n}^0$.

For $k=0,\ 1,\ \cdots$, until convergence:

1. Compute u^{k+1} from

$$u^{k+1}=\arg\min_{v\in H^1(\Omega)}\mathcal{L}_{MC}(v,\psi^k,\mathbf{p}^k,\mathbf{y}^k,\mathbf{n}^k;\lambda_1^k,\boldsymbol{\lambda}_2^k,\lambda_3^k,\boldsymbol{\lambda}_4^k). \qquad (189)$$

2. Compute ψ^{k+1} from

$$\psi^{k+1}=\arg\min_{\varphi\in L^2(\Omega)}\mathcal{L}_{MC}(u^{k+1},\varphi,\mathbf{p}^k,\mathbf{y}^k,\mathbf{n}^k;\lambda_1^k,\boldsymbol{\lambda}_2^k,\lambda_3^k,\boldsymbol{\lambda}_4^k). \qquad (190)$$

3. Compute $\mathbf{p}^{k+1}$ from

$$\mathbf{p}^{k+1}=\arg\min_{\mathbf{q}\in (L^2(\Omega))^3}\mathcal{L}_{MC}(u^{k+1},\psi^{k+1},\mathbf{q},\mathbf{y}^k,\mathbf{n}^k;\lambda_1^k,\boldsymbol{\lambda}_2^k,\lambda_3^k,\boldsymbol{\lambda}_4^k). \qquad (191)$$

4. Compute $\mathbf{y}^{k+1}$ from

$$\mathbf{y}^{k+1}=\arg\min_{\mathbf{z}\in\mathbf{Z}}\mathcal{L}_{MC}(u^{k+1},\psi^{k+1},\mathbf{p}^{k+1},\mathbf{z},\mathbf{n}^k;\lambda_1^k,\boldsymbol{\lambda}_2^k,\lambda_3^k,\boldsymbol{\lambda}_4^k). \qquad (192)$$

5. Compute $\mathbf{n}^{k+1}$ from

$$\mathbf{n}^{k+1}=\arg\min_{\mathbf{m}\in\mathbf{M}}\mathcal{L}_{MC}(u^{k+1},\psi^{k+1},\mathbf{p}^{k+1},\mathbf{y}^{k+1},\mathbf{m};\lambda_1^k,\boldsymbol{\lambda}_2^k,\lambda_3^k,\boldsymbol{\lambda}_4^k). \qquad (193)$$

6. Update $\{\lambda_1^k,\boldsymbol{\lambda}_2^k,\lambda_3^k,\boldsymbol{\lambda}_4^k\}$ by

$$\begin{cases} \lambda_1^{k+1} = \lambda_1^k + r_1(|\mathbf{p}^{k+1}| - \mathbf{p}^{k+1} \cdot \mathbf{y}^{k+1}), \\ \boldsymbol{\lambda}_2^{k+1} = \boldsymbol{\lambda}_2^k + r_2(\{\nabla u^{k+1}, -1\} - \mathbf{p}^{k+1}), \\ \lambda_3^{k+1} = \lambda_3^k + r_3 \left(\psi^{k+1} - \left(\frac{\partial n_1^{k+1}}{\partial x_1} + \frac{\partial n_2^{k+1}}{\partial x_2} \right) \right), \\ \boldsymbol{\lambda}_4^{k+1} = \boldsymbol{\lambda}_4^k + r_4(\mathbf{y}^{k+1} - \mathbf{n}^{k+1}). \end{cases} \tag{194}$$

In (189)-(194), the sets $\mathbf{Z}$ and $\mathbf{M}$ are defined by

$$\mathbf{Z} = \{\mathbf{z} | \mathbf{z} \in (L^2(\Omega))^3, |\mathbf{z}(x)| \leq 1, \text{ a.e. in } \Omega\},$$

and

$$\mathbf{M} = \{\mathbf{m} | \mathbf{m} \in (L^2(\Omega))^3, \frac{\partial m_1}{\partial x_1} + \frac{\partial m_2}{\partial x_2} \in L^2(\Omega)\},$$

respectively.

We observe that that the minimization sub-problems (190), (191) and (192) have closed form solutions which can be computed point-wise. On the other hand, the Euler-Lagrange equations of the sub-problems (189) and (193) are well-posed linear elliptic equations with constant coefficients; fast solvers exist for the solution of the discrete analogues of these elliptic problems (see [186] for details and the results of numerical experiments validating the above algorithm). An important issue is the tuning of the augmentation parameters r_1, r_2, r_3 and r_4; the comments we did in Section 6.2.5, concerning the adjustment of r_1 and r_2 in algorithm (176)-(178), still apply here.

Remark 42. Another augmented Lagrangian based solution method for the L^1-mean curvature problem (184) is discussed and numerically tested in ref. [133]. The related ADMM algorithm involves only three Lagrange multipliers, and three augmentation parameters. Moreover, the various vector-valued functions encountered in the approach discussed in [133] map Ω into $\mathbb{R}^2$ (instead of $\mathbb{R}^3$, as it is the case for algorithm (189)-(194)).

7 Further comments and complements

There is much more to say about *operator-splitting* and *ADMM* algorithms; fortunately, many of these issues and topics we left behind, or said very little about, are developed in the other chapters of this book. There are however some issues we would like to-briefly-comment to conclude this chapter, namely:

(i) The convergence of operator-splitting methods and *ADMM* algorithms, when applied to the solution of problems involving *non-monotone operators* and/or *non-convex functionals*.

(ii) The choice of the *augmentation parameters* and their dynamical adjustment when applying *ADMM* algorithms.

(iii) The derivation of operator-splitting schemes of *high* (or *higher*) *orders* of accuracy.

(iv) Trying to understand why the *Douglas-Rachford* scheme is more robust than the *Peaceman-Rachford* one, using simple model problems to clarify this issue.

(v) Very few problems have generated as many operator-splitting based solution methods than the *Navier-Stokes equations* modelling viscous fluid flows. From this fact, providing the reader with a significant number of related references is a must in a book like this one. These references will conclude this chapter.

Concerning the *first issue*, to the best of our knowledge, there is no general theory concerning the convergence of operator-splitting methods and *ADMM* algorithms when the problem under consideration involves at least one non-monotone operator and/or a non-convex functional. Actually, one can find in the litterature convergence results for some problems lacking monotonicity and/or convexity, but, most often, the proofs of these results are very specific of the problem under consideration, and therefore are not easy to generalize to other situations. However, some recent results obtained by *R. Luke* [96, 115] and *W. Yin* [166], and collaborators, suggest that a fairly general theory is not out of reach. However, we think that there always will be situations where one not will be able to prove the convergence of operator-splitting methods and *ADMM* algorithms. This is not surprising since these methods and algorithms have been quite successful at solving problems for which the existence of solutions has not been proved.

The *second issue*, concerning the choice and the dynamical adaptation of the augmentation parameters is another complicated one, particularly for those non-convex and non-monotone situations involving more than one of such parameters. Indeed, numerical experiments have shown that the optimal values of these parameters may have several orders of magnitude (as shown in, e.g., [80] and [133]), and, from the possible existence of multiple solutions, that bifurcations can take place depending also of the values of these parameters (and of the algorithm initialization). However, for particular problems, heuristics have been found, significantly improving the speed of convergence of these *ADMM* algorithms (see, e.g., [46]).

In order to address the *high* (or *higher*) *orders* of accuracy issue (our *third issue*) we return to Section 2.3 of this chapter (the one dedicated to the Strang symmetrized operator-splitting scheme), and consider the following initial value problem

$$\begin{cases} \dfrac{dX}{dt} + (A+B)X = 0 \text{ on } (0,T), \\ X(0) = X_0, \end{cases} \tag{195}$$

where A and B are *linear* operators *independent* of t. When applied to the solution of the initial value problem (195), the Strang symmetrized scheme (7)-(10) can be written in the following more compact form

$$\begin{cases} X^0 = X_0, \\ X^{n+1} = e^{-A\triangle t/2} e^{-B\triangle t} e^{-A\triangle t/2} X^n, \ \forall n \geq 0. \end{cases} \tag{196}$$

The relation
$$e^{-(A+B)\triangle t} - e^{-A\triangle t/2}e^{-B\triangle t}e^{-A\triangle t/2} = O(\triangle t^3),$$

shows that scheme (196) is second order accurate (and exact if $AB = BA$). For those situations requiring an order of accuracy *higher than two*, several options do exist, the best known being:

(a) The 4$^{\text{th}}$ order *Strang-Richardson* scheme discussed in [49, 50, 48] where it is applied (among other problems) to the numerical solution of real-valued or vector-valued *reaction-diffusion* equations such as

$$\frac{\partial \mathbf{u}}{\partial t} - \mathbf{M}\nabla^2\mathbf{u} + \mathbf{F}(\mathbf{u}) = \mathbf{0},$$

where $\mathbf{u}(x,t) \in I\!R^d$, ∇^2 denotes the Laplace operator, $\mathbf{M}$ is a $d \times d$ symmetric definite matrix, and $\mathbf{F}$ is a smooth mapping from $I\!R^d$ into $I\!R^d$.

(b) The *exponential operator-splitting schemes*. Actually, the Lie and Strang splitting schemes belong to this family of time discretization methods, whose origin (concerning schemes of order higher than two) is not easy to track back, early significant publications being [150, 151] (see also the references therein and those in [161], and in Google Scholar). Arbitrary high accuracy can be obtained with these methods, the price to pay being their reduced stability (compared to the Strang scheme, for example).

The best way to introduce the *Strang-Richardson* scheme is to start, one more time, from the simple initial value problem (195). Applied to the solution of (195), the Strang-Richardson scheme reads as

$$\begin{cases} X^0 = X_0, \\ X^{n+1} = \frac{1}{3}\left[4e^{-A\triangle t/4}e^{-B\triangle t/2}e^{-A\triangle t/2}e^{-B\triangle t/2}e^{-A\triangle t/4} \right. \\ \qquad\qquad \left. -e^{-A\triangle t/2}e^{-B\triangle t}e^{-A\triangle t/2}\right]X^n, \ \forall n \geq 0. \end{cases} \tag{197}$$

A more practical equivalent formulation of the symmetrized scheme (197) can be found in the Chapter 6 of [70]; it avoids the use of matrix exponentials and can be generalized easily to nonlinear problems (it requires the solution of eight sub-initial value problems per time step). Scheme (197) is *fourth order accurate* but not as stable as the original Strang scheme (scheme (196)). Also, its application to decompositions involving more than two operators becomes a bit complicated to say the least (higher order methods of the same type are discussed in [85]).

In a similar fashion, we consider again the initial value problem (195) to introduce *exponential splitting* methods. Applied to the solution of (195) the typical *exponential operator-splitting scheme* reads as follows:

$$\begin{cases} X^0 = X_0, \\ X^{n+1} = \left(\prod_{j=1}^{J} e^{-b_jB\triangle t}e^{-a_jA\triangle t}\right)X^n, \ \forall n \geq 0. \end{cases} \tag{198}$$

where $a_j, b_j \in \mathbb{R}$, for $1 \le j \le J$. The Strang symmetrized scheme (196) is a particular case of (198) (corresponding to $J = 2$, $b_1 = 0$, $a_1 = 1/2$, $b_2 = 1$, $a_2 = 1/2$). By an appropriate choice of J, and of the coefficients a_j and b_j, scheme (198) can be made of order higher than two (as shown in, e.g., [16]), the price to pay being that some of the coefficients a_j, b_j are *negative* making the scheme inappropriate to those situations where some of the operators are dissipative. On the other hand, these higher order schemes produce spectacular results when applied to reversible systems, like those associated with some linear and nonlinear Schrödinger operators, as shown in, e.g.,[51, 161]. Their generalization to those (fairly common) situations involving more than two operators is rather complicated, although theoretically doable.

Concerning the *fourth issue*, the *Peaceman-Rachford* and *Douglas-Rachford* schemes have been briefly discussed in Sections 2.4 and 2.5, respectively. In order to have a better idea of their *accuracy* and *stability* properties, we will consider the particular situation where, in problem (14), $\phi_0 \in \mathbb{R}^d$, $T = +\infty$, and where A_1 (resp., A_2) is given by $A_1 = \alpha A$ (resp., $A_2 = \beta A$), A being a real symmetric positive definite $d \times d$ matrix, and α, β verifying $0 \le \alpha, \beta \le 1$ and $\alpha + \beta = 1$. The exact solution of the associated problem (14) reads as

$$\phi(t) = e^{-At}\phi_0, \ \forall t \ge 0,$$

which implies (by projection on an orthonormal basis of eigenvectors of matrix A, and with obvious notation)

$$\phi_i(t) = e^{-\lambda_i t}\phi_{0i}, \ \forall t \ge 0, \ \forall i = 1,\dots,d, \tag{199}$$

where $0 < \lambda_1 \le \cdots \le \lambda_i \le \cdots \le \lambda_d$, the λ_i's being the eigenvalues of matrix A. Applying the *Peaceman-Rachford* scheme (15) to the particular problem (14) defined above, we obtain the following discrete analogue of (199):

$$\phi_i^n(t) = (R_1(\lambda_i \triangle t))^n \phi_{0i}, \ \forall n \ge 0, \ \forall i = 1,\dots,d, \tag{200}$$

R_1 being the rational function defined by

$$R_1(\xi) = \frac{\left(1 - \dfrac{\alpha}{2}\xi\right)\left(1 - \dfrac{\beta}{2}\xi\right)}{\left(1 + \dfrac{\alpha}{2}\xi\right)\left(1 + \dfrac{\beta}{2}\xi\right)}. \tag{201}$$

Since $|R_1(\xi)| < 1$, $\forall \xi > 0$, the Peaceman-Rachford scheme (15) is *unconditionally stable* in the particular case considered here. However, the property $\lim_{\xi \to +\infty} R_1(\xi) = 1$

shows that the above scheme is *not stiff A-stable*, making it not a first choice scheme to capture steady state solutions or to simulate fast transient phenomena. Actually, the stability drawback we just mentioned is not specific to the particular case we are considering, but seems to hold in general for scheme (15). Incidentally, the relation

$$R_1(\xi) - e^{-\xi} = O(\xi^3) \text{ in the neighborhood of } \xi = 0$$

implies that in the particular case under consideration (where A_1 and A_2 commute) scheme (15) is *second order accurate*. Applying now the *Douglas-Rachford* scheme (17) to the same particular case of problem (14), we obtain

$$\phi^{n+1} = (I + \alpha \triangle t A)^{-1} (I + \beta \triangle t A)^{-1} (I + \alpha \beta (\triangle t)^2 A^2) \phi^n, \ \forall n \geq 0,$$

which implies

$$\phi^n = (I + \alpha \triangle t A)^{-n} (I + \beta \triangle t A)^{-n} (I + \alpha \beta (\triangle t)^2 A^2)^n \phi_0, \ \forall n \geq 0. \tag{202}$$

By projection of (202) on an orthonormal basis of $\mathbb{R}^d$ consisting of eigenvectors of A, we obtain the following variant of (200):

$$\phi_i^n(t) = (R_2(\lambda_i \triangle t))^n \phi_{0i}, \ \forall n \geq 0, \ \forall i = 1, \ldots, d, \tag{203}$$

R_2 being the rational function defined by

$$R_2(\xi) = \frac{1 + \alpha \beta \xi^2}{(1 + \alpha \xi)(1 + \beta \xi)}. \tag{204}$$

Since $0 < R_2(\xi) < 1$, $\forall \xi > 0$, the Douglas-Rachford scheme (17) is *unconditionally stable* in the particular case considered here. However, the property $\lim_{\xi \to +\infty} R_2(\xi) = 1$ shows that the above scheme is *not stiff A-stable*, making it not a first choice scheme to capture steady state solutions or to simulate fast transient phenomena. Actually, the stability drawback we just mentioned is not specific to the particular case we are considering, but seems to hold in general for scheme (17). Concerning the accuracy of scheme (17), we observe that in the neighborhood of $\xi = 0$, we have

$$R_2(\xi) = 1 - \xi + \xi^2 + O(\xi^3),$$

which implies, by comparison with $e^{-\xi} = 1 - \xi + \frac{\xi^2}{2} + O(\xi^3)$, that scheme (17) is no better than first order accurate in the particular case we are considering. Since this particular case is the most favorable one can think about, one expects the Douglas-Rachford scheme (17) to be *generically first order accurate*, a prediction supported by the results of various numerical experiments. It is worth mentioning that in order to improve the accuracy of the Douglas-Rachford scheme (17), *J. Douglas & S. Kim* introduced in the late 90s-early 2000s ([56]), the following variant of the above scheme

$$\phi^0 = \phi_0. \tag{205}$$

For $n \geq 0$, $\phi^n \to \hat{\phi}^{n+1} \to \phi^{n+1}$ as follows:

Solve

$$\frac{\hat{\phi}^{n+1} - \phi^n}{\triangle t} + A_1 \left(\frac{\hat{\phi}^{n+1} + \phi^n}{2}, t^{n+1/2} \right) + A_2(\phi^n, t^n) = 0, \tag{206}$$

and

$$\frac{\phi^{n+1} - \phi^n}{\triangle t} + A_1\left(\frac{\hat{\phi}^{n+1} + \phi^n}{2}, t^{n+1/2}\right) + A_2\left(\frac{\phi^{n+1} + \phi^n}{2}, t^{n+1/2}\right) = 0. \quad (207)$$

The *Douglas-Kim* scheme (205)-(207) is clearly inspired from the *Crank-Nicolson* scheme. Scheme (205)-(207) is *second order accurate* if the operators A_1 and A_2 are sufficiently smooth, the price to pay for this accuracy enhancement being a *reduction of stability and robustness* compared to the original Douglas-Rachford scheme (17).

At those wondering how to choose between *Peaceman-Rachford* and *Douglas-Rachford* schemes we will say that on the basis of many numerical experiments, it seems that the second scheme is more robust and faster for those situations where one of the operators is *non-smooth* (multivalued or singular, for example), particularly if one is interested at capturing steady state solutions. Actually, this behavior is consistent with the fact that the rational function R_1 associated with the Peaceman-Rachford scheme (the one defined by (201)), may change sign when ξ varies on $(0, +\infty)$, unlike the rational function R_2 defined by (204) (the one associated with the Douglas- Rachford scheme) which stays positive on the above interval. These sign changes, suggest a more oscillatory behavior for the associated scheme if fast transients take place, or if one tries to capture steady state solutions starting far away from these solutions.

As a final comment on *ADI* methods we have to mention that one their main contributors (if not the main one), beyond their founders (*J. Douglas*, *H. Rachford* and *D. Peaceman*), is definitely *E. Wachpress*: His wonderful book *The ADI Model Problem* [164] is an invaluable source of information and references on the Peaceman-Rachford and Douglas-Rachford methods, from the theoretical and practical points of view.

As a conclusion, let observe that the *Navier-Stokes equations* modelling the flow of viscous fluids have been mentioned quite a few times in this chapter (Section 4 in particular), and in other chapters of this book. There is no doubt that very few partial differential equation problems have motivated such a large number of operator-splitting based solution methods. Focusing on those publications with which we have some familiarity, let us mention: [11, 12, 13, 23, 35, 43, 47, 70, 72, 73, 90, 91, 92, 93, 94, 105, 107, 111, 112, 116, 122, 123, 158, 159, 160] (see also the references therein, Google Scholar, and Chapters 21, 22 and 23 of this book).

References

1. Aftalion, A.: Vortices in Bose-Einstein Condensates, Birkhäuser, Boston, MA (2006)
2. Ambrosio, L., Masnou, S.: A direct variational approach to a problem arising in image reconstruction. Interfaces and Free Boundaries, **5**, 63–82 (2003)
3. Arrow, K., Hurwicz, L., Uzawa, H.: Studies in Linear and Nonlinear Programing. Stanford University Press, Stanford, CA (1958)
4. Aujol, J.F.: Some first-order algorithms for total variation based image restoration. Journal of Mathematical Imaging and Vision, **34**, 307–327 (2009)

5. Bae, E., Lellmann, J., Tai, X.C.: Convex relaxations for a generalized Chan-Vese model. In: Heyden, A., Hahl, F., Olsson, C., Oskarsson, Tai, X.C. (eds) Energy Minimization Methods in Computer Vision and Pattern Recognition, pp. 223–236. Springer, Berlin (2013)

6. Bae, E., Tai, X.C.: Efficient global minimization methods for image segmentation models with four regions. Journal of Mathematical Imaging and Vision, **51**, 71–97 (2015)

7. Bae, E., Yuan, J., Tai, X.C.: Global minimization for continuous multiphase partitioning problems using a dual approach. International Journal of Computer Vision, **92**, 112–129 (2011)

8. Bae, E., Yuan, J., Tai, X.C., Boykov, Y.: A fast continuous max-flow approach to non-convex multilabeling problems. In: Bruhn, A., Pock, T., Tai, X.C. (eds.) Efficient Algorithms for Global Optimization Methods in Computer Vision, pp. 134-154. Springer, Berlin (2014)

9. Bao, W., Jaksch, D., Markowich, P.A.: Numerical solution of the Gross-Pitaevskii equation for Bose-Einstein condensation. J. Comp. Phys., **187**, 318–342 (2003)

10. Bao, W., Jin, S., Markowich, P.A.: On time-splitting spectral approximations for the Schrödinger equation in the semi-classical regime. J. Comp. Phys, **175**, 487–524 (2002)

11. Beale, J.T., Greengard, C.: Convergence of EulerStokes splitting of the NavierStokes equations. Communications on Pure and Applied Mathematics, **47** (8),1083-115 (1994)

12. Beale, J.T., Greengard, C., Thomann, E.: Operator splitting for Navier-Stokes and Chorin-Marsden product formula. In: Vortex Flows and Related Numerical Methods, NATO ASI Series, Vol. 395, pp. 27-38. Springer-Netherlands (1993)

13. Beale, J.T., Majda, A.: Rates of convergence for viscous splitting of the Navier-Stokes equations. Mathematics of Computation, **37** (156), 243-259 (1981)

14. Belytschko, T., Hughes, T.J.R.(editors): Computational Methods for Transient Analysis. North-Holland, Amsterdam (1983)

15. Bertozzi, A.L., Greer, J.B.: Low curvature image simplifiers: global regularity of smooth solutions andLaplacian limiting schemes. Comm. Pure Appl. Math., 57, 764-790 (2004)

16. Blanes, S., Moan, P.C.: Practical symplectic partitioned Runge-Kutta and Runge-Kutta-Nyström methods. J. Comp. Appl. Math., **142** (2), 313-330 (2002)

17. Bonito, A., Glowinski, R.: On the nodal set of the eigenfunctions of the Laplace-Beltrami operator for bounded surfaces in R-3: A computational approach. Commun. Pure Appl. Analysis, **13**, 2115–2126 (2014)

18. Boyd, S., Parikh, N., Chu, E., Peleato, B., Eckstein, J.: Distributed optimization and statistical learning via the alternating direction method of multipliers. Foundations and Trends in Machine Learning, **3**, 1–122 (2011)

19. Boykov, Y., Kolmogorov, V.: An experimental comparison of min-cut/max-flow algorithms for energy minimization in vision. IEEE Transactions on Pattern Analysis and Machine Intelligence, **26**, 359–374 (2001)

20. Bredies, K.: Recovering piecewise smooth multichannel images by minimization of convex functionals with total generalized variation penalty. In: Bruhn, A., Pock, T., Tai, X.C. (eds.) Efficient Algorithms for Global Optimization Methods in Computer Vision, pp. 44–77. Springer, Berlin (2014)

21. Bredies, K., Pock, T., Wirth, B.: Convex relaxation of a class of vertex penalizing functionals. Journal of Mathematical Imaging and Vision, **47**, 278–302 (2013)

22. Bresson, X., Esedoglu, S., Vandergheynst, P., Thiran, J.P., Osher, S.: Fast global minimization of the active contour/snake model. Journal of Mathematical Imaging and Vision, **28**, 151–167 (2007)

23. Bristeau, M.O., Glowinski, R., Périaux, J.: Numerical methods for the Navier-Stokes equations. Application to the simulation of compressible and incompressible viscous flow. Computer Physics Reports, **6**, 73–187 (1987)

24. Brito-Loeza, C., Chen, K.: On high-order denoising models and fast algorithms for vector-valued images. IEEE Transactions on Image Processing, **19**, 1518–1527 (2010)

25. Calder, J., Mansouri, A.,Yezzi, A.: Image sharpening via Sobolev gradient flows. SIAM Journal on Imaging Sciences, **3**, 981–1014 (2010)

26. Chambolle, A., Lions, P.-L.: Image recovery via total variation minimization and related problems. Numerische Mathematik, **76**, 167–188, (1997)

27. Chambolle, A., Pock, T.: A first-order primal-dual algorithm for convex problems with applications to imaging. Journal of Mathematical Imaging and Vision, **40**, 120–145 (2011)
28. Chan, R.H., Lanza, A., Morigi, S., Sgallari, F.: An adaptive strategy for the restoration of textured images using fractional order regularization. Numerical Mathematics: Theory, Methods & Applications, **6**, 276–296 (2013)
29. Chan, T., Esedoglu, S., Nikolova, M.: Algorithms for finding global minimizers of image segmentation and denoising models. SIAM J. Appl. Math., **66**, 1632–1648 (electronic) (2006)
30. Chan, T.F., Glowinski, R.: Finite Element Approximation and Iterative Solution of a Class of Mildly Nonlinear Elliptic Equations. Stanford report STAN-CS-78-674, Computer Science Department, Stanford University, Palo Alto, CA (1978)
31. Chan, T., Kang, S.H., Shen, J.: Euler's elastica and curvature-based inpainting. SIAM Journal on Applied Mathematics, **62**, 564–592 (2002)
32. Chan, T. F., Marquina, A., Mulet, P.: High-order total variation-based image restoration. SIAM J. Sci. Comput., 22(2), 503-516 (2000).
33. Chan, T., Vese, L.A.: Active contours without edges. IEEE Trans Image Proc., **10**, 266–277 (2001)
34. Chiche, A., Gilbert, J.C.: How the augmented Lagrangian algorithm can deal with an infeasible convex quadratic optimization problem. Journal of Convex Analysis, **22**, 30 (2015)
35. Chorin, A.J.: Numerical study of slightly viscous flow. Journal of Fluid Mechanics, **57** (4), 785-796 (1973)
36. Chorin, A.J., Hughes, T.J.R., McCracken, M.F., Marsden, J.E.: Product formulas and numerical algorithms. Com. Pure Appl. Math., **31**, 205–256 (1978)
37. Ciarlet, P.G.: The Finite Element Method for Elliptic Problems. SIAM, Philadelphia, PA (2002)
38. Crandall, M.G., Lions, P.L.: Viscosity solutions of Hamilton-Jacobi equations. Transactions of the American Mathematical Society, **277**, 1–42 (1983)
39. Cuesta, E., Kirane, M., Malik, S.A.: Image structure preserving denoising using generalized fractional time integrals. Signal Processing, **92**, 553–563 (2012)
40. Dahiya, D., Baskar, S., Coulouvrat, F.: Characteristic fast marching method for monotonically propagating fronts in a moving medium. SIAM J. Scient. Comp., **35**, A1880–A1902 (2013)
41. Dean, E.J., Glowinski, R.: On some finite element methods for the numerical simulation of incompressible viscous flow In: Gunzburger, M.D., Nicolaides, R.A. (eds.) Incompressible Computational Fluid Dynamics, pp. 109–150. Cambridge University Press, New York, NY (1993)
42. Dean, E.J., Glowinski, R.: An augmented Lagrangian approach to the numerical solution of the Dirichlet problem for the Monge-Ampère equation in two dimensions. Electronic Transactions on Numerical Analysis, **22**, 71–96 (2006)
43. Dean, E;J., Glowinski, R., Pan, T.W.: A wave equation approach to the numerical simulation of incompressible viscous fluid flow modeled by the Navier-Stokes equations. In: J.A. de Santo (ed.) Mathematical and Numerical Aspects of Wave Propagation, pp. 65-74. SIAM, Philadelphia, PA (1998)
44. Deiterding, R., Glowinski, R., Olivier, H., Poole, S.: A reliable split-step Fourier method for the propagation equation of ultra-fast pulses in single-mode optical fibers. J. Lightwave Technology, **31**, 2008–2017 (2013)
45. Delbos, F., Gilbert, J.C.: Global linear convergence of an augmented Lagrangian algorithm for solving convex quadratic optimization problems. Journal of Convex Analysis, **12**, 45–69 (2005)
46. Delbos, F., Gilbert, J.C., Glowinski, R., Sinoquet, D.: Constrained optimization in seismic reflection tomography: A Gauss-Newton augmented Lagrangian approach. Geophys. J. Internat., **164**, 670–684 (2006)
47. Demkowicz, L., Oden, J.T., Rachowicz, W.: A new finite element method for solving compressible Navier-Stokes equations based on an operator splitting method and h-p adaptivity. Comp. Meth. Appl. Mech. Eng., **84** (3), 275-326 (1990)

48. Descombes, S.: Convergence of splitting methods of high order for reaction-diffusion systems. Math. Comp., **70** (236), 1481-1501 (2001)
49. Descombes, S., Schatzman, M.: Directions alternées d'ordre élevé en réaction-diffusion. C.R. Acad. Sci. Paris, Sér. I, Math., **321** (11), 1521-1524 (1995)
50. Descombes,S., Schatzman,M.: On Richardson extrapolation of Strang's formula for reaction-diffusion equations. In : Equations aux Dérivées Partielles et Applications : Articles dédiés à J.L. Lions, Gauthier-Villars-Elsevier, Paris, 429-452 (1998)
51. Descombes, S., Thalhammer, M.: The Lie-Trotter splitting for nonlinear evolutionary problems with critical parameters: a compact local error representation and application to nonlinear Schrödinger equations in the semiclassical regime. IMA J. Num. Anal., **33** (2), 722-745 (2013)
52. Desjardin, B., Esteban. M.: On weak solution for fluid-rigid structure interaction: compressible and incompressible models. Archives Rat. Mech. Anal., **146**, 59–71 (1999)
53. Didas, S., Weickert, J., Burgeth, B.: Properties of higher order nonlinear diffusion filtering. Journal of Mathematical Imaging and Vision, **35**, 208–226 (2009)
54. Douglas, J.: Alternating direction methods in three space variables. Numer. Math., **4**, 41–63 (1962)
55. Douglas, J.: Alternating direction methods for parabolic systems in m-space space variables. J. ACM, **9**, 42–65 (1962)
56. Douglas, J., Kim, S.: Improved accuracy for locally one-dimensional methods for parabolic equations. Math. Models Meth. Appl. Sciences, **11** (9), 1563-1579 (2001)
57. Douglas, J., Rachford, H.H.: On the solution of the heat conduction problem in 2 and 3 space variables. Trans. Amer. Math. Soc., **82**, 421–439 (1956)
58. Duan, Y., Huang, W.: A fixed-point augmented Lagrangian method for total variation minimization problems. Journal of Visual Communication and Image Representation, **24**, 1168–1181 (2013)
59. Duvaut, G., Lions, J.L.: Inequalities in Mechanics and Physics. Springer, Berlin (1976)
60. Eckstein, J., Bertsekas, D.P.: On the Douglas-Rachford splitting method and the proximal point algorithm for maximal monotone operators. Math. Progam., **55**, 293–318 (1992)
61. Esser, E.: Applications of Lagrangian-based alternating direction methods and connections to split Bregman. CAM report, 9(31), Department of Mathematics, UCLA, Los Angeles, CA (2009)
62. Fortin, M., Glowinski, R.: Lagrangiens Augmentés: Application à la Résolution Numérique des Problèmes aux Limites. Dunod, Paris (1982)
63. Fortin, M., Glowinski, R.: Augmented Lagrangians: Application to the Numerical Solution of Boundary Value Problems. North-Holland, Amsterdam (1983)
64. Gabay, D.: Application de la méthode des multiplicateurs aux inéquations variationnelles. In: Fortin, M., Glowinski, R. (eds.) Lagrangiens Augmentés: Application à la Résolution Numérique des Problèmes aux Limites, pp. 279–307. Dunod, Paris (1982)
65. Gabay, D.: Application of the methods of multipliers to variational inequalities In: Fortin, M., Glowinski, R. (eds.) Augmented Lagrangians: Application to the Numerical Solution of Boundary Value Problems, pp. 299–331. North-Holland, Amsterdam (1983)
66. Glowinski, R.: Numerical Methods for Nonlinear Variational Problems. Springer, New York, NY (1984, 2nd printing: 2008)
67. Glowinski, R.: Viscous flow simulation by finite element methods and related numerical techniques. In: Murman, E.M., Abarbanel, S.S. (eds.) Progress and Supercomputing in Computational Fluid Dynamics, pp. 173–210. Birkhäuser, Boston, MA, (1985)
68. Glowinski, R.: Splitting methods for the numerical solution of the incompressible Navier-Stokes equations. In: Balakrishnan, A.V., Dorodnitsyn, A.A., Lions, J.L. (eds.) Vistas in Applied Mathematics, pp. 57–95. Optimization Software, New York, NY (1986)
69. Glowinski, R.: Finite element methods for the numerical simulation of incompressible viscous flow. Application to the control of the Navier-Stokes equations. In: Anderson, C.R., Greengard, C. (eds.) Vortex Dynamics and Vortex Methods, pp. 219–301. American Mathematical Society, Providence, RI (1991)

70. Glowinski, R.: Finite element methods for incompressible viscous flow In: Ciarlet, P.G., Lions, J.L. (eds.) Handbook of Numerical Analysis, Vol. IX, pp. 3–1176. North-Holland, Amsterdam, (2003)

71. Glowinski, R.: On alternating direction methods of multipliers: A historical perspective. In: Fitzgibbon, W., Kuznetsov, Y.A., Neittaanmäki, P., Pironneau, O. (eds.) Modeling, Simulation and Optimization for Science and Technology, Vol. 34, pp. 59–82. Springer, Dordrecht (2014)

72. Glowinski, R.: Variational Methods for the Numerical Solution of Nonlinear Elliptic Problems. SIAM, Philadelphia, PA, (2015)

73. Glowinski, R., Dean, E.J., Guidoboni, G., Juarez, H.L., Pan, T.-W.: Applications of operator-splitting methods to the direct numerical simulation of particulate and free-surface flows and to the numerical solution of the two-dimensional elliptic Monge-Ampère equation. Japan J. Ind. Appl. Math., **25**, 1–63 (2008)

74. Glowinski, R., Le Tallec, P.: Augmented Lagrangian and Operator-Splitting Methods in Nonlinear Mechanics. SIAM, Philadelphia, PA (1989)

75. Glowinski, R., Leung, Y., Qian, J.: An operator-splitting based fast sweeping method for an anisotropic eikonal equation. SIAM J. Scient. Comp. (accepted for publication in 2016).

76. Glowinski, R., Lions, J.L., Trémolières, R.: Numerical Analysis of Variational Inequalities. North-Holland, Amsterdam (1981).

77. Glowinski, R., Marrocco, A.: Sur l'approximation par éléments finis d'ordre un et la résolution par pénalisation-dualité d'une classe de problèmes de Dirichlet non-linéaires. C. R. Acad. Sci. Paris, **278A**, 1649–1652 (1974)

78. Glowinski, R., Marrocco, A.: Sur l'approximation par éléments finis d'ordre un et la résolution par pénalisation-dualité d'une classe de problèmes de Dirichlet non-linéaires. ESAIM : Math. Model. Num. Anal., **9**(R2), 41–76 (1975)

79. Glowinski, R., Pan, T.-W., Hesla, T.I., Joseph, D.D., Périaux, J.: A fictitious domain approach to the direct numerical simulation of incompressible viscous fluid flow past moving rigid bodies: application to particulate flow. J. Comp. Phys., **169**, 363–426 (2001)

80. Glowinski, R., Quaini, A.: On an inequality of C. Sundberg: A computational investigation via nonlinear programming. Journal of Optimization Theory and Applications, **158** (3), 739-772 (2013)

81. Glowinski, R., Shiau, L., Sheppard, M.: Numerical methods for a class of nonlinear integro-differential equations. Calcolo, **50**, 17–33 (2013)

82. Glowinski, R., Sorensen, D.C.: Computing the eigenvalues of the Laplace-Beltrami operator on the surface of a torus: A numerical approach. In: Glowinski, R., Neittaanmäki, P. (eds.) Partial Differential Equations: Modeling and Numerical Solution, pp. 225–232. Springer, Dordrecht (2008)

83. Glowinski, R., Wachs, A.: On the numerical simulation of visco-plastic fluid flow. In: Ciarlet, P.G., Glowinski, R., Xu, J. (eds.) Handbook of Numerical Analysis, Vol. XVI, pp. 483-717. North-Holland, Amsterdam (2011)

84. Godlewsky, E.: Méthodes à Pas Multiples et de Directions Alternées pour la Discrétisation d'Equations d'Evolution. Doctoral Dissertation, Department of Mathematics, University P. & M. Curie, Paris, France (1980)

85. Goldman, D., Kaper, T.J.: N th-order operator-splitting schemes and non-reversible systems. SIAM J. Num. Anal., **33** (1), 349-367 (1996)

86. Goldstein, T., Osher, S.: The split-Bregman method for $L1$-regularized problems. SIAM Journal on Imaging Sciences, **2**, 323–343 (2009)

87. Grandmont, C., Maday, Y.: Existence for an unsteady fluid-structure interaction problem. Math. Model. Num. Anal., **34**, 609–636 (2000)

88. Greer, J.B., Bertozzi, A.L.: Traveling wave solutions of fourth order pdes for image processing. SIAM Journal on Mathematical Analysis, **36**, 38–68 (2004)

89. Guidotti, P., Longo, K.: Two enhanced fourth order diffusion models for image denoising. Journal of Mathematical Imaging and Vision, **40**, 188–198 (2011)

90. Guermond, J.L.: Some implementations of projection methods for Navier-Stokes equations. RAIRO-Model. Math. Anal. Num., **30** (5), 637-667 (1996)

91. Guermond, J.L., Minev, P., Shen, J.: An overview of projection methods for incompressible flows. Comp. Meth. Appl. Mech. Eng., **195** (44), 6011-6045 (2006)
92. Guermond, J.L., Quartapelle, L.: Calculation of incompressible viscous flows by an unconditionally stable projection FEM. J. Comp. Phys., **132** (1),12-33(1997)
93. Guermond, J.L., Quartapelle, L.: On the approximation of the unsteady Navier-Stokes equations by finite element projection methods. Numer. Math., **80** (2), 207-238 (1998)
94. Guermond, J.L., Shen, J.: A new class of truly consistent splitting schemes for incompressible flows. J. Comp. Phys., **192** (1), 262-276 (2003)
95. He, B., Yuan, X.: On the O(1/n) convergence rate of the Douglas-Rachford alternating direction method. SIAM J. Numer. Anal., **50**, 700–709 (2012)
96. Hesse, R, Luke, D.R.: Nonconvex notions of regularity and convergence of fundamental algorithms for feasibility problems. SIAM Journal on Optimization, **23** (4), 2397-2419 (2013)
97. Hou, S., T.-W. Pan, Glowinski, R.: Circular band formation for incompressible viscous fluid-rigid-particle mixtures in a rotating cylinder. Physical Review E, **89**, 023013 (2014)
98. Hu, H.H., Patankar, N.A., Zhu, M.Y.: Direct numerical simulation of fluid-solid systems using arbitrary Lagrangian-Eulerian techniques. J. Comp. Phys., **169**, 427–462 (2001)
99. Hu, L., Chen, D., Wei, G.W.: High-order fractional partial differential equation transform for molecular surface construction. Molecular Based Mathematical Biology, **1**, 1–25 (2013)
100. Ito, K., Kunisch, K.: Lagrange Multiplier Approach to Variational Problems. SIAM, Philadelphia, PA (2008)
101. Jidesh, P., George, S.: Fourth–order variational model with local–constraints for denoising images with textures. International Journal of Computational Vision and Robotics, **2**, 330–340 (2011)
102. Jin, S., Markowich, P.A., Zheng, C.: Numerical simulation of a generalized Zakharov system. J. Comp. Phys., **201**, 376–395 (2004)
103. Johnson, A.A., Tezduyar, T.E.: 3-D simulations of fluid-particle interactions with the number of particles reaching 100. Comp. Meth. Appl. Engrg., **145**, 301–321 (1997)
104. Kao, C.Y., Osher, S.J., Qian, J.: Lax-Friedrichs sweeping schemes for static Hamilton-Jacobi equations. J. Comput. Phys., **196**, 367–391 (2004)
105. Karniadakis, G.E., Israeli, M., Orszag, S.A.: High-order splitting methods for the incompressible Navier-Stokes equations. J. Comp. Phys., **97** (2), 414-443 (1991)
106. Kass, M., Witkin, A., Terzopoulos, D.: Snakes: Active contour models. International Journal of Computer Vision, **1**, 321–331 (1988)
107. Kim, J., Moin, P.: Application of a fractional-step method to incompressible Navier-Stokes equations. Journal of Computational Physics, **59** (2), 308-323 (1985)
108. Kimmel, R., Malladi, R., Sochen, N.: Images as embedded maps and minimal surfaces: movies, color, texture, and volumetric medical images. International Journal of Computer Vision, **39**, 111–129 (2000)
109. Lanza, A., Morigi, S., Sgallari, F.: Convex image denoising via non-convex regularization. In: Aujol, J.F., Nikolova, M., Papadakis, N. (eds.) Scale Space and Variational Methods in Computer Vision, pages 666-677, Proceedings, LNCS 9087, Springer International Publishing (2015).
110. Layton, W.J., Maubach, J.M., Rabier, P.J.: Parallel algorithms for maximal monotone operators of local type. Numer. Math., **71**, 29–58 (1995)
111. Le, H., Moin, P.: An improvement of fractional step methods for the incompressible Navier-Stokes equations. Journal of Computational Physics, **92** (2), pp.369-379.
112. Lee, M.J., Do Oh, B., Kim, Y.B.: Canonical fractional-step methods and consistent boundary conditions for the incompressible Navier-Stokes equations. J. Comp. Phys.,**168** (1), 73-100 (2001)
113. Lehoucq, R.B., Sorensen, D. C., Yang, C.: ARPACK Users' Guide: Solution of Large-Scale Eigenvalue Problems with Implicitly Restarted Arnoldi Methods. SIAM, Philadelphia, PA (1998)
114. Lellmann, J., Schnörr, C.: Continuous multiclass labeling approaches and algorithms. SIAM J. Imaging Sci., **4**, 1049–1096 (2011)

115. Lewis, A.S., Luke, D.R., Malick, J.: Local linear convergence for alternating and averaged nonconvex projections. Foundations of Computational Mathematics, **9** (4), 485-513 (2009)
116. Li, C.H., Glowinski, R.: Modeling and numerical simulation of low-Mach number compressible flows. Int. J. Numer. Meth. Fluids, **23** (2), 77-103 (1996)
117. Lie, J., Lysaker, M., Tai, X.-C.: A binary level set model and some applications to Mumford-Shah image segmentation. IEEE Transactions on Image Processing, **15**, 1171–1181 (2006)
118. Lions, P.L., Mercier, B.: Splitting algorithms for the sum of two nonlinear operators. SIAM J. Num. Anal., **16**, 964–979 (1979)
119. Lu, T., Neittaanmäki, P., Tai, X.-C.: A parallel splitting up method for partial differential equations and its application to Navier-Stokes equations. RAIRO Math. Model. and Numer. Anal., **26**, 673–708 (1992)
120. Lysaker, M., Lundervold, A., Tai, X.C.: Noise removal using fourth-order partial differential equation with applications to medical magnetic resonance images in space and time. Image Processing, IEEE Transactions on, **12**, 1579–1590 (2003)
121. Marchuk, G.I.: Splitting and alternating direction methods. In: Ciarlet, P.G., Lions, J.L. (eds.) Handbook of Numerical Analysis, Vol. I, pp. 197–462. North-Holland, Amsterdam (1990)
122. Marion, M., Temam, R.: Navier-Stokes equations: Theory and approximation. In: Ciarlet, P.G., Lions, J.L. (eds.) Handbook of Numerical Analysis, Vol. VI, pp. 503-689. North-Holland, Amsterdam (1998)
123. Marsden, J.: A formula for the solution of the Navier-Stokes equation based on a method of Chorin. Bulletin of the American Mathematical Society, **80** (1),154-158 (1974)
124. Masnou, S., Morel, J.M.: Level lines based disocclusions. In: Proceedings IEEE International Conferenceon Image Processing, Chicago, IL, pp. 259-263 (1998).
125. Mason, P., Aftalion, A.: Classification of the ground states and topological defects in a rotating two-component Bose-Einstein condensate. Physical Review A, **84**, 033611 (2011)
126. Mason, P., Aftalion, A.: Vortex-peak interaction and lattice shape in rotating two-component Bose-Einstein condensates. Physical Review A, **85**, 033614 (2012)
127. Maury, B.: Direct simulation of 2-D fluid-particle flows in bi-periodic domains. J. Comp. Phys., **156**, 325–351 (1999)
128. Maury, B.: A time-stepping scheme for inelastic collisions. Numer. Math., **102**, 649–679 (2006)
129. Maury, B., Venel, J.: Handling of contacts in crowd motion simulations. In: Appert-Rolland, C., Chevoir, F., Gondret, P., Lassarre, S., Lebacque, J.P., Schreckenberg, M. (eds.) Traffic and Granular Flow'07, pp. 171–180. Springer, Berlin Heidelberg (2009)
130. Min, L., Yang, X., Gui, C.: Entropy estimates and large-time behavior of solutions to a fourth-order nonlinear degenerate equation. Communications in Contemporary Mathematics, **15**, (2013)
131. Mouhot, C., Villani, C.: On Landau damping, Acta Mathematica, **207**, 29–201 (2011)
132. Mumford, D., Shah, J.: Optimal approximation by piecewise smooth functions and associated variational problems. Comm. Pure Appl. Math, 42, **42**, 577–685 (1989)
133. Myllykoski, M., Glowinski, R., Kärkkäinen, T., Rossi, T.: A new augmented Lagrangian approach for L^1-mean curvature image denoising. SIAM Journal on Imaging Sciences, **8**, 95–125 (2015)
134. Nadernejad, E., Forchhammer, S.: Wavelet-based image enhancement using fourth order pde. In Intelligent Signal Processing (WISP), 2011 IEEE 7th International Symposium on, pages 1–6. IEEE (2011)
135. Nitzberg, M., Mumford, D., Shiota, T.: Filtering, segmentation and depth. Lecture Notes in Computer Science, 662 (1993)
136. Pan, T.-W., Glowinski, R.: Direct numerical simulation of the motion of neutrally buoyant circular cylinders in plane Poiseuille flow. J. Comp. Phys., **181**, 260–279 (2002)
137. Pan, T.-W., Glowinski, R., Hou, S.: Direct numerical simulation of pattern formation in a rotating suspension of non-Brownian settling particles in a fully filled cylinder. Computers & Structures, **85**, 955–969 (2007)

138. Papafitsoros, K., Schönlieb, C.B.: A combined first and second order variational approach for image reconstruction. Journal of Mathematical Imaging and Vision, **48**, 308–338 (2014)
139. Peaceman, D.H., Rachford, H.H.: The numerical solution of parabolic and elliptic differential equations. J. Soc. Ind. Appl. Math., **3**, 28–41 (1955)
140. Prignitz, R., Bänsch, E.: Numerical simulation of suspension induced rheology. Kybernetika, **46**, 281–293 (2010)
141. Prignitz, R., Bänsch, E.: Particulate flows with the subspace projection method. J. Comp. Phys., **260**, 249–272 (2014)
142. Rosman, G., Bronstein, A.M., Bronstein, M.M., Tai, X.C., Kimmel, R.: Group-valued regularization for analysis of articulated motion. In: Fusiello, A., Murino, V., Cucchiara, R. (eds.) Computer Vision–ECCV 2012. Workshops and Demonstrations, pages 52–62. Springer, Berlin (2012)
143. Rosman, G., Wang, Y., Tai, X.C., Kimmel, R., Bruckstein, A.M.: Fast regularization of matrix-valued images. In: Bruhn, A., Pock, T., Tai, X.C. (eds.) Efficient Algorithms for Global Optimization Methods in Computer Vision, pages 19–43. Springer, Berlin (2014)
144. Rudin, L., Osher, S., Fatemi, E.: Nonlinear total variation based noise removal algorithms. Physica D, **60**, 259–268 (1992)
145. San Martin, J.A., Starovoitov, V., Tucksnak, M.: Global weak convergence for the two-dimensional motion of several rigid bodies in an incompressible viscous fluid. Archives Rat. Mech. Anal., **161**, 113–147 (2002)
146. Schoenemann, T., Kahl, F., Cremers, D.: Curvature regularity for region-based image segmentation and inpainting: A linear programming relaxation. In Computer Vision, 2009 IEEE 12th International Conference on, pages 17–23. IEEE (2009)
147. Schönlieb, C.B., Bertozzi, A.: Unconditionally stable schemes for higher order inpainting. Communications in Mathematical Sciences, **9**, 413–457 (2011)
148. Schwartz, L.: Théorie des Distributions. Hermann, Paris (1966)
149. Setzer, S., Steidl, G.: Variational methods with higher order derivatives in image processing. Approximation, 12, 360-386 (2008).
150. Sheng, Q.: Solving linear partial differential equations by exponential splitting. IMA J. Num. Anal., **9** (2), 199-212 (1989)
151. Sheng, Q.: Global error estimates for exponential splitting. IMA J. Num. Anal., **14** (1), 27-56 (1994)
152. Sigurgeirson, H., Stuart, A.M., Wan, J.: Collision detection for particles in flow. J. Comp. Phys., **172**, 766–807 (2001)
153. Strang, G.: On the construction and comparison of difference schemes. SIAM J. Num. Anal., **5**, 506–517 (1968)
154. Tai, X.C., Hahn, J., Chung, G.J.: A fast algorithm for Euler's elastica model using augmented Lagrangian method. SIAM Journal on Imaging Sciences, **4**, 313 (2011)
155. Tai, X.C., Neittaanm`̈ki, P.: Parallel finite element splitting–up method for parabolic problems. Numerical Methods for Partial Differential Equations, **7**, 209–225 (1991)
156. Tai, X.C., Wu, C.: Augmented Lagrangian method, dual methods and split Bregman iteration for ROF model. In: Tai, X.C., Morken, K., Lysaker, M., Lie, K.-A. (eds.) Scale Space and Variational Methods in Computer Vision, pages 502–513. Springer, Berlin (2009)
157. Tartar, L.: An Introduction to Sobolev Spaces and Interpolation Spaces. Springer, Berlin (2007)
158. Temam, R.: Sur l'approximation de la solution des équations de Navier-Stokes par la méthode des pas fractionnaires (I). Archive for Rational Mechanics and Analysis, **32** (2), 135-153 (1969)
159. Temam, R.: Sur l'approximation de la solution des équations de Navier-Stokes par la méthode des pas fractionnaires (II). Archive for Rational Mechanics and Analysis, **33** (5), 377-385 (1969)
160. Temam, R.: Navier-Stokes Equations: Theory and Numerical Analysis. American Mathematical Society, Providence, RI (2001)
161. Thalhammer, M.: High-order exponential operator-splitting methods for time-dependent Schrödinger equations. SIAM J. Num. Anal., **46** (4), 2022-2038 (2008)

162. Turek, S., Rivkind, L., Hron, J., Glowinski, R.: Numerical study of a modified time-stepping θ-scheme for incompressible flow simulations. J. Scient. Comp., **28**, 533–547 (2006)
163. Villani, C.: Birth of a Theorem: A Mathematical Adventure. Ferrar, Strauss & Giroux, New York, NY. (2015)
164. Wachpress, E.L.: The ADI model problem. Springer, New York, NY (2013)
165. Wan, D., Turek, S.: Fictitious boundary and moving mesh methods for the numerical simulation of rigid particulate flows. J. Comp. Phys., **222**, 28–56 (2007)
166. Wang, Y., Yin, W., Zeng, J.: Global Convergence of ADMM in nonconvex nonsmooth optimization. arXiv preprint arXiv:1511.06324 (2015)
167. Weickert, J., ter Haar Romeny, B.M., Viergever, M.A.: Efficient and reliable schemes for nonlinear diffusion filtering. Image Processing, IEEE Transactions on, **7**, 398–410 (1998)
168. Wekipedia. Co-area formula (http://en.wikipedia.org/wiki/coarea_formula) (2013)
169. Wikipedia. Total variation (http://en.wikipedia.org/wiki/total_variation), 2014.
170. Wu, C., Tai, X.C.: Augmented Lagrangian method, dual methods, and split Bregman iteration for ROF, vectorial TV, and high order models. SIAM Journal on Imaging Sciences, **3**, 300–339 (2010)
171. Yang, F., Chen, K., Yu, B.: Efficient homotopy solution and a convex combination of ROF and LLT models for image restoration. International Journal of Numerical Analysis & Modeling, **9**, 907–927 (2012)
172. Yin, W., Osher, S., Goldfarb, D., Darbon, J.: Bregman iterative algorithms for l_1-minimization with applications to compressed sensing. SIAM Journal on Imaging Sciences, **1**, 143–168 (2008)
173. Yuan, J., Bae, E., Tai, X.C.: A study on continuous max-flow and min-cut approaches. In Computer Vision and Pattern Recognition (CVPR), 2010 IEEE Conference on, pages 2217–2224. IEEE (2010)
174. Yuan, J., Bae, E., Tai, X.C., Boykov, Y.: A continuous max-flow approach to Potts model. In: Daniilidis, K., Maragos, P., Paragios, N. (eds.) Computer Vision–ECCV 2010, pages 379–392. Springer, Berlin (2010)
175. Yuan, J., Bae, E., Tai, X.C., Boykov, Y.: A study on continuous max-flow and min-cut approaches. In Computer Vision and Pattern Recognition (CVPR), 2010 IEEE Conference on, pages 2217–2024. IEEE (2010)
176. Yuan, J., Bae, E., Tai, X.C., Boykov, Y.: A spatially continuous max-flow and min-cut framework for binary labeling problems. Numerische Mathematik, **126**, 559–587 (2014)
177. Yuan, J., Schnorr, C., Steidl, G.: Simultaneous higher-order optical flow estimation and decomposition. SIAM J.Scientific Computing, 29(6), 2283-2304 (2007).
178. Yuan, J., Shi, J., Tai, X.C.: A convex and exact approach to discrete constrained $TV - L^1$ image approximation. East Asian Journal on Applied Mathematics, **1**, 172–186 (2011)
179. Zach, C., Gallup, D., Frahm, J.-M., Niethammer, M.: Fast global labeling for real-time stereo using multiple plane sweeps. In Vision, Modeling and Visualization Workshop (VMV) pages 243–252 (2008)
180. Zakharov, V.E.: Collapse of Langmuir waves. Soviet Journal of Experimental and Theoretical Physics, **35**, 908–914 (1972)
181. Zeng, W., Lu, X., Tan, X.: Nonlinear fourth-order telegraph-diffusion equation for noise removal. IET Image Processing, **7**, 335–342 (2013)
182. Zhao, H. K.: Fast sweeping method for Eikonal equations. Math. Comp., **74**, 603–627 (2005)
183. Zhu, W., Chan, T.: Image denoising using mean curvature of image surface. SIAM Journal on Imaging Sciences, **5**, 1–32 (2012)
184. Zhu, W., Chan, T.: A variational model for capturing illusory contours using curvature. Journal of Mathematical Imaging and Vision, **27**, 29–40 (2007)
185. Zhu, W., Chan, T., Esedoglu, S.: Segmentation with depth: A level set approach. SIAM Journal on Scientific Computing, **28**, 1957–1973 (2006)
186. Zhu, W., Tai, X.-C., Chan, T.: Augmented Lagrangian method for a mean curvature based image denoising model. Inverse Problems and Imaging, **7**, 1409–1432 (2013)
187. Zhu, W., Tai, X.C., Chan, T.F.: Image segmentation using Euler's elastica as the regularization. Journal of Scientific Computing, **57** (2), 414-438 (2013).